LANGMUIR PROBE MEASUREMENTS IN 13.56MHz DISCHARGES

A thesis for the degree of PhD

Presented to

DUBLIN CITY UNIVERSITY

by

JOHN V. SCANLAN

School of Physical Sciences

DUBLIN CITY UNIVERSITY

Research supervisor

Dr. Michael B. Hopkins

September 1991

DECLARATION

This thesis is based on my own work.

John Scanlan, Sept. '91

CONTENTS

page

CHAPTER ONE.....*RF DISCHARGES*

1.1 Introduction 1

1.2 rf plasmas 5

1.3 rf plasma modeling 19

1.4 Outline of proposed research 25

CHAPTER TWO.....*THE LANGMUIR PROBE*

2.1 Introduction 30

2.2 Langmuir probe theory 31

2.3 Evaluation of the eedf 37

2.4 Sources of error in probe measurements 39

2.5 Langmuir probes in rf plasmas 43

2.6 Techniques to obtain probe characteristics in rf plasmas 49

2.7 The tuned probe 54

2.8 Operating conditions of the developed tuned probe 61

CHAPTER THREE.....*THE EXPERIMENTAL RF SYSTEM*

3.1 Introduction 62

3.2 The experimental set-up 63

3.3 rf matching units 66

3.4 rf power measurement 72

3.5 rf grounds and shielding 75

3.6 Data acquisition and analysis 78

page

CHAPTER FOUR.....*RESULTS AND DISCUSSION OF PLASMA PARAMETER MEASUREMENTS*

4.1 Introduction 79
4.2 The bulk electron temperature 82
4.3 Pressure dependence of rf plasma parameters 86
4.4 Spatial dependence of rf plasma parameters 95
4.5 Power dependence of rf plasma parameters 101
4.6 Accuracy of the measured plasma parameters 103

CHAPTER FIVE.....*RESULTS AND DISCUSSION OF EEDF MEASUREMENTS*

5.1 Introduction 105
5.2 eedf's measured in argon rf plasmas 107
5.3 eedf's measured in nitrogen rf plasmas 113
5.4 Afterglow eedf's and the influence of super-elastic collisions on the eedf structure 124

CHAPTER SIX.....*ELECTROSTATIC CONFINEMENT IN RF PLASMAS*

6.1 Introduction 130
6.2 The confinement mechanism 132

CHAPTER SEVEN.....*CONCLUSIONS*

7.1 Summary of work 136
7.2 Suggestions for future work 139

REFERENCES 141

ABSTRACT

Low pressure, radio-frequency (rf) glow discharges have been used extensively in plasma processing in recent years. To exploit the advantages of the rf plasma fully, a detailed knowledge of the discharge physics is required. Many powerful models have evolved which attempt to describe the plasma and predict plasma parameters under varying conditions. However, in the absence of versatile and reliable diagnostic experimental tools, such models cannot be tested and the processing operator must rely on the so-called "*Response Surface Methodology*" to predict plasma-chemistry and physical reaction rates.

This thesis reports on the development of a tuned Langmuir probe, which has been used to monitor plasma parameters, including the electron energy distribution function (eedf), in 13.56MHz argon and nitrogen plasmas under various discharge conditions. The development and application of the tuned probe is described, as is the rf environment, since successful measurements rely on a thorough understanding of the subtleties of the two.

The plasma parameter measurements are presented as a function of gas pressure, spatial distribution and input rf power. The results are generally interpreted in terms of accepted rf plasma theory, which is still evolving. The eedf measurements demonstrate that the argon and nitrogen plasmas are created via different ionization processes, and may be strongly influenced by inelastic and super-elastic collision processes.

Plasma heating, a topic of much recent debate, is discussed, and an electron trapping mechanism, which resolves some of the questions posed by the eedf measurements and the current plasma heating theories, is presented.

CHAPTER ONE
RF DISCHARGES

1.1 Introduction

Over the years, gas discharges have been used in several pure and applied research applications. For example, dc glows have been used extensively in gas laser research, resulting in the development of molecular nitrogen, argon ion and atomic neutral helium-neon lasers[1]. Such developments rely on the understanding of the fundamental processes involved in the glow discharge. In particular, gas lasers exploit the knowledge of both the cross-sections of the applied atomic and molecular processes (e.g. N_2 vibrational excitation, He metastable excitation), and the values of relevant plasma parameters. Macroscopic parameters such as gas pressure, gas type, chamber dimension and discharge voltage and current (discharge power), determine the microscopic parameters, neutral gas density, n_o, electron temperature, kT_e, electron density, n_e, positive ion density, n_+, and electron energy distribution function (eedf). In order to properly understand and exploit the glow discharge, the

microscopic parameters, and their dependence on the macroscopic parameters, must be known.

Glow discharges have also been used extensively in materials processing[2]. In particular, they have been successfully applied to plasma enhanced chemical vapour deposition, sputter deposition, substrate sputter etching, plasma etching, reactive ion etching and ion implantation. Microelectronic device fabrication is performed almost exclusively in the glow discharge. The advantage over chemically based systems is that while the background gas (argon, fluorine, etc.) remains cold, the electron energy is typically between 1eV and 20eV. Collisions of these energetic electrons with the neutral carrier gas atoms or molecules generates the ionic etchant species. Dissociation reactions, for example, which have large activation energies, can proceed at essentially room temperature. This non-equilibrium between the different gas species, and low temperature environment, is the key to device integrity. Also, the disparity in the diffusion coefficients of electrons and ions results in the plasma biasing itself positive with respect to the discharge chamber. This plasma potential, depending on the mode of plasma generation and voltage coupling, can be anywhere between a few volts and a few hundred volts. As the positive ions traverse the plasma sheath they are accelerated by the plasma potential. This energetic ion bombardment is the distinction between plasma etching and

reactive ion etching (RIE), and enhances the etch rate as well as improving directionality.

Recently, trends toward improved etch profiles, etch rate and shrinking dimensions have rendered the dc plasma processing system all but obsolete[2],[3]. The reasons for this are as follows. Firstly, the dc glow is spatially inhomogeneous; secondly, discharge current densities are low; and thirdly, the dc glow greatly depends on secondary electron emission for ionisation, and thus varies with the surface condition of the electrodes. It is thus unsuited to the processing environment. As a result, processing systems have instead turned to radio-frequency (rf) generated plasmas. The rf plasma, while not having the mentioned disadvantages of the dc system, has the added advantages that it can be operated at low pressures, favouring improved anisotropy; it can be operated in electrodeless systems, and does not necessarily depend on γ (secondary electron emission coefficient); and also can be used to process insulating materials. Furthermore, the time-averaged rf plasma potentials are normally quite high, favouring RIE.

Many other configurations have been applied to plasma processing. For example, electron cyclotron resonance (ECR) discharges[2],[4],[5], surface wave discharges[6], magnetrons[7] and helical resonators[8]. Very often magnetic fields are employed to confine ionizing electrons, so that the discharge operation is extended to

lower pressures. None, however, have achieved the ubiquity of the rf system. Recently, rf plasmas have been used to drive low pressure multipole ion sources[9], favoured over the conventional hot filament sources because of its limitless lifetime compared to tungsten filaments. RF excitation is again employed *in lieu* of dc because of its lower pressure limit, a pre-requisite for large aperture ion sources.

As a result of the forementioned applications of the rf discharge, much experimental and theoretical interest has been directed at this type of plasma. As stated earlier, the rf plasma can only be exploited fully when the dependence of the microscopic parameters upon the external discharge variables are determined. It is also necessary that the plasma be understood in terms of production (electron heating mechanisms) and loss rates (diffusion, recombination, etc.), as different modes of operation are possible. Since rf plasmas are time-varying, the temporal evolution of the plasma is an added parameter, and one which is proving to be increasingly important.

This thesis is an attempt to link and extend the current knowledge of rf plasmas. The experimental investigation has resulted in the development of a diagnostic tuned Langmuir probe, which has been used to characterise an rf plasma, resulting in a clearer picture of rf plasma operation.

1.2 RF Plasmas

Although rf plasmas are used extensively, rf plasma physics has not been developed in depth and our understanding of the subject is still evolving at a considerable rate. The current knowledge of rf plasmas is summarized in four sections below. This knowledge has arisen from both experimental and theoretical research endeavours, the techniques of which are described in subsequent sections of this chapter.

(i) Configurations, rf glow and plasma potentials

Although the rf plasma can be inductively or capacitively coupled, most commercial processing systems are parallel plate, capacitively coupled, and driven at the allotted frequency of 13.56MHz. One electrode is grounded, while the other is powered by the rf voltage supply, through an intervening matching network and a blocking capacitor (see section 3.1). Discharge stability is maintained by the blocking capacitor which prevents dc current from flowing in the plasma and the external circuit (see fig.3.1). If the electrodes are of equal area, the system is termed symmetric, while unequal electrode areas constitutes an asymmetric arrangement. Although, in many processing systems, the electrodes are of equal area, since one electrode is normally grounded and equipotential with the chamber walls, the arrangement does constitute an asymmetric system.

The chamber pressure is usually maintained between 10mTorr and 500mTorr[2]. When the discharge is operating the glow fills the space between the electrodes. This is the plasma or quasi-neutral region of the discharge. Dark spaces (or sheaths) provide the interface between the plasma and the electrodes or chamber walls. The electric fields in the quasi-neutral region are weak compared to the fields in the space-charge dominated sheaths. In fact most of the applied rf voltage appears across the sheaths. The rf plasma is weakly ionized, with n_e/n_o of the order of 10^{-6}.

On a time averaged scale the plasma is positive with respect to all chamber surfaces in order to maintain quasi-neutrality. Electrons, which diffuse faster than ions, are thus contained within the discharge by the ambipolar fields which are established. Figure 1.1 is an illustrative diagram of plasma potentials, $V_p(t)$, and excitation electrode voltages, $V_{rf}(t)$, assuming a purely capacitive sheath behaviour, for three different geometries and for dc and capacitively coupled excitation electrodes taken from Köhler et al.[10]. The plasma potential of a 13.56MHz low pressure argon glow discharge was determined for the various configurations by measuring the time resolved positive ion energy distribution. The capacitively coupled, asymmetric set-up, the smaller electrode being powered, is the most widely used (top right of fig 1.1). In this configuration, in order to

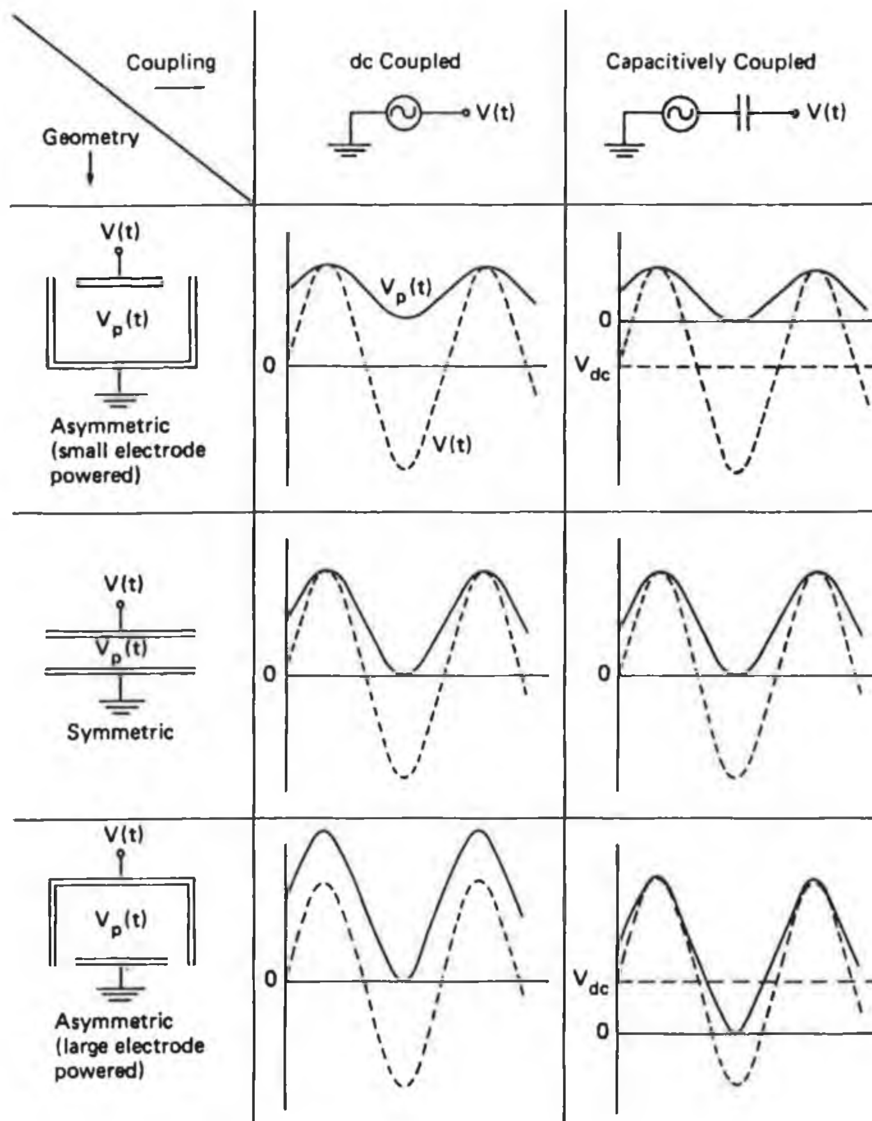

FIG.1.1: RF plasma potentials for different discharge geometries (taken from ref.10)

preserve electronic current continuity on each rf half cycle (since no dc current can flow), a dc negative bias establishes itself on the powered, smaller electrode. The

development of this self bias is illustrated in figure 1.2[11]. The current drawn by an electrode in the rf plasma is given by the IV curve (fig.1.2(a)). In order to draw a net zero current, the electrode adopts a negative bias (fig.1.2(b)). Many processing systems exploit this configuration, since ions are accelerated toward the negatively biased driven electrode.

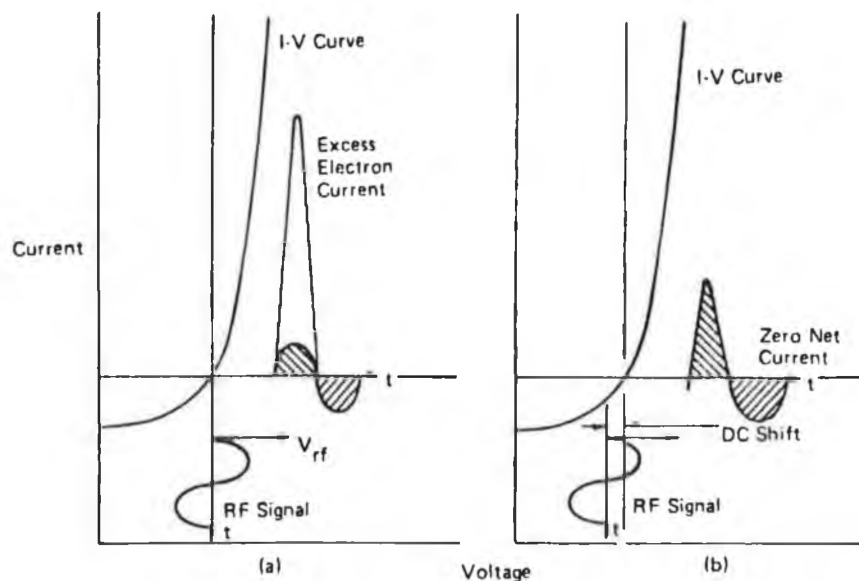

FIG.1.2: The development of the dc self-bias (taken from ref.11)

(ii) Frequency response and the rf sheath

If the rf driving frequency, ω, is less than the ion plasma frequency, ω_i, then the discharge ions can respond to the rf field variations. The ion plasma frequency is given by

$$\omega_i = (n_e e^2/m_i \varepsilon_o)^{1/2} \quad ..... \quad \textbf{(1.1)}$$

and is typically of the order of a few MHz. The electron plasma frequency is nominally of the order of 1GHz. If $\omega < \omega_i$, then the rf sheath is resistive, since both electron and ion currents flow, and the plasma potential appears as V_{p1} in figure 1.3. If $\omega > \omega_i$, then the rf sheath is capacitive, since only electrons respond to the rf field variations, and the plasma potential appears as V_{p2}. At a driving frequency of 13.56MHz, an intermediate case is probably more appropriate, the rf sheath containing both resistive and capacitive terms, shown as V_{p3}.

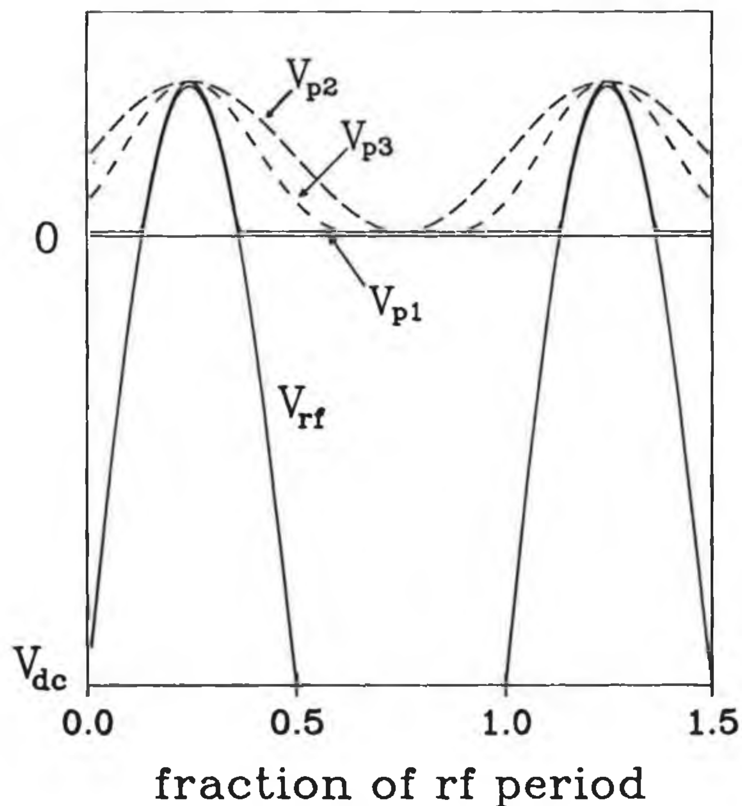

FIG.1.3: Illustration of the expected temporal evolution of the driving potential, $V_{rf}(t)$, and the plasma potential, $V_p(t)$, for rf discharges.

(iii) Production mechanisms in rf plasmas

The exact mechanisms of rf plasma excitation are quite complex, and have proved difficult to study, from both experimental and modeling viewpoints. However, considerable progress has been made, particularly at higher pressures (0.1 to 2Torr), and it has been shown that the rf discharge can operate in several different modes[12],[13]. Two distinct modes, which are of particular importance, are the so-called γ-regime and α-regime.

The electron ionization mean free path[1] is given by

$$\lambda_i = 1/n_o\sigma_i \qquad \ldots\ldots \qquad (1.2)$$

where σ_i is the ionization cross-section, shown in figure 1.4 as a function of electron energy in argon[14]. Also, the total inelastic collision mean free path is given by

$$\lambda_{inel} = 1/n_o\sigma_{inel} \qquad \ldots\ldots \qquad (1.3)$$

and σ_{inel} is also shown in fig. 1.4[15]. Figure 1.5 shows σ_i and σ_{inel} for electrons in nitrogen[16].

At high gas pressures, greater than 500mTorr, the mean free paths of plasma electrons are such that ionization occurs locally and is generally a bulk process, except near the sheaths. For example, for 50eV electrons in argon at 1Torr, with n_o = pressure (Torr) x 3.54×10^{16}cm^{-3} and $\pi a_o^2 = 8.82 \times 10^{-17}$cm^2, λ_i = 1.1mm, and for nitrogen λ_i = 1.5mm. This is known as the α-regime, and bulk electrons (i.e. electrons with energies below the ionization threshold) are heated by the bulk plasma

electric field and contribute to ionization. In this respect, the plasma resembles a dc positive column[17].

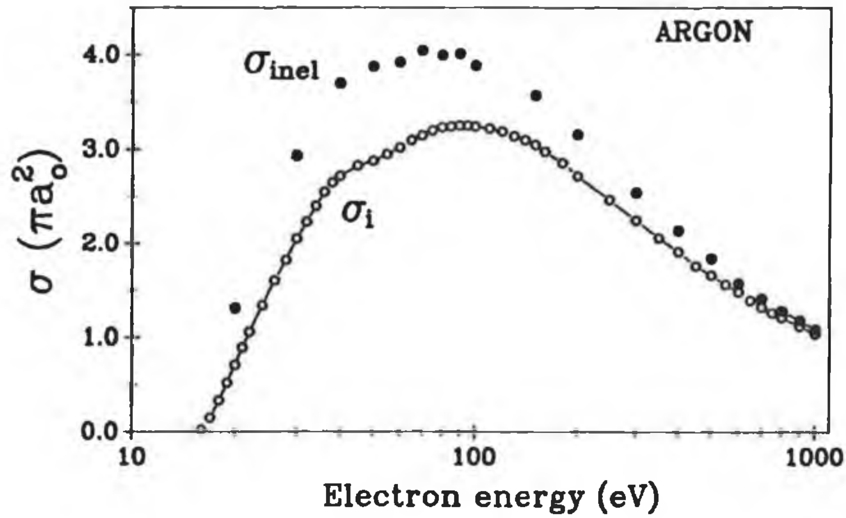

FIG.1.4: Total inelastic (σ_{inel}) and ionization (σ_i) cross-sections for electrons in argon (from refs. 14,15).

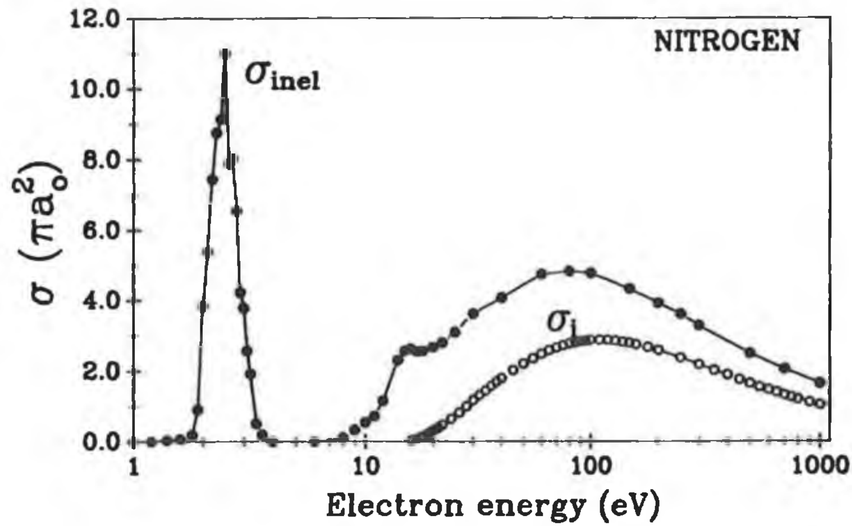

FIG.1.5: Total inelastic (σ_{inel}) and ionization (σ_i) cross-sections for electrons in nitrogen (from ref.16).

Associated with such plasmas is a high (2eV-4eV) bulk electron "temperature" (if the eedf is Maxwellian)[17].

If the rf sustaining voltage is now increased, secondary electrons emitted from the electrodes under ion bombardment are accelerated by the sheath field to very high energies. These high energy electrons undergo collisions in the sheath region, creating more secondary electrons, leading to an avalanche of electron current growth. This avalanche of electrons in the sheath region occurs because the electron mean free path begins to increase with increasing electron energy (see fig.1.4; σ decreases, λ increases) so that the electrons can be accelerated to higher energies, and also because as the electron energy increases, many successive ionizing collisions in the sheath are possible. Thus, an electron beam with energies up to the rf voltage amplitude enters the glow region. Most of the ionization takes place at the plasma-sheath boundary, although a non-negligible part of the total ionization takes place within the plasma since the cathode emitted electrons can penetrate deeply into the plasma and release their energy there. The secondary electrons begin to contribute to ionization in the glow region[18] and the ion density increases, resulting in a further increase in secondary electron emission. This positive feedback results in an abrupt transition from the α-regime to the γ-regime, where ionization is produced by the secondary electrons. The

γ-regime has been likened to a dc negative glow or hollow cathode discharge, since the plasma is non self-sustained. An external beam, originating at the electrodes, is the primary source of ionization in the plasma bulk[12]. Since the plasma is sustained by an external electron beam, the bulk electron temperature is normally low (<1eV).

At lower gas pressures, typically 100mTorr to 500mTorr, the plasma ionization is dominated by a type of α-process. Although secondary electron emission still occurs, the electron ionization mean free paths (approximately 5mm for a 300eV electron in argon at 300mTorr) are such that the majority of secondary electrons traverse the sheath region without making ionizing collisions, and little or no electron amplification occurs. Secondary electrons may, however, cross the sheath and penetrate the plasma bulk. A heating mechanism peculiar to rf plasmas, which is described below, also contributes to a fast electron component in the eedf. Therefore, electrons in the tail of the energy distribution function, which have energies just above the ionization threshold, and have short ionization mean free paths account for ionization in the plasma bulk. The electric field in the plasma is weak, and does not contribute significantly to electron heating.

Decreasing the gas pressure further, below the point where a dc discharge would extinguish for similar

sustaining voltages, the rf plasma persists. The plasma is now maintained by a heating mechanism peculiar to the rf system. The problem has been investigated extensively by Godyak[19],[20],[21], Boeuf[12], and Kushner[17]. It appears that the sheath oscillations (the rf sheaths oscillate in space and energy), which are characteristic of rf discharges, can also constitute an important source of energy for the electrons. Models[12],[22],[23] have predicted that an rf discharge can be self-sustaining even without secondary electron emission. The role of the sheath oscillation in the electron energy gain and deposition mechanisms has been considered in two extreme cases:

(a) Firstly, the "wave-riding" (this term is a misnomer and should not be confused with Landau damping) regime[17],[22] corresponds to a situation where the sheath is collisional for the electrons (i.e. the electron mean free path is small with respect to the sheath length) and applies to the pressure regimes already described. As the rf sheath oscillates, the local plasma potential oscillates. During the portion of the rf cycle when the sheath is in retreat, either spatially or energetically, the plasma potential near and in the sheath increases. Thermal electrons from the plasma diffuse or drift toward the electrodes. During the second half of the rf cycle, the sheath spatially or energetically extends back into

the plasma (sheath expansion). The electrons that followed the sheath in its retreat towards the electrodes suddenly find themselves in a region with a lower plasma potential. These largely thermal electrons are then accelerated into the plasma, riding the wave of the lower plasma potential. The energy gained by an electron which is in the path of the extending sheath is approximately equal to the difference between the minimum potential and plasma potential at the location of the electron's closest approach. The result is a broad high energy tail in the eedf located at the boundary of the sheath and the plasma. Since the sheath is collisional, the electrons "riding" the expanding sheath undergo collisions, imparting energy to the plasma.

(b) Secondly, the "stochastic" heating[21] regime corresponds to a low pressure (less than 100mTorr) regime, where the electron mean free path is of the order of or greater than the gap length. In this regime, the electron has a larger probability to interact with the sheaths than to undergo a collision with a gas molecule. The electron is supposed to exchange momentum with the sheath and can be reflected by it (Fermi acceleration). The regime of interest is where the chaotic dynamics dominate the electron motion, which is the range of pressures in the near-collisionless regime where electrons experience many interactions with the sheaths before suffering collisions

with neutrals. That is, the regime where the electron bounce time is much less than the mean time for elastic collisions. The electron motion occurs in two distinct parts, the unperturbed motion through the bulk plasma, where the electron velocity is constant, and the rapidly varying velocity region in the sheath. It is possible for electrons to be stochastically heated in such a fashion up to the point where their energy equals the escape energy, which in the physical discharge is the ambipolar sheath potential. This is discussed in further detail in section 1.4.

(iv) Loss mechanisms in rf plasmas

The three primary electron loss processes in glow discharges are diffusion, recombination and attachment[1]. In electropositive gases, such as argon or nitrogen, at low pressures, ambipolar diffusion is the primary plasma loss mechanism. The electron loss rate is

$$dn_e/dt = -D_a n_e/\Lambda^2 \quad ..... \quad (1.4)$$

where D_a is the ambipolar diffusion coefficient, and Λ is the characteristic diffusion length, given by

$$1/\Lambda^2 = (\pi/L)^2 + (2.405/a)^2 \quad .. \quad (1.5)$$

for a cylindrical chamber of length L and radius a[1].

The ambipolar diffusion coefficient is given by

$$D_a = (D_e\mu_+ + D_+\mu_e)/(\mu_e + \mu_+) \quad (1.6)$$

where μ_e and μ_+ are the respective electron and ion

mobilities. In the usual case of interest,

$$D_e >> D_+ \quad \text{and} \quad \mu_e >> \mu_+$$

Also, if the eedf is Maxwellian then,

$$D_e = kT_e/m\nu_{eN} \qquad ..... \qquad (1.7)$$

where ν_{eN} is the electron neutral collision frequency, and

$$D_+ = kT_+/M\nu_{iN} \qquad ..... \qquad (1.8)$$

where ν_{iN} is the ion neutral collision frequency.

Therefore,

$$D_a = (kT_e/e).\mu_+ + D_+ \qquad ... \qquad (1.9)$$

or

$$D_a = D_+(1 + T_e/T_+) \qquad ..... \qquad (1.10)$$

The electron-neutral collision frequency is given by

$$\nu_{eN} = n_o\sigma_{tot}v_e \qquad ..... \qquad (1.11)$$

for an electron velocity v_e. σ_{tot} is the total collision cross-section.

At pressures greater than 1Torr, recombination becomes an increasingly significant loss process. The electron loss rate is

$$dn_e/dt = -\alpha n_e n_+ \qquad ..... \qquad (1.12)$$

where α is the recombination coefficient. In a quasi-neutral plasma

$$dn_e/dt = -\alpha n_e^2 \qquad ..... \qquad (1.13)$$

The most important recombination process in glow discharges is dissociative recombination.

Electron attachment is an important loss process in electronegative gases, and is thus significant in many processing systems (O_2, Cl_2, Fl_2), and negative ion sources (H^-, D^-). The electron loss rate is

$$dn_e/dt = -h\nu_{eN}n_e \quad \ldots\ldots \quad \textbf{(1.14)}$$

ν_{eN} is the electron neutral collision frequency and h is the attachment coefficient.

In recombination and attachment dominated plasmas, the electron density spatial distribution tends to be uniform whereas in diffusion dominated plasmas, the electron density distribution is greatest in the centre of the plasma, falling off in a sinusoidal (or Bessel function) mode towards the walls of the chamber. Also, in the plasma afterglow (i.e. the post-discharge, **E**=0) the electron density decays linearly with time in recombination dominated discharges, while it decays exponentially in diffusion and attachment dominated discharges.

1.3 RF Plasma Modeling

The modeling of capacitively coupled rf glow discharges has proceeded along several paths and focused its attention on different aspects of the discharge physics. The principle approaches are summarized below.

(i) The Boltzmann equation (microscopic model)

The ideal way of representing the electron and ion kinetics in a weakly ionized gas is through the Boltzmann equation[(1),(24)]. The Boltzmann equation is an integro-differential equation in a 7-dimensional space (time plus 6-D phase space: position-velocity) whose solution yields the particle velocity distribution function $f(\mathbf{r},\mathbf{v},t)$. The excitation, dissociation, and ionization rates can be deduced from the eedf. In a discharge, the charged particle motion is coupled with the electric field, and the transport equations must be solved together with Poisson's equation for the electric field. Although numerical methods for solving the Boltzmann equation for a given electric field distribution are available[(25)], the coupling between the electron and ion Boltzmann equations and Poisson's equation is a formidable numerical problem. For this reason, and also to reduce the computer time for solution convergence, several methods of modeling simplifications have been adopted.

(ii) Continuum models

Continuum models are based on the fluid (or moment) equations[1], in which the plasma is considered to behave as a conducting fluid, rather than as individual particles. A fundamental condition for validity is that the gas pressure be approximately greater than a few tenths of a Torr (≃300mTorr). The model is thus suited to the medium or high pressure regime. Belenguer and Boeuf[12] have used the scheme to model the transition from the α-regime to the γ-regime in a simulated helium rf glow. As in other fluid models, the electron kinetics are described in terms of a two electron (tail and bulk of the eedf) group. Transport coefficients and electron induced process cross-sections are taken from experimental measurements reported in the literature. The technique, however, does employ certain assumptions, such as a bi-Maxwellian energy distribution with a value (nominally 1eV) for the bulk electron energy, and a local field approximation (valid only at high pressures, where the tail of the eedf is modulated by the rf field).

(iii) Particle-in-cell or Monte Carlo models

More recently, kinetic simulations (which are valid at low gas pressures) have been applied to the rf discharge[17],[22],[26]. Particle-in-cell and Monte Carlo models of rf glows provide kinetic information

self-consistently by integrating the equations of motion of many super-particles representing electrons and ions, with a simultaneous numerical solution of Poisson's equation on a spatially discrete mesh, and with a Monte Carlo treatment of electron-neutral and ion-neutral collisions. The advantage over other simulation methods is that the eedf is the result of the calculation (and need not be Maxwellian). Time-averaged spatially dependent eedf's can be computed, although a functional form for the spatial variation of the rf field is employed.

(iv) Analytical models

Godyak has proposed several analytical modeling approaches to aspects of the rf discharge. In particular, he has derived relationships for sheath heating of electrons in low-pressure rf discharges[21],[27], for the transition from bulk to sheath heating[20] (stochastic heating) and for the transition from α to γ mechanisms in the high pressure regime[18]. Many of these models are supported by experimental measurements and have improved our knowledge of the rf plasma immensely. For instance, the transitions between different plasma heating mechanisms is now perceived as fundamental in the rf glow. Associated with these regime transitions are abrupt changes in kT_e and n_e via positive feedback.

Stochastic sheath heating has also been analytically modeled by Goedde et al.[28], in which it is shown that the electron motion is only stochastic (i.e. described by non-linear dynamics with chaotic regimes, so that it is possible for the electron to gain very large energies from the oscillating sheath) at very low pressures (<10mTorr) and at high sheath oscillation frequencies (>50MHz).

The rf sheath has also been described analytically[29],[30],[31], in which predictions of sheath conductance and capacitance are presented. These values are relevant in determining, for example, the harmonic components of the plasma potential and the degree of net sheath heating possible.

(v) Equivalent circuit models

Measurements of the electrical characteristics of capacitively coupled, parallel plate, rf discharges have led to the development of equivalent circuit models[32],[33],[34]. Such a circuit model is shown in figure 1.6[10]. The bulk plasma is represented simply by a resistor, representing the power deposition due to collisions. Since the field in the bulk discharge is typically of the order of 2V/cm (see chapter four) and the discharge current is typically 50mA, the bulk plasma resistance is low. The sheaths are primarily capacitive due to the positive ion space charge and the fact that

only the electrons respond to the rf field. These capacitances are estimated from typical sheath thicknesses, using equations 2.23 and 2.24. A parallel diode allows for the asymmetry of the ion and electron currents, and a large parallel resistor represents collisional power deposition in the sheaths. Typical plasma sheath resistances may be estimated from Langmuir probe IV characteristics (see chapter two).

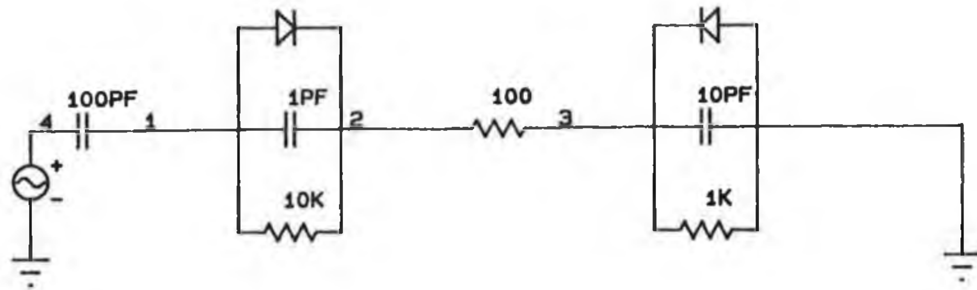

FIG.1.6: Equivalent circuit model of rf plasma

The effectiveness of such a model can easily be demonstrated using, for example, a pc software package such as ORCAD. Figure 1.7 is the result of an ORCAD circuit simulation of the potentials appearing at nodes 1 (the driving voltage at the driven electrode) and 3 (the plasma potential) when the circuit is driven by a 13.56MHz, 500v rf signal. The dc offset, which reaches an equilibrium value after a few cycles, appears as a result

of the unequal electrode areas (represented by differing values of sheath capacitance) and the coupling capacitor. The plasma potential is essentially positive throughout the rf cycle (simulated via the diode, representing the different electron and ion mobilities), and with contributions from higher harmonics of the driving frequency (the non-linearity of the sheath is introduced by the finite sheath resistances).

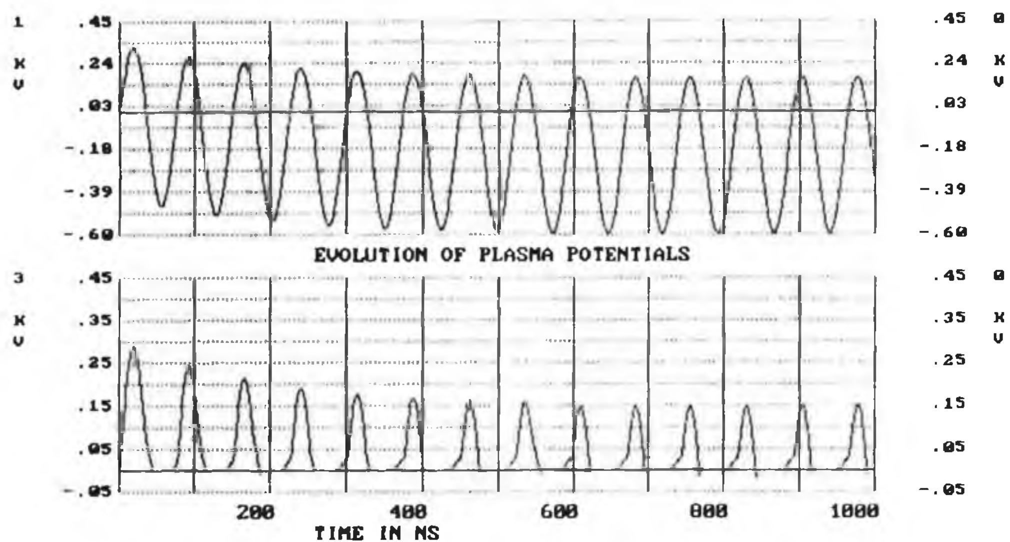

FIG.1.7: Software simulation of the evolution of the dc self-bias and the rf plasma potential using the circuit model of fig.1.6

Electrical models of this type, used and developed in conjunction with experimental measurements, have been used to predict transitions from different power-deposition pressure regimes and the influence of different attaching gases on the discharge impedance[35].

1.4 Outline of proposed research

Although our understanding of rf plasma physics has greatly increased in the last few years, a number of key issues need to be addressed. To date, rf plasma modeling has been developed to a sophisticated level and indeed surpasses the experimental development. Experimental research has been hampered by the lack of suitable diagnostic tools, which are important both in terms of fundamental research and in terms of industrial applications. This thesis is an attempt to, firstly, develop a suitable rf plasma diagnostic, and secondly, to use such a device to answer some of the pertinent research questions.

The current level of understanding of rf plasmas has been discussed in section 1.2. Several points of interest have been raised which are worthy of further research. Not least among these is a better understanding of how rf sheath oscillation heating operates. The scheme is widely quoted as been the operative plasma heating mechanism at low pressures. It is argued here[36], however, that the described scenarios of sheath heating are alone insufficient to account for gas ionization at low pressures for the following reasons. The rf period (for the normal driving frequency of 13.56MHz) is about 74ns. Hence the sheath expands and contracts every 37ns. Assuming that the spatial sheath oscillation is about 1cm, then the sheath has an effective velocity of 2.7×10^7cm/s.

Fast, ionizing electrons (with energies greater than 15eV), whose velocity is much greater than the sheath velocity cannot be heated by the sheath, since they do not experience its motion. Slow electrons, however do experience some energy gain, the maximum being

$$E = 1/2m_e v_s^2 \quad ..... \quad (1.16)$$

where v_s is the sheath velocity, and is approximately 0.2eV. However, the sheath expansion is not linear in time, so that it may travel at much higher velocities. The electron energy gain may therefore be significantly higher. However, as the electron velocity increases, the sheath oscillations become ineffective in electron heating, since the electron velocity is much greater than the sheath velocity, it is difficult to see how the electrons can be heated to ionizing energies, unless very many collisions with the rf sheaths are possible. Sheath oscillations tend to cool electrons during their contraction half-cycle, so that there is no net energy gain if the rf sheath is capacitive. It is the conductance of the rf sheath which makes the sheath impedance non-linear, resulting in net sheath heating. (Note that the energy gained by the electrons is proportional to the square of the sheath velocity and hence to the square of the driving frequency. Thus, rf sheath heating should become increasingly important as the driving frequency is increased).

As mentioned in section 1.2, electrons may be

stochastically heated up to energies equal to the escape energy if many successive collisions with the sheath are possible. If the escape energy, which in the physical system is the plasma to anode sheath potential, is large then many successive collisions with the sheaths are possible, and the plasma electrons can attain quite large energies. Thus, electrons cannot be stochastically heated via collisions with the oscillating sheath unless they are "trapped" in the plasma by some mechanism. Although such a mechanism, described below and in detail in chapter six, appears inherently in the advanced plasma models, so that rf sheath heating appears the dominant mechanism, it has not been stressed, to the knowledge of this author, that the electron trapping mechanism is also very essential.

It is proposed here(36),(37) that fast electrons are electrostatically confined or trapped by the rf sheaths, and can only escape to the chamber walls or electrodes during limited portions of the rf cycle. This is supported by the eedf measurements at low pressures which display a group of isotropic ionizing electrons, even though their mean free paths greatly exceed the chamber dimensions (see chapters five and six). The situation is similar to low pressure magnetically confined multipole ion sources, where fast electron lifetimes are at least an order of magnitude greater than normally the case for similar diffusion dominated plasmas. Fast electron confinement (via wall surface magnetic fields) means that

the electrons undergo much more ionizing collisions in their increased lifetime. Similarly, in the case of electrostatic sheath confinement, the fast electrons "see" an increased chamber length. Thus, it is suggested here that, firstly, electrostatic confinement of fast electrons is the primary source of plasma heating at low pressures and that, secondly, net stochastic heating by the rf sheaths can only occur if electron confinement holds true. Since it is suggested that fast electrons are trapped by large ambipolar sheath fields, the plasma potential measurements will reveal the degree of electron trapping possible.

The value of the bulk electron temperature in rf plasmas has been the subject of much debate in recent years(19),(22),(38), particularly since it has been realised that associated with transitions between different modes of rf plasma operation, are transitions in the value of the electron temperature. In particular, the variation of kT_e with discharge pressure and power and its spatial variation are questions which must be addressed, so that a more complete picture of the rf plasma may be developed.

Other relevant plasma parameters such as V_p and n_e will also be determined over a range of operating conditions. Spatial measurements of V_p will reveal the plasma bulk electric fields, while spatial measurements of

n_e will determine the operative plasma loss processes. The electron energy distribution function measurements will also be presented for both argon and nitrogen discharges in chapter five. EEDF measurements are important from both a plasma chemistry point of view, since any process rate coefficient is determined by the eedf, and from a fundamental physics point of view, since electrons are responsible for almost all gas discharge processes. Argon and nitrogen are particularly interesting since the cross-sections of the many important plasma processes can be very different.

CHAPTER TWO

THE LANGMUIR PROBE

2.1 Introduction

Langmuir probe measurements are a powerful and experimentally simple means of determining key internal discharge parameters; in particular the charged particle concentrations and the eedf (or electron temperature if the distribution is Maxwellian). Several excellent reviews of the technique are available[39],[40]. The probe technique has traditionally been applied to dc discharges and afterglows; its use in rf discharges being hampered by the problems of rf interference. This chapter is devoted to a discussion of the technique and the viability of Langmuir probe measurements in rf discharges.

2.2 Langmuir probe theory

The Langmuir probe method consists of measuring the current drawn from the plasma to the probe, recorded as a function of the probe voltage relative to a reference electrode, usually the grounded chamber wall. The potential difference between the probe and the plasma causes a sheath to form around the probe, and most of the voltage drop occurs across this sheath. The probe is fabricated from a refractory metal, such as tungsten, and the probe sleeve usually from ceramic. Most glow discharge workers employ cylindrical probes, as the sheath expansion theory is well developed[41], although plane and spherical probes are sometimes used. Also the cylindrical probe can be made small, so that plasma depletion of low-energy electrons is reduced.

The theoretical basis of the probe technique divides roughly into two categories distinguished by the probe/plasma conditions to which they apply. The first provides a scheme for plasma parameter evaluation in the case of low pressure/small probe systems. The second deals with probe applications in high pressure plasmas and in the presence of magnetic fields. We concern ourselves only with the former. The validity of low pressure theory for a given application is estimated from the criteria

$$r_p \ll \lambda \; ; \quad \lambda_D \ll \lambda \qquad \ldots \qquad (2.1)$$

where r_p is the probe radius, λ is the electron

collisional mean free path, and λ_D is the Debye length given by

$$\lambda_D = (kT_e \varepsilon_o / n_e e^2)^{1/2} \quad .... \quad \textbf{(2.2)}$$

Other implicit assumptions in low pressure theory are:

(a) The electrons and ions have Maxwellian energy distributions, with $kT_e >> kT_+$

(b) The probe sheath thickness is small compared to the length of the probe.

A typical probe set-up is shown in figure 2.1, and the measured probe IV characteristic is shown in figure 2.2. There are three regimes of probe operation.

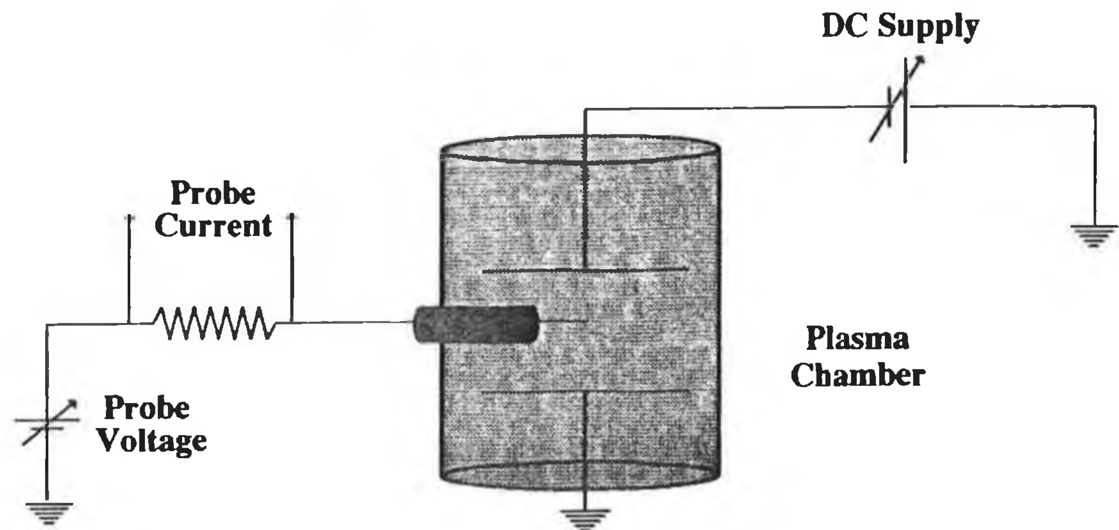

FIG.2.1: Experimental set-up of Langmuir probe

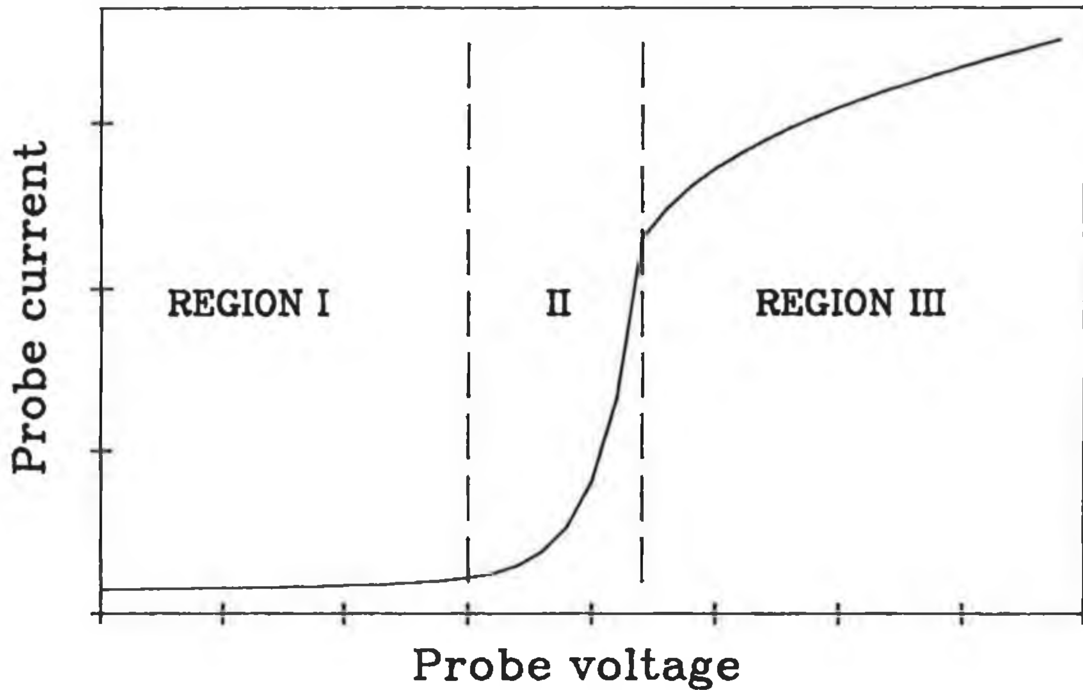

FIG.2.2: Typical probe IV characteristic

When the probe is biased strongly negative with respect to the plasma, the plasma electrons are repelled, while positive ions are collected, resulting in the ion saturation current, shown as region I in figure 2.2. The ion saturation current is given by

$$I_+ = (n_+ e v_+ A)/4 \quad ..... \quad (2.3)$$

where V_+ is the average (or acoustic) ion velocity and A is the probe area. More accurately, A is the probe sheath area, a function of the bias voltage, and usually calculated from the Laframboise ion sheath expansion curves[41].

The probe current consists of both an electron and an ion current component, and separating the two is one of the perennial problems associated with Langmuir probes. A good theory of ion current expansion permits an estimation of n_+ at highly negative voltages, so that the fast electron current to the probe can be calculated. When the sheath is thin with respect to the probe radius ($r_p/\lambda_D>>1$), the sheath can be considered planar, and space charge limited ion motion prevails. In the opposite limit of a thick sheath, only some of the particles entering the sheath are captured by the probe, because of the possibility of orbital motions. This is the Orbit Motion Limit regime. This theory has been extended by Laframboise, and the results of his numerical calculations have been widely used[(42),(43)].

As the probe bias is made less negative, an increasing fraction of electrons are collected by the probe. This is the electron retardation or electron collection regime, shown as region II in fig. 2.2. At the floating potential, V_f, the probe collects equal fluxes of electrons and positive ions, so that the net current is zero. The electron current to a probe in a retarding field is

$$I_e = I_o.\exp[e(V-V_p)/kT_e] \qquad (2.4)$$

$$\Rightarrow \quad \ln I_e - \ln I_o = eV/kT_e - eV_p/kT_e \quad \ldots \qquad (2.5)$$

$$\Rightarrow \quad d/dV\,(\ln I_e) = e/kT_e \quad \ldots \qquad (2.6)$$

Thus, a plot of ln I_e against probe potential yields a slope of e/kT_e, from which the electron temperature can be determined. Alternatively[42], the maximum in dI_e/dV occurs at the plasma potential, and

$$I_e/(dI_e/dV)|_{V=V_p} = kT_e/e \quad .. \qquad (2.7)$$

i.e. the ratio of probe electron current to the first derivative of the probe electron current at the plasma potential is equal to the electron temperature. Therefore, to determine the electron temperature, it is necessary to determine initially the electron current, so that the ion current contribution must be subtracted from the total probe current in region II. The ion current contribution is normally estimated from a linear extrapolation of the ion saturation current, although this procedure is suspect since the laws governing the ion current extrapolation in region II are not accurately known. Note also that the plasma potential is given by the voltage corresponding to the maximum in the first derivative of the probe current. The precise location of the plasma potential on the probe IV curve is also, however, one of the classic problems associated with the technique. It is found that the maximum in the first derivative can occur below the point where the saturation current is reached[42], and V_p is corrected via the method of intersecting slopes on a plot of ln I_e vs probe bias. This technique compensates to some extent for low energy

electron reflection by the probe.

The plasma potential, V_p, marks the transition between electron collection in two different regimes. When the bias voltage is greater than the plasma potential, electron saturation current is collected, and

$$I_o = (n_e e v_e A)/4 \quad ..... \quad (2.8)$$

where the average electron velocity, v_e, is given by

$$v_e = (8kT_e/\pi m_e)^{1/2} \quad ..... \quad (2.9)$$

for a Maxwellian electron energy distribution. The electron saturation is shown as region III in figure 2.2. The electron saturation current allows the electron density to be determined.

2.3 Evaluation of the eedf

One of the most basic characteristics of any gas discharge is the electron energy distribution function. For example, it has important consequences in calculating the rate coefficients of electron induced processes, such as ionization and excitation[43]. The eedf is integrated over the relevant cross-section to produce a value for the rate coefficient of some electronic process

$$\langle \sigma v \rangle = \int_{threshold}^{\infty} f(\varepsilon)\sigma(\varepsilon)v(\varepsilon).d\varepsilon \qquad (2.10)$$

where ε is the electron energy, $f(\varepsilon)$ is the experimentally measured, normalized eedf, $\sigma(\varepsilon)$ is the reaction cross-section, and $v(\varepsilon)$ is the electron velocity[44].

Provided that the eedf is isotropic, the second derivative of the probe characteristic is proportional to the eedf[45], and

$$n(\varepsilon) = n_e f(\varepsilon) = 2/eA.d^2I_e/dV^2.(2m_e\varepsilon/e)^{1/2} \qquad (2.11)$$

Thus the eedf can be determined simply by the second derivative of the probe current with respect to the probe bias. This can be obtained via numerical or analogue differentiation, the former being favoured since it does not mask or suppress eedf structure. The contribution of the extrapolated ion current is not subtracted in this work, since it is normally found to be negligible at low eedf energies. Averaging (typically 10^5 points per

characteristic) and wide energy half-widths (varying from $\Delta\varepsilon = 0.5eV$ at low energies to $\Delta\varepsilon = 4.0eV$ at high energies), has been employed in this and previous[46] work, and is favoured over smoothing routines.

The second derivative can also be determined by superimposing an ac signal on the dc probe bias. Several variations are possible, but in general the second derivative is obtained from a harmonic of the applied ac signal[47],[48].

2.4 Sources of error in probe measurements

Of all the diagnostic procedures of plasma physics, the probe method is arguably the most susceptible to error, both at the levels of measurement and interpretation. The debatable subjects of ion current extrapolation and plasma potential evaluation have already been mentioned. Other sources of error are:

(i) The limit of low-pressure, collisionless sheath theory, i.e. the regime of validity of equation 2.1, must be respected. Also, the evaluation of the eedf from the second derivative, i.e. the Druyvesteyn method, is only applicable at low pressures[40],[45]. Fortunately, since rf plasmas are usually operated at low pressures (<300mTorr), the low pressure theory is generally valid. Care must be used, however, in choosing the probe dimensions.

(ii) When the probe voltage is within $kT_e/2$ of the plasma potential, the low energy electrons may be deflected or depleted by the probe, resulting in significant error in the measured eedf[49]. This is discussed further in chapter five.

(iii) In low density or tenuous plasmas, electron depletion may be a serious problem, particularly in post-discharge or afterglow measurements. The problem has been considered by Waymouth[50], resulting in some workers[51] employing a pulsed probe technique, in which

the probe is biased only during measurements, so that electron depletion is limited. It has been found[52], however, that serious depletion only occurs at long times into the afterglow, where plasma density is quite low ($\simeq 10^8 cm^{-3}$).

(iv) Observations in rf plasmas have indicated that the probe bias may cause shifts in the potential of a floating probe positioned in a different region of the plasma, particularly for bias voltages greater than V_p. This "pushing" or perturbing of the local plasma potential has also been observed, but to a lesser degree, in dc cold cathode discharges. In dc discharges, the plasma-wall sheaths are resistive, so that the plasma couples to the wall resistively and the plasma potential is low. In rf discharges, however, the sheaths are capacitive, with very little resistive coupling, and the plasma potential is high. As a result, the rf plasma is more susceptible to probe perturbation, since small fractional changes in the plasma potential result in greater absolute voltage shifts. It is possible, however to make probe measurements with respect to another probe (similar to a double probe with the exception that the reference probe is connected via a voltage follower grounded to the chamber wall, so that the return current is not limited by the positive ion saturation current; see section 2.6), so that small shifts in the plasma potential are compensated.

(v) The eedf measured by the Langmuir probe may also

differ from that in the undisturbed plasma due to perturbations induced by the insulated sleeve of the probe holder. There are two ways in which this can happen. Firstly, electron recombination losses at the probe surface must be replaced by collisional ionization, so that the tail of the eedf "becomes hotter"[39] close to the probe. It is thus desirable that the radius of the probe sleeve exposed to the plasma satisfy eqn. 2.1. Secondly, the positive space charge sheath forming around the probe holder may alter the electron density measurement[47]. For this reason, cylindrical probes should have long collectors and thin sleeves.

(vi) The Druyvesteyn relationship (equation 2.11) for evaluation of the eedf is only valid when the eedf is isotropic. Measurements by this author with flat, planar probes designed to detect anisotropies have not revealed any beam effects. These measurements included both monitoring the floating potential of the flat probe in perpendicular orientations and measurement of the eedf at values up to 200eV[53].

(vii) In high pressure or high current/high power discharges, sputter deposition of electrode material onto the probe and probe holder may be significant. It results in either plasma perturbation due to an increased probe collection area, or erroneously deduced plasma parameters. The problem can be avoided by continuously cleaning the probe. This is achieved via ionic bombardment of the

probe surface, by biasing at negative voltages, prior to the measurement scan. Thorough cleaning can be achieved by biasing at highly positive voltages, well into electron saturation, so that the probe surface acts as an electrode and can be made to glow. If a discharge is ignited in the presence of oxygen and nitrogen mixtures, it is possible to coat walls, electrodes and probes with an insulating layer. It is thus important that the chamber be evacuated to high vacuum before running the discharge.

2.5 Langmuir probes in rf plasmas

In a dc discharge the plasma potential is invariant with time, and the probe current is given by eqn. 2.4. In an rf discharge, however, the plasma potential fluctuates with time, as shown in figure 1.1. Thus if the probe is maintained at a fixed dc bias, the fluctuating voltage across the plasma-probe sheath results in the collection of a time varying current. Since the variation of the plasma potential with time is generally unknown, the instantaneous probe current cannot be used to infer the plasma parameters. The rf voltage that occurs across the the plasma-probe sheath shifts the apparent floating potential to more negative values and distorts the probe IV characteristic. The electron temperature inferred from the convoluted characteristic generally exceeds the true value, while the electron density is underestimated[54].

The probe current in an rf plasma is a function of time and is given by

$$I_e(t) = I_o.\exp[e(V-V_p(t))/kT_e] \qquad (2.12)$$

In the following analysis the plasma potential will be assumed to be sinusoidal, although this is not necessarily the case. The result, however, does apply to probe analysis in all rf plasmas, regardless of the harmonic content of the plasma potential, (except where $\omega_e < \omega$, in which case the electrons cannot follow the rf field variations and the plasma potential is unmodulated).

The probe current is thus

$$I_e(t) = I_o.\exp[e(V-V_{pdc}+V_{prf}\mathrm{Sin}\omega t)] \quad (2.13)$$

where V_{pdc} is the dc component of the rf plasma potential and $V_{prf}\mathrm{Sin}\omega t$ is the corresponding rf component, i.e.

$$V_p(t) = V_{pdc} - V_{prf}\mathrm{Sin}\omega t \quad .. \quad (2.14)$$

There is also a displacement current component, which may indeed be larger than the conduction current, but averages to zero. The time averaged current is thus

$$\bar{I}_e = I_o/T\int_0^T \exp[e(V-V_{pdc})].\exp[e(V_{prf}\mathrm{Sin}\omega t)]dt \quad (2.15)$$

Therefore,

$$\bar{I}_e = I_o/T.\exp[e(V-V_{pdc})].\int_0^T \exp[e(V_{prf}\mathrm{Sin}\omega t)]dt \quad (2.16)$$

It is thus apparent that the "true" probe characteristic is simply multiplied by a factor r, given by the integral term of eqn. 2.16. The floating potential in a dc plasma is given by setting $I_e = 0$. Thus

$$V_f = V_p - kT_e\ln I_o \quad ..... \quad (2.17)$$

In the rf plasma analysis, the floating potential becomes

$$V_f = V_p - kT_e\ln[rI_o] \quad .... \quad (2.18)$$

Since r is greater than zero, the effect of the rf convolution is to shift the apparent floating potential to lower values.

It is apparent from eqn. 2.16 that the electron temperature is unaffected by the factor r, and can be obtained in the usual way. However, the rf distorting voltage is normally quite high, of the order of tens of volts (or greater), so that the averaging of electron current extends into both the electron saturation current and ion saturation current regions. The averaged electron current in this case is a much more complicated function, the net result being an overestimation of kT_e and an underestimation of n_e. This is illustrated in figure 2.3.

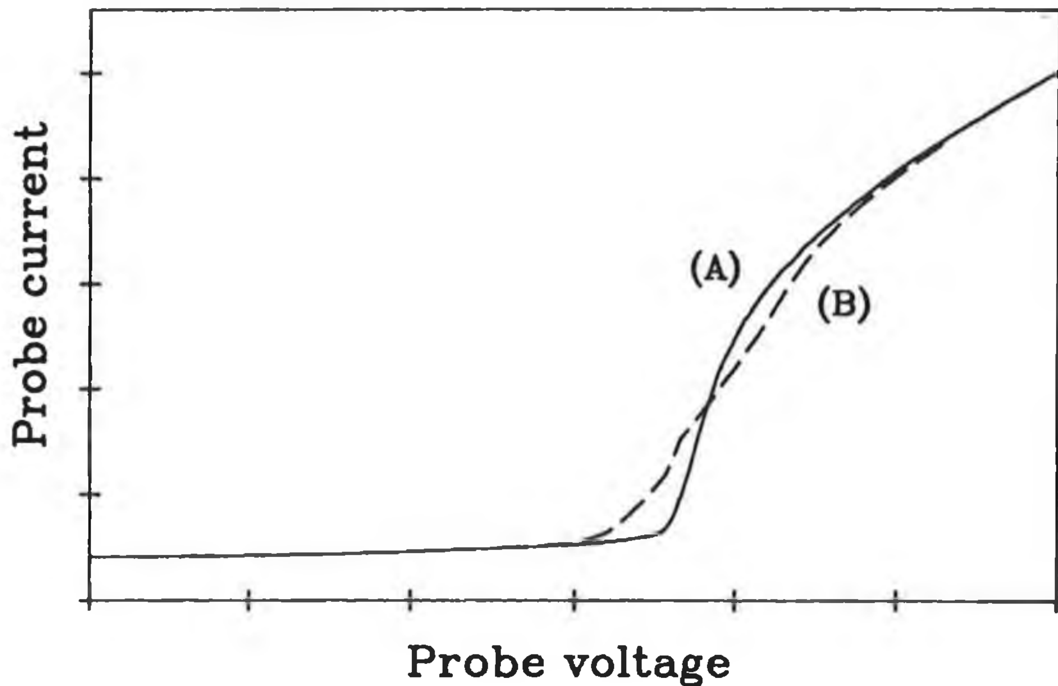

FIG.2.3: Software simulation of rf distortion of probe IV characteristic. Trace A is a characteristic measured in a dc plasma, trace B is the same characteristic with a simulated rf convolution.

Trace A is an IV characteristic measured in a dc discharge. Trace B is the same characteristic with 2volts peak-to-peak rf convolution, generated via a computer simulation. The distortion is essentially a consequence of the rectification of the rf voltage by the non-linear impedance of the probe sheath[(55),(19)]. Not only is the IV characteristic flattened, but also its derivatives, and the second derivative, i.e. the eedf, is extremely sensitive to the presence of rf fluctuating voltages[(56),(57)].

Note that in the above analysis, only the plasma potential is assumed to vary with time. Thus the effect of rf convolution would be much more complicated if the electron density or temperature were modulated at the driving frequency. It is generally accepted that n_e is constant throughout the rf cycle, satisfied if

$$f >> z \qquad ..... \qquad (2.19)$$

where f is the field frequency and z is the ionization frequency[(58)]. The ionization frequency is

$$z = n_o \sigma_i v_e \qquad ..... \qquad (2.20)$$

where σ_i is the ionization cross-section[(14)]. At low pressures, and in 13.56MHz discharges, the inequality of eqn. 2.19 is generally satisfied. For example, in a 10mTorr argon plasma, $z = 5.3 \times 10^6 s^{-1}$ for 20eV electrons. Nitrogen is similar, since the ionization cross-sections are comparable.

The electron temperature is unmodulated if

$$f >> \kappa\nu_{eN} \quad ..... \quad (2.21)$$

where ν_{eN} is the electron neutral collision frequency and κ is the fraction of energy transferred in a collision[58]. At low gas pressures, this inequality is also satisfied, but some models have shown the tail of the eedf to modulated at high pressures[22]. For example, in a 100mTorr argon plasma, $\kappa\nu = 2.7x10^{-5} \times 1.33x10^{9} = 3.59x10^{4}s^{-1}$ for 10eV electrons (close to the peak value of ν/P), using eqn. 1.11 and the total collisional cross-section given in ref.15. In a 100mTorr nitrogen plasma, $\kappa\nu = 3.84x10^{-5} \times 1.34x10^{9} = 5.1x10^{4}$ for 2.5eV electrons (close to the peak value of ν/P), using the total collisional cross-section given in ref.16.

Capitelli et al.[59] suggest that if the reduced frequency, $\bar{\omega}$, given by

$$\bar{\omega} = \omega/p \quad ..... \quad (2.22)$$

where p is the gas pressure in Torr, is less than the energy dissipation frequency, $\bar{\nu}_E$, then the eedf is modulated at the rf driving frequency. Thus, as the gas pressure is increased, it becomes increasingly possible that the eedf is not constant over the rf cycle.

The above essay highlights the problems associated with Langmuir probe analysis in rf plasmas. In effect, the IV characteristic is convoluted by the time varying component of the plasma potential. Deconvolution is impossible, since the variation of $V_p(t)$ is not known. In addition to this interference, a further serious problem exists which must also be overcome if rf plasma parameters are to be correctly determined from the probe technique.

If a conventional Langmuir probe, i.e. a piece of wire, is biased to collect electrons in an rf plasma, then the current collected is a function of time, oscillating at the rf driving frequency. A typical 100pF co-axial cable has a capacitive impedance of about 100Ω at 13.56MHz!. Thus, serious loading of the plasma will occur unless the impedance between the probe and ground is greatly increased. The problem is non-trivial, especially in chamber with metallic walls, where parasitic capacitances are virtually impossible to remove.

2.6 Techniques to obtain probe characteristics in rf plasmas

Several techniques have been adopted in an attempt to negate the problem of rf convolution of the probe IV characteristic. Below is a summary of some of these methods. Section 2.7 is a description of the technique adopted by this author.

(i) Accurate measurements of rf plasma parameters using a conventional Langmuir probe are possible using time resolved measurements of the IV characteristic. The characteristic is obtained by simultaneously sampling the current and voltage, synchronously with the rf driving voltage, and in a time which is short compared to its period[60]. The technique, however, is only valid up to frequencies of about 1MHz, for two reasons. Firstly, probe theory requires that a quasi-stationary sheath forms around the probe, and it becomes increasingly difficult to satisfy this in the increasingly short sample times as the driving frequency increases[61]. A quasi-stationary sheath can only occur in rf plasmas with $\omega > \omega_i$ on a time-averaged scale since the ions cannot respond to the rf fields. Secondly, large capacitive loading of the probe signal is incurred and data acquisition more difficult as the sample time decreases. The technique has been successfully employed to measure eedf's up to frequencies of 100KHz[62] and plasma parameters up to frequencies of 1MHz.

One advantage of this technique is that it permits temporal resolution of probe measurements. Thus, it is possible to measure the evolution of the eedf over the rf cycle. Furthermore, it may be possible to time resolve measurements of the tail of the eedf in 13.56MHz discharges, since these electrons, having greater velocities, are more likely to respond to rapid probe biasing. Such measurements would be interesting in the light of recent debate of "ionization waves" traversing the spatial and temporal regimes of rf plasmas(63),(64),(65), as mentioned in chapter one.

(ii) Capacitive probes that have a high impedance to ground have been used to monitor the time-varying plasma potential in the rf discharge. A numerical simulation of the convoluting effect of this rf potential on the probe characteristic is then used to estimate the true IV characteristic, and the correct plasma parameters deduced(66). The technique is suspect in two regards. Firstly, numerical simulation of the convolution effect of the measured rf potential requires that a Maxwellian distribution be assumed. This is usually not the case. Secondly, the simulation must include the fact that the rf potential will normally drive the probe from electron collection to electron saturation during a cycle. Such a simulation proves to be quite complex.

(iii) Another technique involves superimposing on the probe signal, an rf bias of the same frequency, amplitude and phase as the rf component of the plasma potential[67],[68],[69]. The rf voltage between probe and plasma is thus removed and the characteristic obtained is equivalent to that of a dc discharge. The driving signal for the probe is derived from the driven electrode, and the phase and amplitude of the signal can be adjusted independently. The applied bias is adjusted in phase and amplitude until the floating potential is maximized. However, since there is likely to be differences in the harmonic content of the rf plasma potential and the driving voltage, mismatch is likely to occur[70], causing distortion of the characteristic. Another drawback is the complex experimental arrangement, since the phase and amplitude of the applied signal need to be adjusted prior to each measurement[71].

(iv) Floating double probes can be used to combat the rf distortion of the characteristic. The probes follow the rf plasma potential, so that a dc characteristic can be obtained provided that the probes are not loaded by capacitive coupling to ground. At low frequencies, the problem is not so grave, whereas at 13.56MHz parasitic capacitances result in considerable loading of the probe signal. The double probe is also limited by the fact that electron current collected by one of the probes must be

balanced by positive ion current collected by the other. As a result, only those electrons in the tail of the eedf are collected, and the double probe cannot measure the bulk electron temperature[40].

The return current of the double probe can be increased by increasing the area of one of the probes (the reference probe) relative to the other (the collecting probe), which is in fact a single probe. Thus double probes are often referred to as symmetric and single probes as asymmetric. This scenario is unacceptable, the reference probe in asymmetric arrangement usually being one of the discharge electrodes.

(v) Attempts have been made to use the floating property of the double probe, while also attempting to solve the problem of the limited return current[72]. One of the techniques developed uses a voltage follower on the reference probe line, so that both probes are still the same area but the follower sinks limitless current, via the chamber wall. With high frequency voltage followers readily available, the technique could easily be successfully operated up to frequencies of about 100kHz. Thereafter, capacitive loading becomes significant. Such loading can be removed by installing high impedance inductors on the probe lines near the collecting surfaces.

A similar idea uses a hot filament as a current return *in lieu* of the voltage follower. Again the system is essentially a double probe with the reference probe

replaced by a hot filament. When the filament is cold, a conventional double probe characteristic is obtained. If the emission current of the filament is increased to greater than the electron saturation current, a single probe characteristic can be obtained.

Both of these techniques seem to operate successfully at low frequencies. At high frequencies, the main concern is capacitive loading. Attempting to float the entire measuring arrangement at rf voltages is virtually impossible. Placing inductive coils on the probe lines will prevent capacitive loading if the impedance of the coils is sufficiently high. However, the technique described in the following section is simpler and has been successful in measuring rf plasma parameters.

2.7 The tuned probe

The rf voltage across the plasma-probe sheath can be minimized by ensuring that the impedance of the sheath is small compared with the impedance between the probe and ground[(73),(74),(75),(76)]. Thus, most of the rf voltage appears across the probe to ground impedance and not the plasma-probe sheath impedance. In order to avoid rf convolution of the probe characteristic, the rf voltage across the sheath should be less than kT_e. Typically, kT_e is of the order of 1eV, whereas the rf fluctuation in V_p may be as high as 100V, peak-to-peak.

The equivalent circuit of the tuned Langmuir probe is shown in figure 2.4. On the circuit there are three voltage nodes. Node A corresponds to a reference point outside the plasma, usually the grounded chamber wall. Node B corresponds to the probe tip, i.e. the probe collecting surface, while node C corresponds to a point in the undisturbed plasma just outside the plasma-probe sheath. The impedance of the plasma-probe sheath is denoted Z_p. It consists of a resistive term R_p and a capacitive term C_p in parallel. As discussed in chapter one, when $\omega > \omega_i$, then the rf sheath is essentially capacitive. The value of the sheath capacitance may be estimated as follows. The plasma-probe sheath thickness is given by the Langmuir equation

$$r_s \simeq (1+V/kT_e)^{1/2}.\lambda_D \quad \ldots \quad (2.23)$$

where V is the probe voltage with respect to the plasma potential. For kT_e=1eV and $n_e=1\times10^{10}cm^{-3}$, $\lambda_D\simeq0.1mm$. Taking $r_s\simeq2\lambda_D$, then r_s=0.2mm.

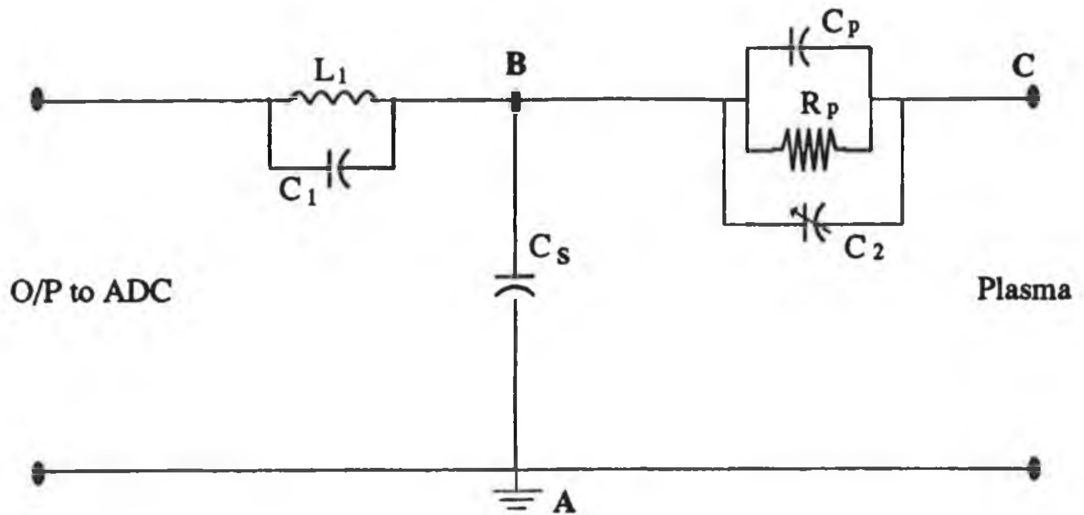

FIG.2.4: Equivalent circuit of tuned Langmuir probe

The capacitance of the co-axial sheath is

$$C_p = 2\pi\varepsilon_o/\ln[(r_s+r_p)/r_p] \quad .. \quad (2.24)$$

where r_p is the probe radius. For a probe radius of 0.25mm, the probe sheath capacitance is 9.5×10^{-11}F/m, so that for a probe length of 10mm, C_p=0.95pF. At 13.56MHz, this represents an impedance $Z_p=1.2\times10^4\Omega$. This analysis is valid for low-pressure, collisionless sheaths.

The impedance between the probe collecting surface and the reference point is denoted Z_s. It is determined solely by a parasitic capacitance C_s. This has a typical value of 5pF, so that $Z_s=2.3\times10^3\Omega$. Thus, $Z_p \gg Z_s$, so that almost the entire rf voltage appears across Z_p, causing rf induced distortion of the probe characteristic.

The value of Z_p can be reduced by adding a shunt impedance across the plasma-probe junction. An ac shunt impedance can be provided by a large conducting surface in contact with the plasma and ac coupled to the collecting probe. This is denoted C_2. The value of C_2 is only dependent on the plasma parameters and is independent of the probe voltage, whereas C_p, being dependent on the plasma-probe sheath thickness, is influenced by the probe bias. Introducing C_2 in parallel with C_p not only reduces Z_p, but also makes the effective probe tip capacitance independent of the probe bias voltage. The conducting sleeve which constitutes C_2 comprises of a stainless steel cylinder of radius 1.5mm and length 25mm, capacitively coupled to the probe tip. Using eqn. 2.24, with the exception that r_s is replaced by λ_D, $C_2=21.5$pF. Thus, the shunt impedance has a value of 546Ω at 13.56MHz. The effective value of Z_p is then $5.2\times10^2\Omega$.

Introducing C_2 results in $Z_s \simeq 4.Z_p$. Since Z_s and Z_p are in series, approximately 1/5 of the rf voltage now appears across Z_p. At 50mTorr and 50watts, the rf

component of the plasma potential has been measured at approximately 100volts peak-to-peak. In this case, 20volts of rf will appear across the plasma-probe junction. In order to minimize rf distortion of the probe IV characteristic, the rf voltage dropped across Z_p should be less than kT_e.

Almost the entire rf voltage will appear across Z_s if $Z_s >> Z_p$. This is achieved by introducing the tuned network. An inductor L_1 with an intrinsic self-capacitance C_1, is introduced as shown in figure 2.4. Inductors are available with self-resonant peaks close to 13.56MHz. It is possible to increase Z_s to values of about $1x10^5\Omega$, at the first harmonic. Therefore, $Z_s \approx 200.Z_p$, and non-convoluted characteristics can be obtained. The results presented in chapters four and five have been taken with a tuned network comprised of a pair of inductors (RS 228-179) both resonant close to 13.56MHz. Figure 2.5 is a schematic diagram of the tuned probe construction[77]. The probe is vacuum compatible (sealed with "Torr Seal"™ epoxy) and the inductors are housed within the pyrex body of the probe. The ceramic serves as a insulating support and is vacuum and temperature compatible.

The impedance of the tuned probe network, measured *in situ* as a function of frequency, is shown in figure 2.6. The response curve of this tuned probe is quite broad, so that at the second harmonic of the rf driving frequency,

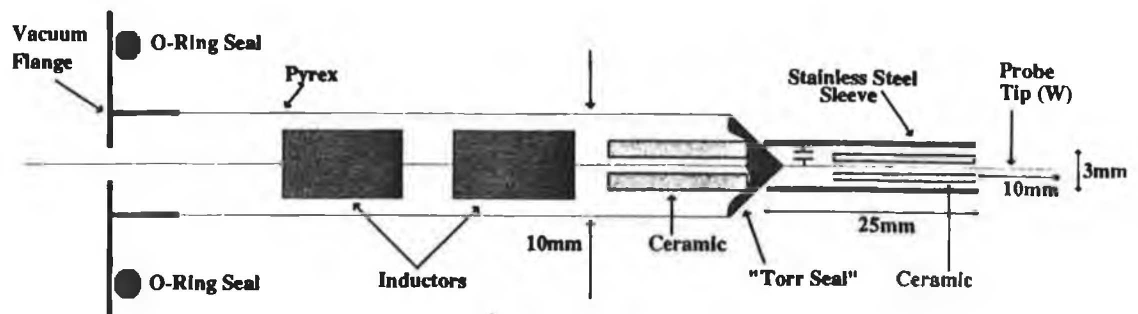

FIG.2.5: Detail of the tuned probe construction

i.e. at 27MHz, the impedance of the network is approximately 10% of its value at the fundamental. Therefore, even if the contribution of the second harmonic to the plasma potential rf component is as high as 30%, the voltage appearing across the plasma-probe sheath is still less than kT_e.

An important aspect of the probe construction is that the pair of inductors are situated close to the probe tip, inside the plasma chamber. Hence, the high frequency components of the probe signal are not loaded by parasitic capacitances[78].

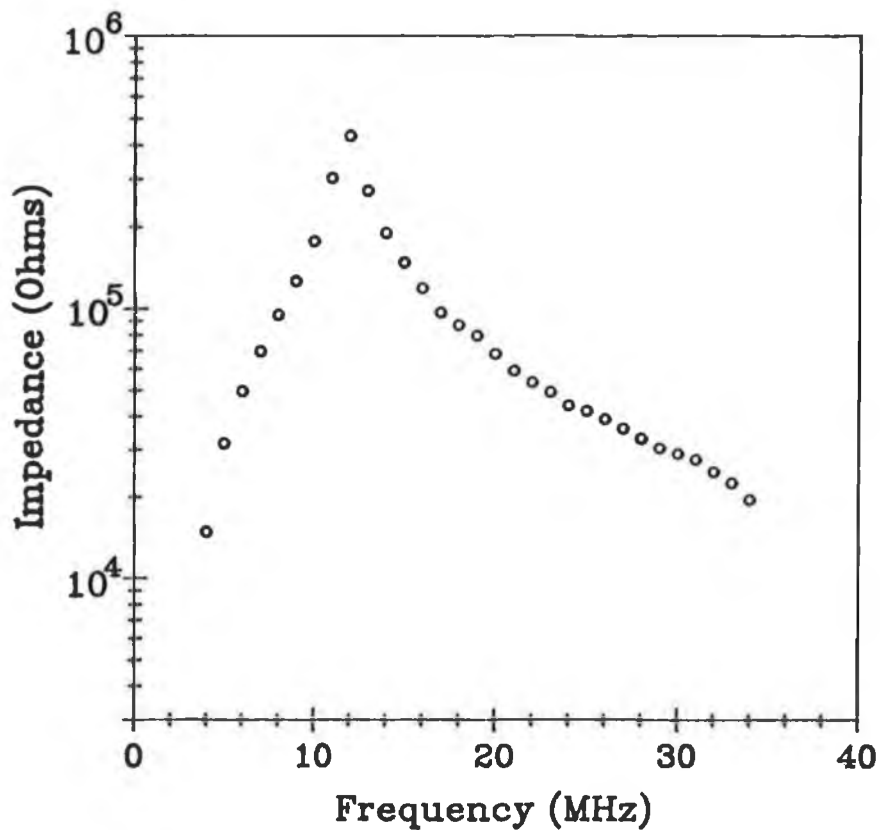

FIG.2.6: Impedance of the tuned probe as a function of frequency

Figure 2.7 shows the IV characteristic of a simple Langmuir probe compared to the tuned probe, in a 13.56MHz nitrogen discharge at 100mTorr. The simple Langmuir probe greatly overestimates kT_e and underestimates n_e. Also apparent is the dc shift of the erroneous characteristic to lower voltages.

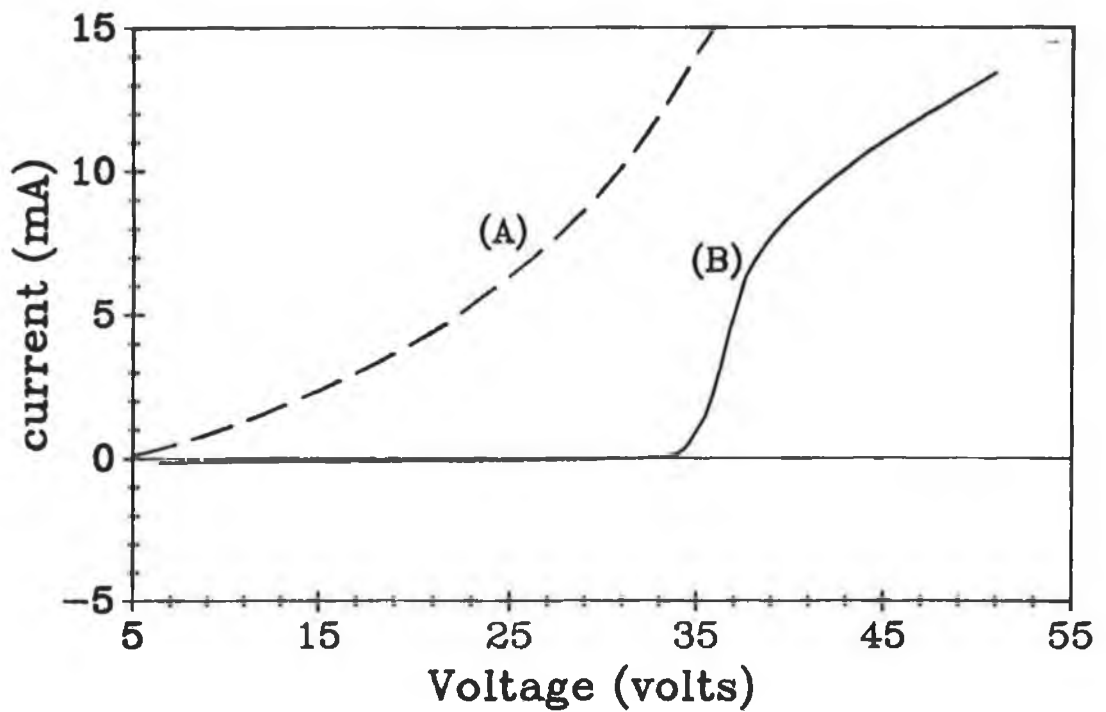

FIG.2.7: IV characteristic of the tuned probe compared with a simple Langmuir probe in a 13.56MHz, 20watt nitrogen plasma at 100mTorr. The simple probe, (A), gives the erroneous values, kT_e=13eV and $n_e=8\times10^{9}cm^{-3}$, while the tuned probe, (B), gives kT_e=1eV and $n_e=1.2\times10^{10}cm^{-3}$.

2.8 Operating conditions of the developed tuned probe

The developed tuned probe described in section 2.7 is designed to operate in 13.56MHz discharges. Its operation and adaptability are similar to a simple Langmuir probe. Since the outer stainless steel cylinder (see fig.2.5) is 3mm in diameter, this represents the spatial resolution of the probe. If the design criteria are adhered to, the probe is adaptable to any rf plasma system. However, if applied to plasmas in processing gas mixtures, or plasmas in gases with low dissociation energies, layer formation on the probe tip and holder must be considered as a source of error in parameter measurement. The inductors have a dc current limit of about 200mA, which must not be exceeded. Equation 2.1 defines the upper pressure limit of Langmuir probe operation. This equation should be satisfied by the 3mm probe sleeve. Thus, in argon and nitrogen[(14),(15),(16)], the upper pressure limit is about 300mTorr. Without the shunt conductor, the upper limit is an order of magnitude greater.

CHAPTER THREE

THE EXPERIMENTAL RF SYSTEM

3.1 Introduction

When working with rf plasmas it is essential to appreciate the subtleties and difficulties associated with radio frequency design. For example, probe measurements can only be hampered by high levels of rf noise, so that it is important to know how to minimize interference. High impedances at low frequencies or dc can become low impedances at radio frequencies; and apparent conductors can acquire significant impedances at high frequencies. Such effects need to be understood and dealt with in order to effectively investigate the rf plasma. Unlike dc discharges, rf plasma power must be distributed via matching networks, and the actual measurement of the rf power deposited in the plasma is non-trivial. These and other aspects of the rf experimental system are discussed in this chapter.

3.2 The Experimental set-up

The rf plasma is generated in a stainless-steel walled chamber with two 80mm diameter parallel electrodes separated by 35mm, as shown in figure 3.1. The top electrode, which is usually the driven one, is movable, by means of a "Wilson" vacuum seal, although 35mm is the nominal electrode spacing used. During the spatial measurements, the original top electrode was replaced by a smaller electrode (70mm), to allow passage of the movable probe. Both electrodes were, however, of the same fundamental design. The electrode is TIG welded to a Kovar to pyrex seal, and the pyrex forms the sliding shaft

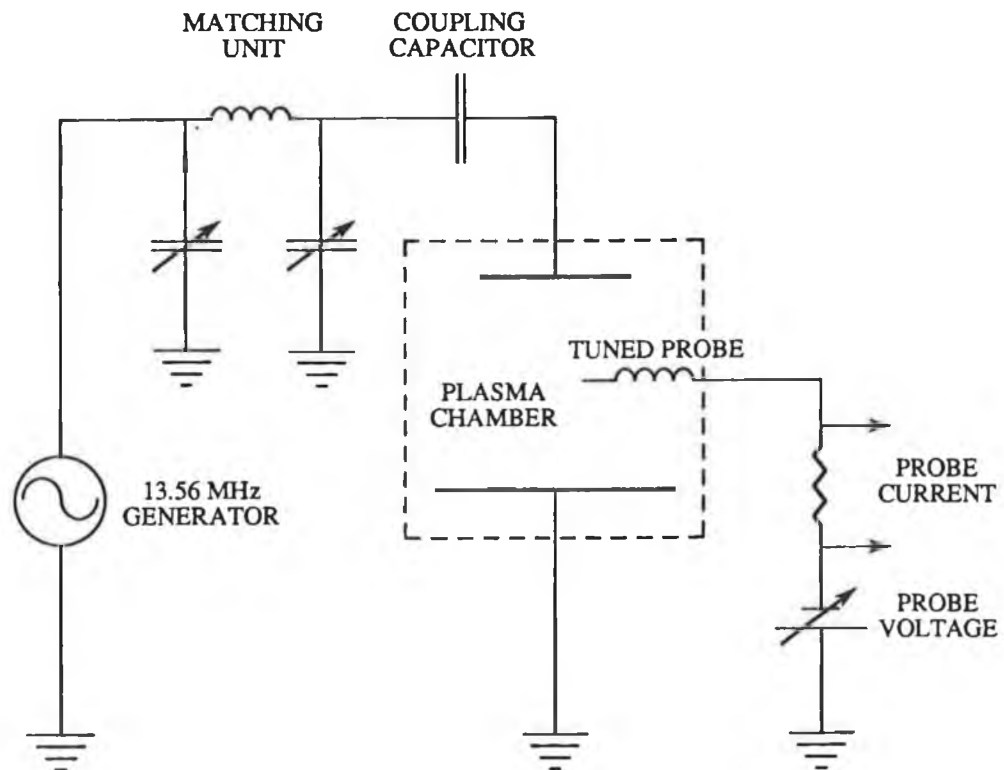

FIG.3.1: Schematic of the experimental set-up

of the "Wilson" seal. The water cooling pipes are situated inside the glass seal. This type of design proved to be most effective, fulfilling the basic requirement of a movable, water cooled electrode.

The chamber is evacuated by a 170l/s turbo-molecular pump resulting in a base pressure of approximately 1×10^{-5}Torr. The pumping unit, consisting of turbo and rotary pumps, is displaced to one side of the chamber, for two reasons. Firstly, because the gas flow rate would be too large if the turbo were placed beneath the chamber operating at typical gas pressures. If the gas flow rate is too large, >15sccm^{-1}, the turbo is subject to considerable torque and may be damaged. Secondly, the water connections to the bottom electrode have been known to leak(!), resulting in corrosion of the turbo pump blades. The present design has operated efficiently but the base pressure could be improved, by at least an order of magnitude, by re-positioning the turbo pump.

The base pressure of the chamber is measured with a Penning gauge. The discharge gas pressure is monitored by a Baratron capacitance manometer rated for full scale operation to 10Torr. Such a range has proved suitable for the rf discharge system and allows the versatility of high pressure measurement which is useful when operating dc cold cathode discharges. The pressure is maintained at a chosen value by means of MKS flow control unit on the gas admittance line. The reactor gas (99.99%) is admitted via

a 1metre long "Teflon" (PTFE) tubing. The chamber contains quite a number of Viton O-ring seals, so that it is not UHV compatible and cannot be baked.

The top electrode is usually capacitively driven with approximately 20watts of rf power at a frequency of 13.56MHz. The second electrode and chamber walls are connected to ground, constituting an asymmetric arrangement. The quoted power is half the difference in forward and reverse power as measured at a ENI ACG-3 13.56MHz rf generator. This allows for 50% power loss in the matching network(79). The power is distributed via a matching network as described in section 3.2. When operating at frequencies other than 13.56MHz, or when operating a pulsed rf discharge, a ENI 320L broadband (250kHz-110MHz) rf amplifier is used. This is driven by an rf signal generator (pulse train modulated in the case of pulsed rf plasmas).

The probes are usually placed parallel to and equidistant from the stainless-steel electrodes, except while making spatial measurements.

3.3 RF Matching Units

The rf generator alone is insufficient to ignite a plasma. It is necessary that a matching unit be placed between the generator and the driven electrode[2]. Matching units can be constructed in different ways, but the fundamental purpose is to match the output impedance of the generator to the input impedance of the load. When this occurs, according to the *maximum power theorem*[80], total power transfer is achieved, i.e. no power is reflected from the load back to the source. In dc systems, maximum power transfer is achieved when the load resistance equals the source resistance. In ac circuits, maximum power transfer occurs when the load impedance Z_l is equal to the complex conjugate of the source impedance Z_s. Thus if $Z_s = R + jX$, then $Z_l = R - jX$, for a matched system.

The primary function of the matching unit is to force the load impedance to look like the complex conjugate of the source impedance, and this is done by inserting the appropriate resistances and reactances between the two. Since we are dealing with reactances, which are frequency dependent, a perfect match is achievable at only one frequency. Hence variable reactances are employed in rf matching units. Figure 3.2 shows the equivalent circuit for the rf generator, the plasma and a typical L-type matching network. The L-type network is the simplest

matching unit and the plasma model of capacitor and resistor, although simplified, serves to illustrate the problem.

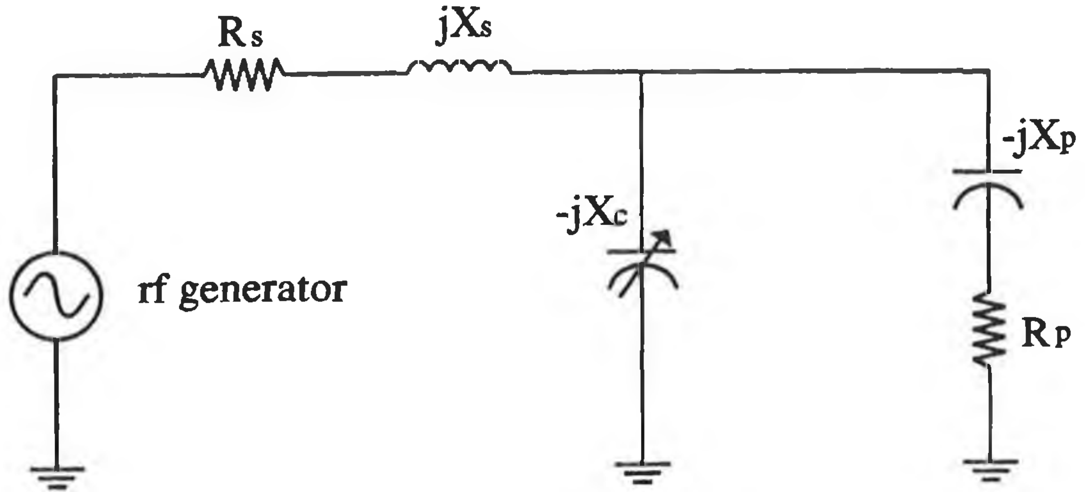

FIG.3.2: Equivalent circuit of rf generator, matching unit and plasma.

The source resistance is the output resistance of the rf generator, R_s. We call this the series resistance. The load impedance is the plasma impedance, $Z_p = R_p - jX_p$. The reactance term is negative since we know the rf plasma impedance to consist mainly of a capacitive term[13]. Thus,

$$X_p = 1/\omega C_p, \qquad ..... \qquad (3.1)$$

where ω is the angular frequency of the rf and C_p is the equivalent capacitance of the plasma (mainly the sheaths).

Finally, the L-network consists of a series reactance,

$$X_s = \omega l_s \quad \ldots\ldots \quad (3.2)$$

where l_s is the inductance in Henries; and a shunt reactance

$$X_c = 1/\omega C_c \quad \ldots\ldots \quad (3.3)$$

The L-network is used in a low-pass filter configuration so that element capacitances are placed in parallel with load capacitances and element inductors are placed in series with stray inductances. The inductive reactances and capacitive reactances are thus in series, and cancel each other.

X_p and X_c are in parallel and can be represented by a single capacitive reactance X_l. Also, let $R_p = R_l$, for the sake of nomenclature.

The output impedance of the source is now

$$R_s + jX_s \quad \ldots\ldots \quad (3.4)$$

The input impedance to the load appears as R_l and $-jX_l$ in parallel, and is therefore given by

$$-jX_l . R_l / -jX_l + R_l \quad \ldots\ldots \quad (3.5)$$

with a complex conjugate

$$jX_l . R_l / jX_l + R_l \quad \ldots\ldots \quad (3.6)$$

Maximum power transfer is achieved when equations (3.4) and (3.6) are equal,

$$\Rightarrow \quad R_s R_l + jX_s R_l + jX_l R_s - X_s X_l = jX_l R_l \quad (3.7)$$

Equating real and complex parts, we get for the real terms

$$R_s R_l = X_s X_l \quad ..... \quad (3.8)$$

Therefore,

$$X_s/R_s = R_l/X_l \quad ..... \quad (3.9)$$

and for the complex terms

$$X_s R_l + X_l R_s = X_l R_l \quad ..... \quad (3.10)$$

From eqn. (3.9)

$$R_l = X_s X_l/R_s \quad ..... \quad (3.11)$$

$$\Rightarrow \quad X_s^2 X_l/R_s + X_l R_s = X_l R_l \quad ..... \quad (3.12)$$

$$\Rightarrow \quad X_s^2 X_l/R_s^2 + X_l = R_l X_l/R_s \quad ..... \quad (3.13)$$

$$\Rightarrow \quad X_s^2/R_s^2 + 1 = R_l/R_s \quad ..... \quad (3.14)$$

Thus,

$$X_s/R_s = R_l/X_l = \sqrt{R_l/R_s - 1} \quad (3.15)$$

This equation applies if $R_l > R_s$.

If $R_s > R_l$, as is usually the case with rf plasmas, then eqn. (3.15) becomes

$$R_s/X_s = X_l/R_l = \sqrt{R_s/R_l - 1} \quad (3.16)$$

Using equation (3.16), we can determine the reactive loads X_s and X_l necessary to achieve an impedance match, at a given frequency, between any source and load. Logan et al.[81] used this equation to determine the impedance of an rf discharge at 13.56MHz by varying the values of X_s and X_l until a perfect match was achieved (no reflected

power, VSWR =1) between the plasma and generator. Typically, the resistive part of the plasma impedance, R_p, ranges from a few ohms to tens of ohms, while the capacitive part, X_p, ranges from a few tens of ohms to hundreds of ohms. In the actual matching unit used in all our 13.56MHz plasma experiments, typically, L_s ranges from 0.1μH to 1.0μH and C_1 ranges from 1pF to 800pF and C_2 from 1pF to 200pF. If we consider C_1 and L_s to represent the L-network then C_2 can be considered a variable on L_s, by adding or subtracting an opposite reactance. Modern processing systems include an automatic matching network, which tracks the plasma impedance as rf power or gas pressure is changed.

The impedance of the plasma depends on electrode area, electrode spacing, gas type, gas pressure and rf power. Godyak[27] has shown that the impedance of the rf plasma may also be governed by the amplitude of the rf voltage, so that the discharge impedance may change over the rf cycle[34].

Matching units can also be constructed using transformers. For example, broadband transformers[80] have been used to match the generator output to the plasma impedance at frequencies between 1MHz and 5MHz. The output impedance of a transformer, Z_o, is related to its input impedance, Z_i, by

$$Z_o = [n_1/n_2]^2.Z_i \quad ..... \quad (3.17)$$

where n_1 is the number of primary turns and n_2 is the number of secondary turns. Thus Z_o can be made equal to the plasma impedance, Z_p, by varying the turns ratio.

Impedance matching can also be achieved using resonance, where the plasma is made to resonate with the matching element at a desired frequency. Indeed, the network of figure 3.2 can be considered as a type of resonant circuit. The forward power at the chamber is

$$P = E^2/Z_p \quad ..... \quad (3.18)$$

where E is voltage on the driven electrode and Z_p is the plasma impedance. Thus, the voltage is

$$E = \sqrt{P.Z_p} \quad ..... \quad (3.19)$$

and the power must be such that the voltage is equal to the striking voltage for the carrier gas at the desired pressure. Resonance effectively boosts the voltage across any element at the resonant frequency by the Q-value of the circuit. Resonant circuits (and also step-up transformers) have also been used to drive low frequency (1kHz to 50kHz) discharges in this work. Such discharges were used to study the merits of the double probes mentioned in section 2.6.

3.4 RF Power Measurement

The measurement of the rf power deposited in the plasma is non-trivial. Processing systems usually employ rf generators with forward and reverse power meters, so that plasma power is taken as the difference. The forward and reverse powers are measured via the voltage drop across a known resistor. Voltage standing wave meters are often used to ensure minimum reflection. Many researchers[74],[82] use high voltage probes to monitor the driving voltage, V_{rf}, and Pearson or Phillips current probes to measure the rf current. The rf power to the plasma is then taken as

$$P = (IV\cos\phi)/2 \quad ..... \quad \textbf{(3.20)}$$

where ϕ is the phase shift between current and voltage, and is usually very close to $\pi/2$[12],[20].

In an attempt to measure the rf power deposited in the plasma, the development of a Rogowski loop[20] was considered. Referring to figure 3.3, the coil operates as follows:

We wish to measure the current, $I = I_o \sin\omega t$, in a long straight wire. A rectangular loop of N turns is placed close to the wire as shown. The magnetic field produced by the current is perpendicular to the plane of the loop and is thus given by Ampere's Law as

$$B = \mu_o I/2\pi r \quad ..... \quad \textbf{(3.21)}$$

and the flux linkage (Faraday Law of Induction) is

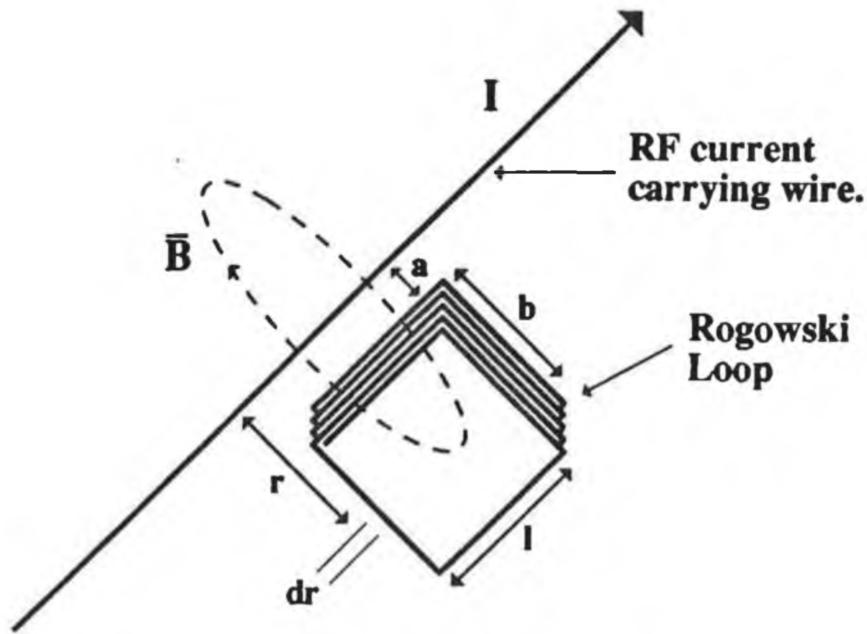

FIG.3.3: A Rogowski loop.

$$\Phi = \int \mathbf{B}.\mathbf{n}A \qquad ..... \qquad (3.22)$$

where **n** is the unit vector perpendicular to **B**, and A is the area of the loop. Thus,

$$\Phi = \mu_o INl/2\pi \int_a^{a+b} dr/r \qquad ..... \qquad (3.23)$$

$$\Rightarrow \qquad \Phi = \mu_o I_o Nl/2\pi . \ln[(a+b)/a] \mathrm{Sin}\omega t \qquad (3.24)$$

and the induced emf (across the ends of the coil) is

$$E = -d\Phi/dt = -\Phi_o \mathrm{Cos}\omega t \qquad ... \qquad (3.25)$$

The amplitude of the induced voltage is thus

$$E_o = \mu_o I_o Nl/2\pi . \ln[(a+b)/a] \qquad (3.26)$$

and for loop dimensions, a=3mm, b=12mm, l=12mm

$$E_o = 3.9\times10^{-9}.I_o.N \qquad ..... \qquad (3.27)$$

so that the peak current can be measured. Typically, I_o is about 100mA for the rf discharge, so that for E_o to be in the μVolt range, N must be approximately 10,000;

although this could be reduced by an order of magnitude with a metallic former. Thus, the construction of an effective home-made loop is un-feasible; in fact, commercial loops are only available for high ac currents (amps).

The problem with the above power measuring techniques is that they assume no power is lost in the matching network. This assumption is generally incorrect, and the inductive elements can become quite hot. Thus, ref.79 suggests that up to 50% losses can occur in the matching unit. (I^2R losses are greater for conductors carrying rf currents than for dc currents because of the "skin effect":- the effective resistance is inversely proportional to the skin depth, and thus proportional to the square root of the frequency). Since the measured rf current is the current flowing in the matching network and plasma, it cannot be used to estimate the plasma power.

Another idea for rf plasma power measurement is to install a calorimeter on the water cooling line of the driven electrode. Temperature change as a function of power could easily be calibrated with a dc plasma, so that the power deposited in the rf system could be established. However, power is also lost from the plasma via radiation (IR, UV, visible) and these power losses differ greatly in the rf and dc systems (at least in the visible). However, the technique may have some potential.

3.5 RF Grounds and Shielding

A few points about grounding and shielding of the rf system worthy of consideration are listed below.

(i) The impedance of any length of conducting wire is

$$Z = R + j\omega L \qquad \ldots\ldots \qquad (3.28)$$

where R is the resistance given by

$$R = \rho l/A \qquad \ldots\ldots \qquad (3.29)$$

and L is the inductance of the wire. At low frequencies Z is dominated by the resistive term and is small, whereas at high frequencies, the inductive term may dominate. The inductance of a length of copper wire is approximately 1μH/m, so that at 13.56MHz, ωL is about 85Ω!, for a 1metre length. Thus, apparent conductors may in fact represent quite large impedances at radio frequencies. At high frequencies, the resistive term increases, due to the decrease in conductive cross-section of the wire by the "skin-effect". Hence, great care must be used when grounding rf systems. In general, grounding wires must be of large surface area, and as short as possible; copper or aluminium straps are normally used. RF compatible connectors and rf co-axial cable should also be used. As in any electronic system, unique grounding points are desirable, avoiding ground current loops. Peculiar to rf systems, however, wire loops should be avoided, since induced fluxes are proportional to the enclosed areas.

(ii) RF filters were installed on the mains-sockets of the rf power supplies. This greatly reduced noise in external circuitry, as there was considerable rf pick-up on the grounds of the rf generator cables. Also, the impedance associated with oscilloscope leads, etc., is capacitive

$$Z = 1/j\omega C \qquad \ldots\ldots \qquad (3.30)$$

and may be very small at high values of ω. Thus, serious signal loading can occur.

(iii) The power radiated from an oscillating voltage source is proportional to the fourth power of the oscillator frequency. As a result, radiation losses become significant at high radio frequencies. Thus, to avoid pick-up in the microcomputer and the data-acquisition electronics, the rf system was surrounded by a Faraday cage.

The characteristic impedance of air is approximately 350Ω, so that it is possible to match the output impedance of cables, etc., to this input impedance with a resulting maximum radiative power transfer. Clearly, this should be avoided, and is best done by using shielded cables with low characteristic impedances. The driven electrode connection is shielded as close to the electrode as possible.

Finally, a word of warning about the safety aspects of rf radiation. The operating frequency of 13.56MHz is not close enough to microwave frequencies to be of great danger. For example, the resonance of H_2O used in μwave cooking is 2.45GHz. Furthermore, the operating frequency is much greater than the ionic plasma frequency, so that ions do not respond to the rf fields, and thus is not suspect as lower frequency radiation may be. However, at high powers it is best to avoid exposure, and a Faraday cage will provide sufficient protection.

3.6 Data acquisition and analysis

The Langmuir probe characteristics are measured via computer controlled, high speed data acquisition hardware. The system provides accurate control of the probe voltage, via a high speed DAC, and the ability to measure the probe current in the μA to mA ranges, via a 16 bit A/D. This system has been described in detail elsewhere[52]. Data analysis is performed in real time via a BASIC code[42], and the eedf is established by numerical differentiation[44],[46].

CHAPTER FOUR

RESULTS AND DISCUSSION OF PLASMA PARAMETER MEASUREMENTS

4.1 Introduction

This chapter is devoted to the presentation and discussion of results of plasma parameter measurements in argon and nitrogen rf plasmas. In particular, the spatial and pressure dependence of the electron temperature, the electron density and the plasma potential are discussed. Ideally, a complete treatise of rf plasma investigation would include the dependence of the parameters on plasma driving frequency and plasma power. However, since the tuned probe has been designed to operate at the widely used allotted frequency of 13.56MHz, the dependence of plasma parameters on driving frequency is beyond the scope of this work. It is worth noting, however, that the rf plasma driving frequency regime can be subdivided into

sections $\omega < \omega_i$, $\omega_i < \omega < \omega_e$ and $\omega > \omega_e$. In this respect, the former regime has been investigated prior to this work[(60),(62)], while the latter is the concern of microwave discharge workers. Thus, since 13.56MHz falls within the $\omega_i < \omega < \omega_e$ regime in the case of glow discharges (low density), it is this regime which has been investigated. However, it is crucial to remember that important transitions in rf discharge physics can occur if ω falls on either side of such parameters as the ionization frequency or the neutral collision frequency (see section 2.5). Furthermore, it has been mentioned that "stochastic" sheath heating may be possible if ω is large enough (see sections 1.2 and 1.4) and both rf sheath heating and electrostatic confinement are certainly functions of ω. The dependence of the plasma parameters on discharge power is also worthy of serious investigation. However, it was not considered a priority in this work, since exact determination of rf power deposited in the plasma is non-trivial. Nonetheless, the dependence of the argon rf plasma parameters was measured as a function of power, but it must be remembered that the quoted power is only accurate to within a factor of two.

The plasma carrier gases chosen were argon and nitrogen. Argon because it is inert and is traditionally used as a discharge gas. Cross-sections for argon are

easily obtained[14], and much recent work, both experimental and modeling, has been done on argon plasmas. It is also widely used in processing as an efficient etchant. Nitrogen was investigated because it is molecular, and the eedf is highly structured. There has been much recent interest in the eedf's of nitrogen plasmas[83],[84]. Helium and hydrogen rf plasmas were also investigated, although not as thoroughly as argon and nitrogen.

4.2 The bulk electron temperature

There has been much controversy in recent years concerning the accurate values of kT_e in rf plasmas. It has arisen for two reasons. Firstly, the problem of rf convolution of the probe characteristic tends to overestimate kT_e. Measured electron temperature values have typically been between 2eV and 10eV. Indeed, probe measurements have been viewed with varying degrees of scepticism. Secondly, models of the rf glow are incomplete, and have tended to treat the plasma as either a self-sustained bulk plasma, analogous to a dc positive column, or a non self-sustained plasma, analogous to a dc negative glow. The electron temperature may differ by almost an order of magnitude in both cases.

Recently, as discussed in section 1.2, it has been realised that the rf plasma may exist in different modes. Depending on the gas pressure and the sustaining voltage, different heating mechanisms are responsible for maintaining the discharge. Positive feedback dependencies result in abrupt transitions between these regimes. Invariably, associated with such transitions, are transitions in the values of kT_e and n_e [18],[19],[20].

Quite recent and relatively complete models[22] predict electron temperatures of the order of 1eV or 2eV in low pressure (≃100mTorr) argon rf plasmas. However, a much debated recent publication[19] reports a measurement

of very low (≈0.4eV) electron temperatures in similar discharges. A tuned probe (similar to that described in section 2.7) is used to avoid the problem of rf distortion of the IV characteristic, and a feedback loop is employed to avoid low frequency noise distortion of the characteristic. The powered symmetric electrodes are both made to follow low frequency fluctuations in the plasma potential as detected via a ring electrode (probe). It is not clear, however, that driving the plasma in this way does not alter discharge conditions.

In the view of this author, accurate probe measurements are possible if the conditions outlined in chapter two are satisfied. However, since probe measurements are regarded with suspicion (by the uninitiated!), the validity of the results presented here were scrutinized via a simple technique. The accuracy of plasma parameter measurements in the rf discharge can be checked by measuring the parameters in the post-discharge or afterglow. This is achieved by square-wave pulsing the rf plasma and taking time resolved measurements with respect to the plasma off-time. Since the perturbing effects of the rf voltage disappear in the afterglow, probe measurements are simplified. Figure 4.1a is a plot of kT_e and n_e as a function of time into the afterglow for a 30mTorr pulsed argon rf discharge. Plasma parameters are measured with a conventional Langmuir probe in the afterglow. The parameters obtained with the tuned probe,

during the plasma on-time, are plotted at 0μs. Extrapolating the parameter values obtained in the afterglow back to 0μs results in good agreement with the values measured in the rf discharge. Such an extrapolation is possible since the afterglow temporal decay is exponential, characteristic of diffusion dominated plasmas (see section 1.2). For example, in fig.4.1a, the electron temperature is shown to decay exponentially, in the early post-discharge, with a characteristic decay time, τ=13μs. Note that 8μs into the afterglow, the value of kT_e is about 1eV. Thus, it must be at least greater than this during the discharge, and the results of ref. 19 are clearly not universal. Figure 4.1b shows a similar result for a 125mTorr discharge, and figure 4.1c for a nitrogen 125mTorr discharge. kT_e is typically of the order of 2eV in the rf argon plasma and 1eV in the rf nitrogen plasma[77].

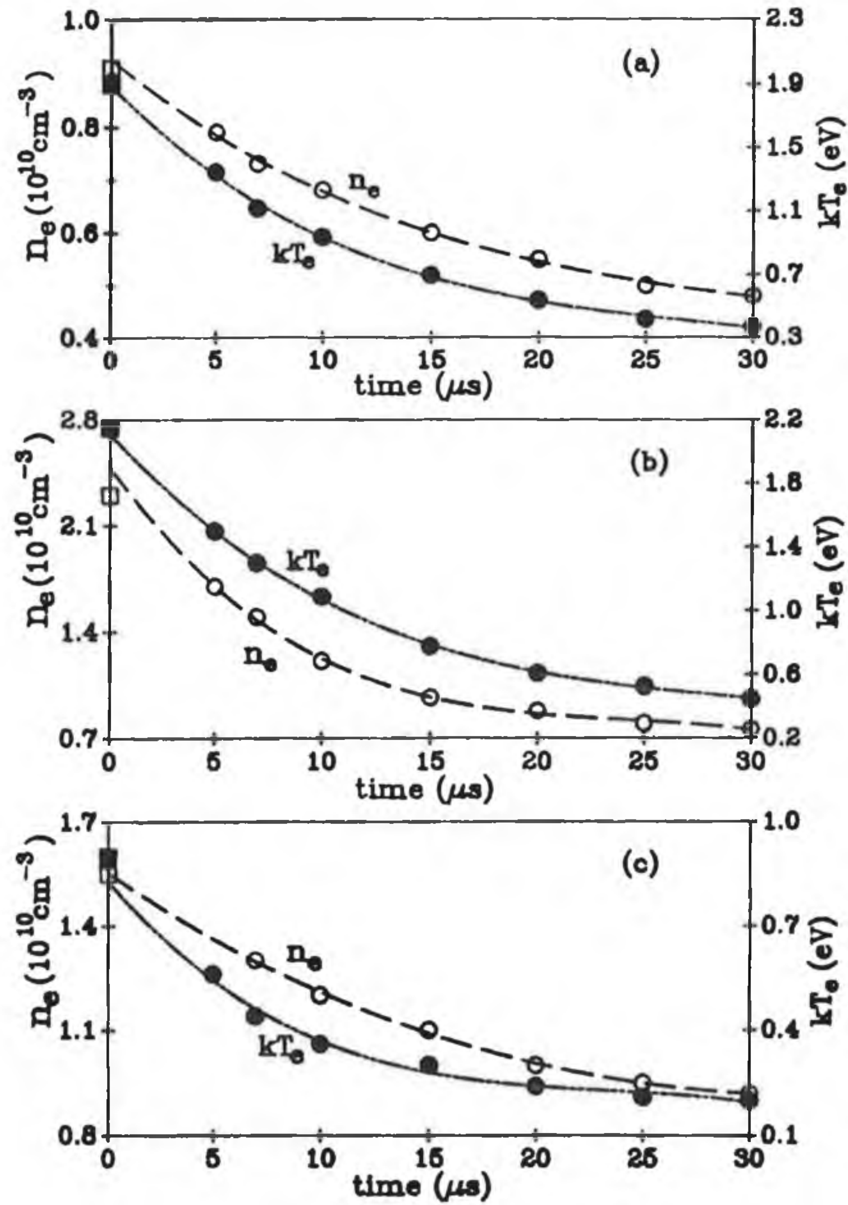

FIG. 4.1: Plot of kT_e and n_e as a function of time into the post-discharge of a 13.56MHz, 20watt (a)argon plasma at 30mTorr, (b)argon plasma at 125mTorr and (c)nitrogen plasma at 125mTorr. Open circles represent n_e in the post-discharge, closed circles represent kT_e in the post-discharge, measured with a simple Langmuir probe. Open squares represent n_e in the rf plasma, closed squares represent kT_e in the rf plasma, measured with the tuned Langmuir probe.

4.3 Pressure dependence of rf plasma parameters

Figure 4.2 shows the measured pressure dependence of kT_e, V_p and n_e in a 13.56MHz, 20watt argon plasma.

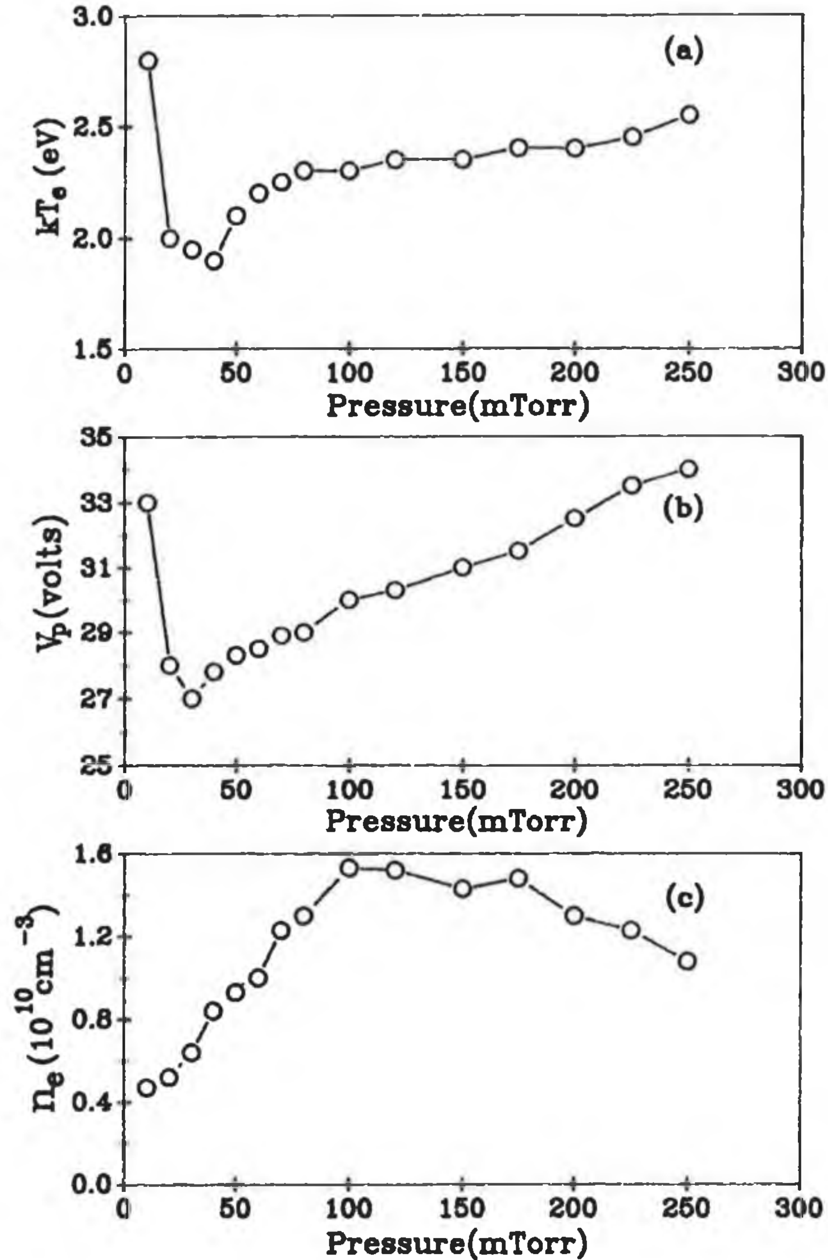

FIG.4.2: Pressure dependence of (a)kT_e, (b)V_p, and (c)n_e in a 13.56MHz, 20watt argon plasma.

It has been found that the argon rf glow appears (visually) almost uniform, both across the glow, and as a function of pressure. The electron temperature in the centre of the discharge does rise steadily as a function of pressure, from about 1.8eV at 40mTorr to 2.5eV at 250mTorr, as shown in fig. 4.2a; with the exception that at very low pressures, just before the discharge is no longer sustainable, kT_e is quite high. A similar dependency has been observed by Godyak[19]. In discharges where bulk fields are responsible for plasma heating, the electron temperature is known to decrease as a function of increasing pressure[1]. As the pressure increases, the number of collisions increases, so that electrons loose energy more rapidly. Stated simply, as the electrons undergo more collisions, they cool down. The plasma production rate (via single step ionization) is

$$P_i = n_e n_o \langle \sigma_i v_e \rangle \quad ..... \quad \textbf{(4.1)}$$

where $\langle \sigma_i v_e \rangle$ represents the ionization rate coefficient obtained by integrating the ionization cross-section over the eedf. Thus, although the eedf cools, since n_o increases, the production rate may remain constant. Similarly, although the collision rate (or frequency) increases as the pressure increases, since the bulk temperature cools, the energy loss rate (energy lost per collision times collision frequency) may also remain constant. These relationships are well understood, and

may apply to pressure regimes in which collisional or diffusion cooling are dominant. The argument is simplified, since only elastic and ionizing inelastic collisions are accounted for, but does explain the observed dependencies.

In the case of the fig. 4.2a, however, since the bulk dc electric field is of the order of 1 or 2 volts/cm in this pressure regime (see figure 4.5b), bulk heating is not a significant plasma production mechanism. Rather, sheath heating (complemented by electrostatic trapping of fast electrons) sustains the plasma (Diffusion is the main loss mechanism, since $\lambda \geq l$, where l is the characteristic dimension of the discharge). Both sheath heating and electrostatic trapping are most efficient when the sheath-plasma voltages are large, and thus at lower pressures (sheaths are more capacitive). As the pressure increases, the production rate from these mechanisms decreases, so that the plasma production rate via the tail of the distribution must increase. Associated with this increase is an increase in the electron temperature.

The average plasma potential, V_p, increases steadily from about 28volts at 50mTorr to 32volts at 200mTorr (figure 4.2b). This is discussed further below, in context with measurements taken in nitrogen.

In ambipolar diffusion dominated plasmas, the continuity equation (i.e. energy balance) for electrons is

$$n_e n_o \langle \sigma_i v_e \rangle = D_a n_e / \Lambda^2 \quad .... \quad (4.2)$$

(see eqn. 1.4). If the eedf is Maxwellian, then using eqns. 1.8 and 1.10, have

$$D_a = k(T_+ + T_e)/M\nu_{iN} \quad .... \quad (4.3)$$

$$n_e = n_e n_o \langle \sigma_i v_e \rangle . \Lambda^2 M\nu_{iN} / k(T_+ + T_e) \quad (4.4)$$

The collision frequency is proportional to the gas pressure (eqn. 1.11). The plasma production rate has been found to be independent of pressure (in argon), as discussed in section 5.2. Since kT_e is relatively unchanging with increasing pressure (fig. 4.2a) and the ion temperature is constant, n_e should be approximately proportional to the gas pressure. Figure 4.2c shows this linear dependence up to pressures of about 100mTorr. Thereafter, n_e remains constant with increasing pressure and eventually begins to decrease. Although this behaviour is not understood, it is not clear that the production rate remains constant[36]. Also, kT_e does increase slightly, especially at these pressures.

In the above argument, the loss rate is taken to be constant. It is estimated from the power input to the plasma, which is constant. This is discussed in detail in section 5.2. The constant production rate must balance this loss rate. Plasma loss is also incurred via recombination, so that if this process is important, then the estimated loss rate (from discharge current) will be

invalid. It is unclear whether or not the production rate increases. Three-body recombination would account for the observed decrease in electron density, but should not be important at these densities in argon.

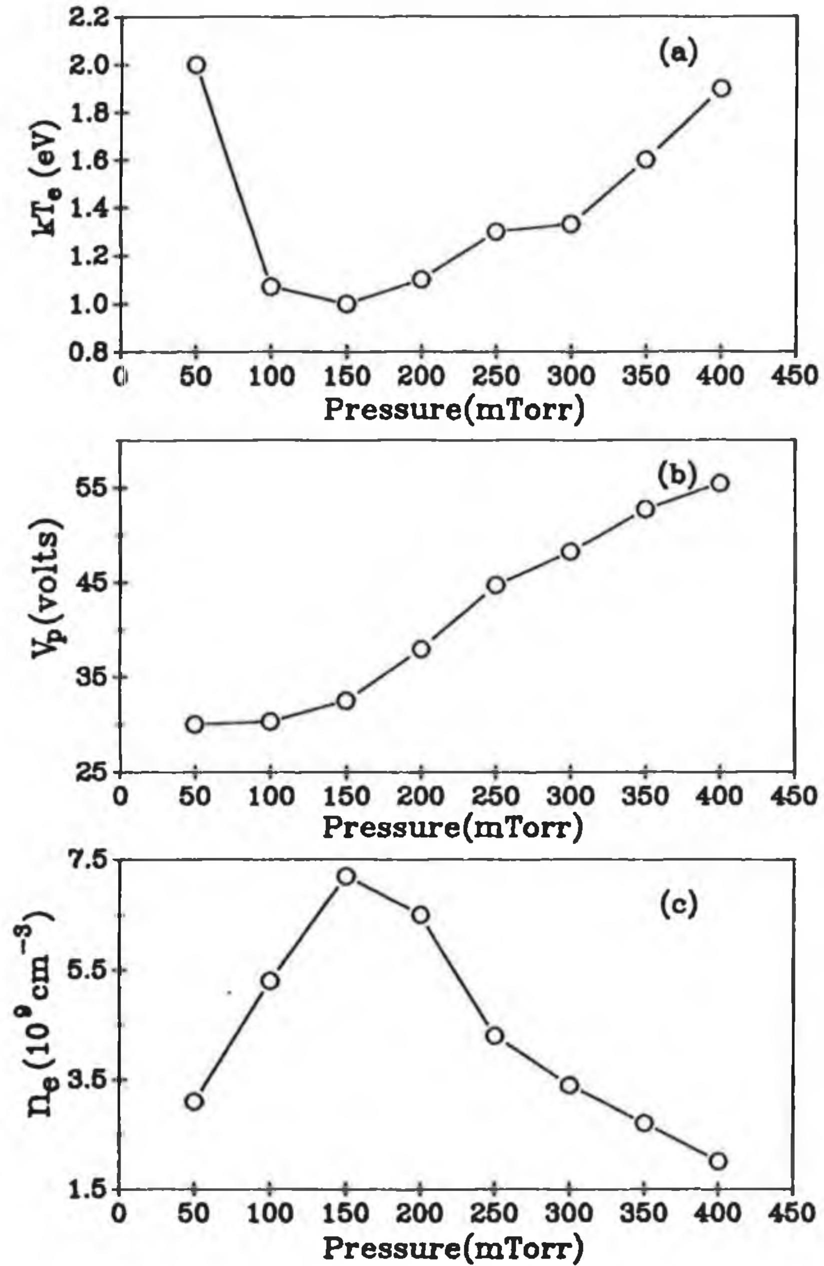

FIG.4.3: Pressure dependence of (a)kT_e, (b)V_p, and (c)n_e in a 13.56MHz, 15watt nitrogen plasma.

Figure 4.3 shows the measured pressure dependence of kT_e, n_e and V_p in a 13.56MHz, 15watt nitrogen plasma.

In the case of nitrogen, kT_e increases much more rapidly as a function of pressure, increasing by almost a factor of two between 100mTorr and 400mTorr (figure 4.3a).

The plasma potential in the nitrogen rf plasma also undergoes a rapid increase as a function of increasing pressure. This suggests that the rf driving voltage, V_{rf}, is increasing (see figs 1.1, 1.3). Since the rf power is constant, such an increase would imply that the plasma impedance must increase with pressure. This is unrealistic in terms of equivalent circuit models of the glow (see section 1.4). Measurement of V_{rf} as a function of increasing pressure reveals that it is relatively

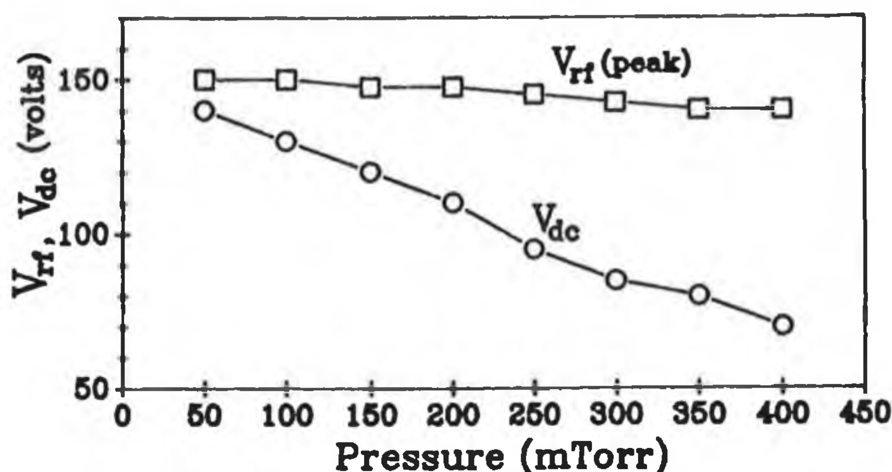

FIG.4.4: RF driving voltage and dc bias as a function of pressure in a 13.56MHz, 15watt nitrogen plasma.

constant (decreasing very slightly), as expected; i.e. the plasma impedance is constant or deceasing slowly. This agrees with the results of Bletzinger[35], and is shown in figure 4.4. Figure 4.4 also shows the pressure dependence of the dc bias on the driven electrode. It decrease steadily, explaining why the plasma potential increases. Since V_{rf} is relatively constant, a decrease in dc bias ensures that the driving voltage is greater on its positive portion of the rf cycle (see figs 1.1, 1.3). Thus the plasma potential increases. The question remains as to why the dc bias should decrease. This is answerable in terms of the equivalent circuit model of fig. 1.5. The driven electrode has a smaller area than the grounded electrode (hence the dc bias). This is modeled by assigning the driven electron sheath capacitance, C_{s1}, a smaller value. As this capacitance decreases with respect to the grounded electrode sheath capacitance, C_{s2}, the dc bias increases. The dc bias will therefore decrease if the ratio of C_{s1} to C_{s2} increases. It has been observed that as the pressure is increased, the driven electrode sheath thickness decreases and the grounded electrode sheath thickness appears to increase. Since the sheath capacitances are inversely dependent on the sheath thickness, an increase in gas pressure will result in an increase in the capacitance ratio. Thus, the dc bias

decreases. The optically observed expansion and contraction of the sheaths (remember that these sheath thicknesses are averaged over the rf cycle) as a function of pressure is supported by spatial measurements and is discussed further in section 4.4. A similar scenario occurs in the case of argon, but much less pronounced.

Figure 4.3c is a plot of the measured pressure dependence of the electron density in the nitrogen rf plasma. Again, it appears that n_e increases linearly with pressure up to about 150mTorr. Thereafter, however, n_e decreases rapidly. Recombination is not significant, the loss rate being

$$dn_e/dt = -\alpha n_e^2 \qquad \ldots\ldots \qquad \textbf{(4.5)}$$

Since n_e is about $1x10^{10}cm^{-3}$, and $\alpha \simeq 3x10^{-7}cm^3s^{-1}$ for the nitrogen ion[1], the loss rate is approximately $3x10^{13}cm^{-3}s^{-1}$. This is well below the diffusion loss rate (see section 5.2), so that recombination can be ignored. Note, however, that the electron temperature does increase significantly, so that the argument presented for argon is not valid. More importantly, it has been noted that the production rate calculated from the eedf (i.e. the production rate via single step ionization of the ground state molecule) is a few orders of magnitude below the estimated loss rate in the case of nitrogen (see section 5.2), and it is suspected that electron-metastable molecule/atom collisions may account for the majority of

plasma production. If the plasma loss rate is virtually constant with pressure, and the production rate from the eedf decreases with pressure, then eqn. 4.4 predicts that n_e will decrease (kT_e and ν_{iN} both increasing). The exact processes which give rise to the observed dependence remain, however, unclear, but it must be appreciated that many complex collisional processes are possible.

4.4 Spatial dependence of rf plasma parameters

Figure 4.5 shows the observed variation of the argon rf plasma parameters with distance from the driven electrode. The driven electrode corresponds to X=0cm and the grounded electrode to X=4.5cm. The probe is moved in steps of 0.5cm parallel to the electrodes and maintained in the vertical central axis of the plasma.

The spatial dependence of kT_e (fig. 4.5a) demonstrates that the argon rf plasma is almost homogeneous, as suspected from its appearance.

The plasma potential variation with distance from the driven electrode is shown in figure 4.5b. It demonstrates that the rf glow is almost field free, with a maximum dc bulk field of 1V/cm. This value increases with pressure, as the plasma becomes more collisional.

The measured value of the bulk field is supported by the spatial variation of the electron density (fig. 4.5c). As mentioned in section 1.2, in diffusion dominated plasmas, the electron density is greatest in the centre of the plasma, falling off toward the electrodes in a sinusoidal or Bessel function mode, dictated by the ambipolar field.

These spatial measurements are substantiated by recently reported PIC simulations(22).

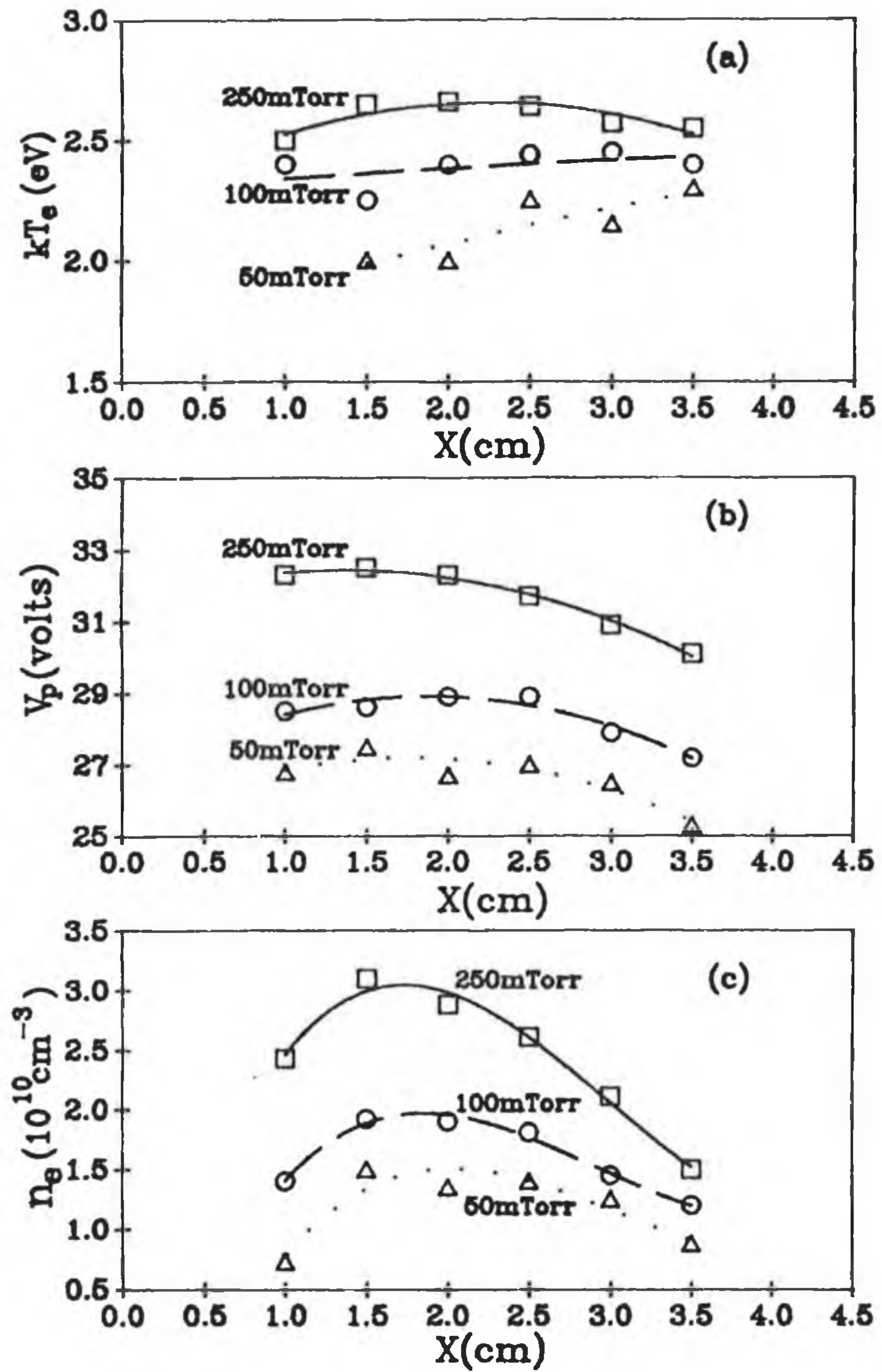

FIG.4.5: Spatial dependence of (a)kT_e, (b)V_p, and (c)n_e in a 13.56MHz, 20watt argon plasma.

Figure 4.6 shows the measured spatial dependence of the rf plasma parameters in nitrogen.

The spatial variation of kT_e, at a few different pressures (fig 4.6a) is again supportive of the visual appearance of the nitrogen glow. The plasma is non-homogeneous, unlike argon, particularly close to the sheaths. At the low pressure (100mTorr), the driven electrode sheath extends about 1cm from the electrode. Thus, the measured electron temperature is high. As the pressure is increased, the driven electrode sheath contracts, and the temperature at X=1cm decreases. Meanwhile, the grounded electrode sheath thickness (averaged over the rf cycle) is expanding, so that eventually the electron temperature at X=3.5cm increases at 350mTorr. This behaviour has already been described above in context with the pressure dependence of V_p in the nitrogen rf plasma.

It must be stressed, however, that the plasma parameters are modulated by the rf field in the sheath regions[22], so that the time averaged probe measurements close to the plasma sheaths may be invalid.

The spatial variation of V_p in the nitrogen glow (fig. 4.6b) demonstrates that the bulk field is about 2V/cm. This will be discussed further in context with the eedf measurements in nitrogen.

The electron density spatial dependence is plotted in figure 4.6c. Again, n_e is greatest in the centre of the glow, with a clear ambipolar dependence.

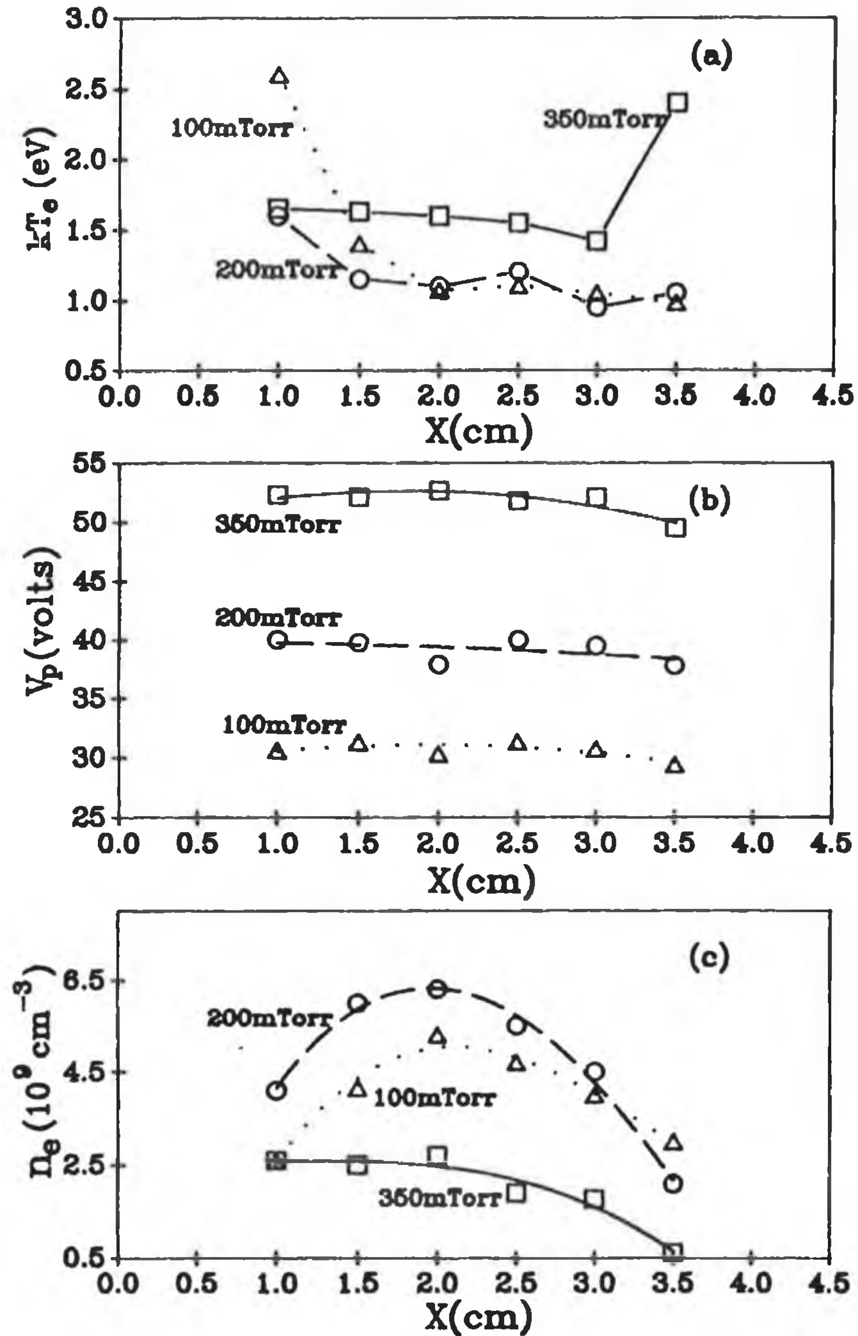

FIG.4.6: Spatial dependence of (a)kT_e, (b)V_p, and (c)n_e in a 13.56MHz, 15watt nitrogen plasma.

The spatial dependence of the diffusion equation can be written as

$$\nabla^2 n = -n/\Lambda^2 \qquad ..... \qquad (4.6)$$

where $\Lambda = \sqrt{D\tau}$ is the characteristic diffusion length. For a long cylinder of radius a,

$$\nabla^2 n = 1/r.\delta/\delta r.r.\delta n/\delta r + 1/r^2.\delta^2 n/\delta\phi^2 + \delta^2 n/\delta z^2 \qquad (4.7)$$

Assuming no z dependence and azimuthal symmetry, it can be shown that the dominant radial diffusion mode is described by a first order Bessel function. The experimental spatial measurements are in the z-direction, i.e. along the length of the cylinder, so that, if radial and azimuthal symmetry are assumed, the simple 1D diffusion equation holds

$$\nabla^2 n = \delta^2 n/\delta z^2 = -n/\Lambda^2 \qquad ... \qquad (4.8)$$

The solution to this equation is a summation of sinusoidal terms, the higher order modes diffusing rapidly, so that only the lowest order need be considered

$$n(z) = n_o \sin(\pi z/L) \qquad ..... \qquad (4.9)$$

where n_o is the maximum value of the electron density, i.e. in the centre of the discharge and L is the chamber length. Note that this solution represents diffusion away from a point source, positioned in this case in the centre of the discharge.

Figure 4.7 is a plot of this diffusion solution fitted to the experimental data. The data is that shown in figure 4.6c, for the 200mTorr case. It is important to note that the diffusion theory solution greatly simplifies the actual discharge conditions. Firstly, it assumes that the ionization occurs at a point source in the centre of the discharge, rather than over a distributed region close to the driven electrode. Secondly, ionization and charge distribution in the sheath regions are not accounted for.

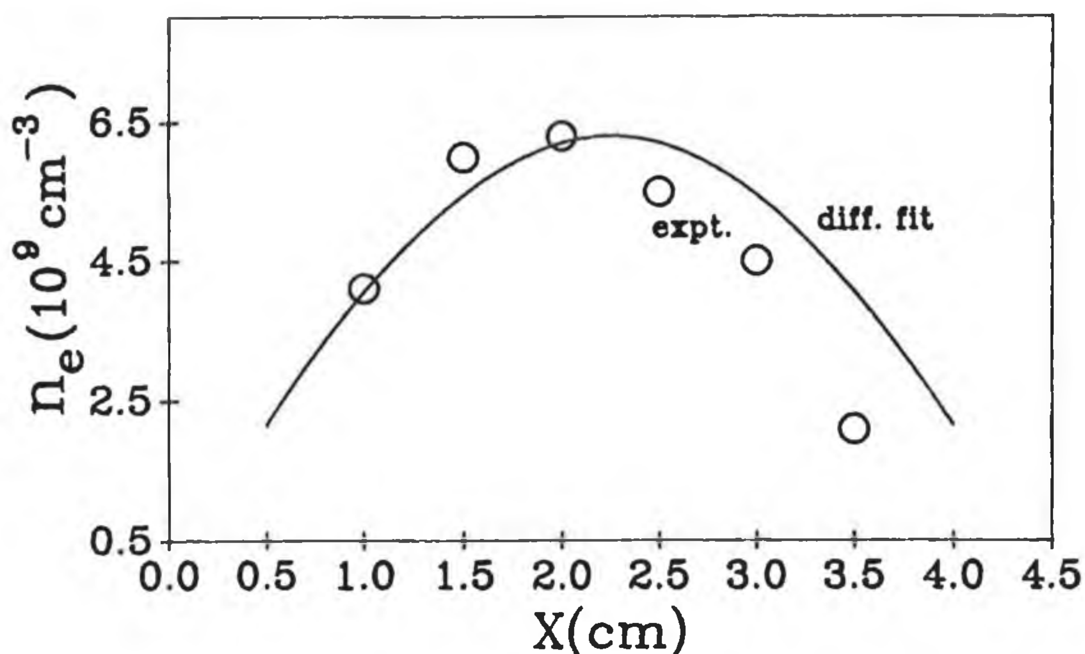

FIG.4.7: Diffusion theory fit of experimental spatial variation of n_e. Open circles are data points from fig.4.6c; solid line is sinusoidal 1D diffusion theory solution.

4.5 Power dependence of rf plasma parameters

Figure 4.8 is a plot of the dependence of the argon rf plasma parameters as a function of input rf power. Although there is considerable uncertainty about the absolute value of plasma power, the results are as expected and agree with other workers[20],[74]. The electron temperature drops slowly as input power is increased, whereas both the plasma potential and the electron density increase with increasing power.

At the low pressure, the electron temperature varies with power in a "bow" shape, with a minimum at about 25watts. As the power increases, the rf component of the plasma potential is likely to increase, so that rf convolution of the probe IV characteristic is increasingly likely. This would result in an apparent increase of electron temperature with rf power, as observed after 25watts.

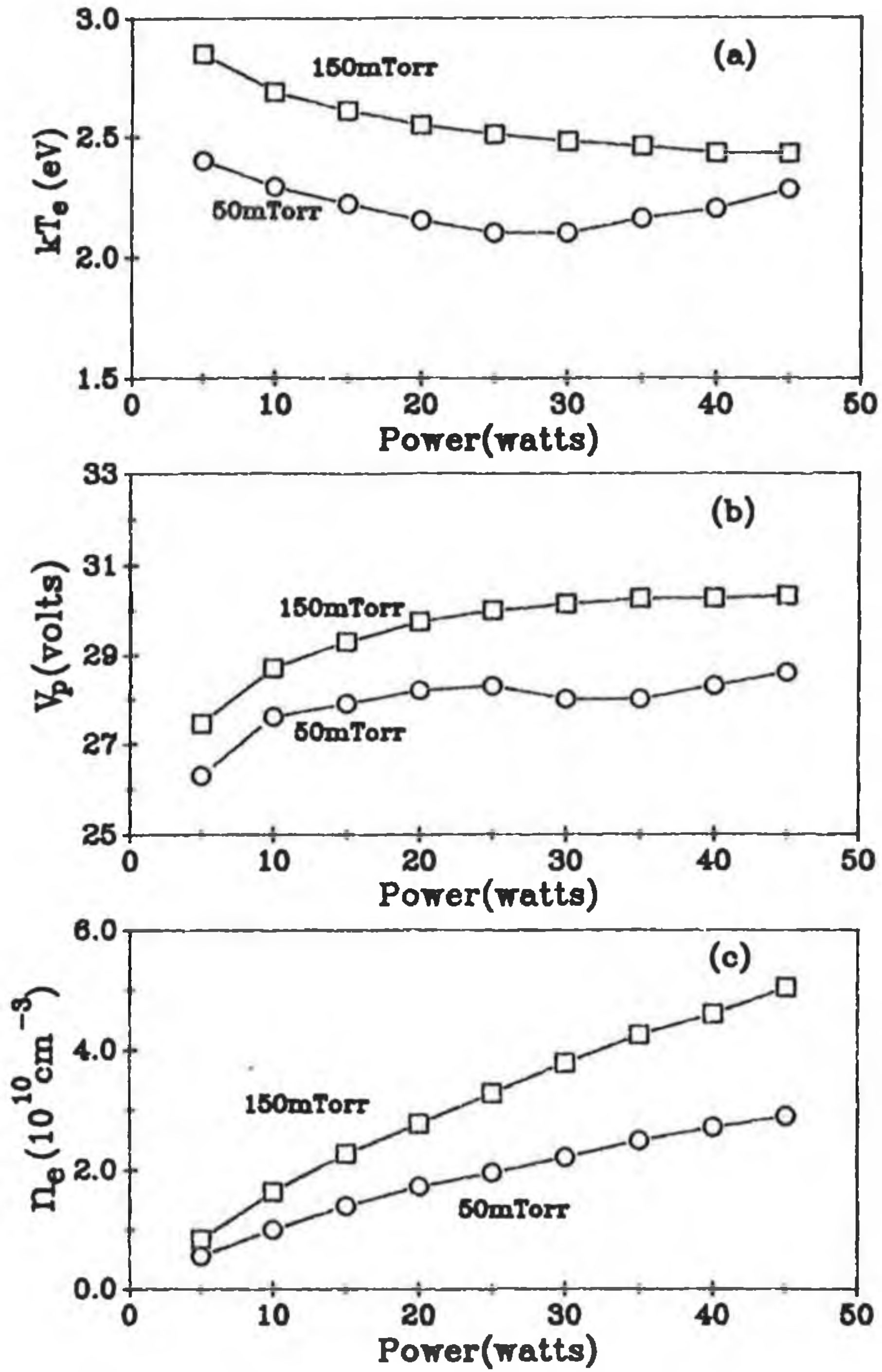

FIG.4.8: Power dependence of (a)kT_e, (b)V_p, and (c)n_e in a 13.56MHz, 20watt argon plasma.

4.6 Accuracy of the measured plasma parameters

The accuracy of the measured plasma parameters depends on (a)the stability of the rf plasma, (b)the successful operation of the tuned probe, (c)the consistency and accuracy of the computer analysis, (d)the operation of the data acquisition system and (e)adherence to the defined (eqn.2.1) pressure regime. It has been found, however, that the plasma parameters are reproducible to within a few percent over extensive data sets, and over long periods of time. For example, after several runs the drifts of less than 10% in kT_e are typical. Similarly for the plasma potential and the electron density. Thus the rf plasma seems to be very stable in time. The successful operation of the tuned probe has been checked by measuring the plasma parameters in the rf afterglow. Systematic errors in the parameter determination has also been addressed. For example, kT_e is also determined via the eedf analysis, and it is found that kT_e determined in this way is always slightly less (of the order of 10% to 15%) than the value obtained from equation 2.7. Thus systematic errors in the software analysis are checked by an independent analysis method. The data acquisition system has been the subject of extensive calibration and improvement[52]. The electron temperature is considered to be accurate to within about 15%.

The electron density is also determined from the integral of the measured eedf (see chapter five) and n_e determined from this method and from equation 2.8 agree to within a factor of two. This defines the accuracy of the electron density measurement. The plasma potential is accurate to within kT_e/e since the characteristic is exponential in the region where V_p is determined[42].

CHAPTER FIVE

RESULTS AND DISCUSSION OF EEDF MEASUREMENTS

5.1 Introduction

As discussed in section 2.3, one of the most basic characteristics of any gas discharge is the electron energy distribution function, since electrons are responsible for the majority of physical and chemical processes. Indeed, the modeling of gas discharges requires knowledge of the rate coefficients for electron induced processes, which requires knowledge of the eedf.

Since rf discharges are widely used, both at research and processing levels, it is important that the eedf's of rf discharges be measured. The problems associated with Langmuir probes (which are extremely effective in measuring eedf's, permitting both spatial and temporal resolution) has made this task difficult. Since the eedf is obtained from the second derivative of probe current,

the eedf is particularly sensitive to both rf interference and improper employment of probe technique or improper interpretation of probe results. However, if all problems are surmounted, which is possible, probe measurements will remain the most effective in returning valuable information on rf discharges.

Similar to the plasma parameter measurements, eedf measurements have been concentrated, for the most part, on argon and nitrogen discharges. Some rf plasma afterglow eedf's have also been measured. Related to these measurements, and to the eedf's of rf discharges in general, the role of super-elastic collisions and metastable states is also discussed in this chapter.

5.2 EEDF's measured in argon rf plasmas

Figure 5.1a shows an eedf measured in a 20watt, 13.56MHz argon plasma at 30mTorr. It can be approximated by a bi-Maxwellian distribution with a bulk electron temperature of 1.7eV and a "fast" electron temperature, kT_{fe}, of 3.2eV. The low energy group is thermalized by electron-electron collisions, while the high energy group temperature is probably a consequence of rf sheath heating[36]. Figure 5.1b shows an eedf measured in a

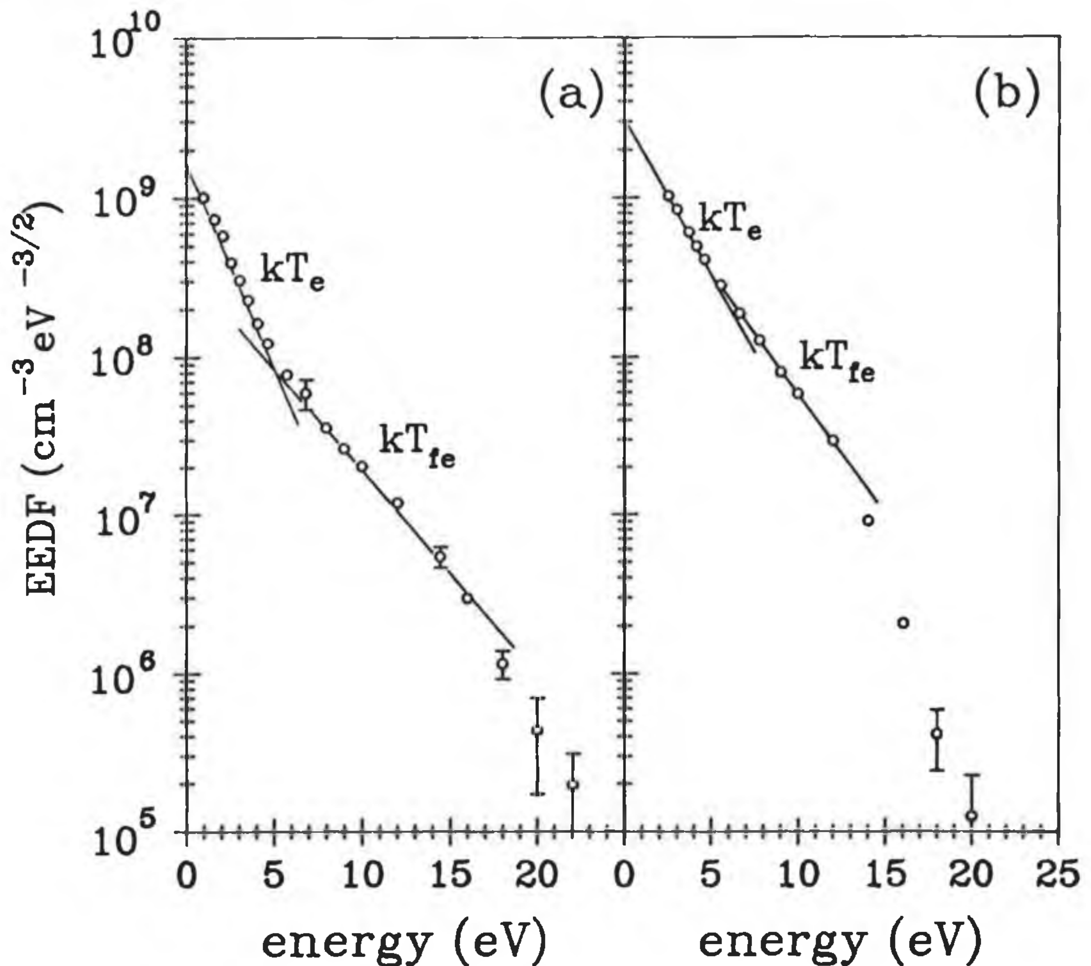

FIG.5.1: EEDF measured in a 13.56MHz, 20watt argon plasma at (a)30mTorr and (b)125mTorr.

20watt, 13.56MHz argon plasma at 125mTorr, with kT_e=2.1eV and kT_{fe}=2.9eV. Both eedf's decay rapidly above the ionization potential (15eV), especially in the high pressure case, due to increased inelastic collisions with the neutral gas.

Electrostatic probe measurements are, in general, inaccurate close to the plasma potential, particularly at low electron energies when the probe bias is within kT_e of V_p. This results in very large error bars, and these results are not plotted. No evidence of rf convolution (which would tend to broaden the eedf) is apparent. As found from the plasma parameter measurements, the general tendency is for the bulk electron temperature to increase with increasing pressure. The values of kT_e extracted from the eedf measurements are always slightly lower than those deduced from the probe IV characteristic. This is due to difficulties associated with accurate determination of the plasma potential (see eqn. 2.7 and section 2.2) in the software analysis. The error, however, is small and may be ignored. The eedf measurements are taken to be accurate. As is evident from figure 5.1, the eedf can be determined to five orders of magnitude with the tuned probe.

The electron density n_e, determined from the probe electron saturation current, agrees to within a factor of two with the electron density measured from the integral of the eedf.

The plasma production rate, P_i, is given by eqn. 4.1. It has been calculated using the cross-sections listed in ref.14 and the measured eedf's at several discharge gas pressures. Figure 5.2 is a plot of P_i as a function of argon pressure. P_i lies in the range $1x10^{15}cm^{-3}s^{-1}$ to $2x10^{15}cm^{-3}s^{-1}$, displays no marked dependence on pressure, but appears relatively constant. At pressures greater than 100mTorr, the contribution of the extrapolated ion current to the tail of the eedf may become significant. This contribution is not corrected for, since the exact

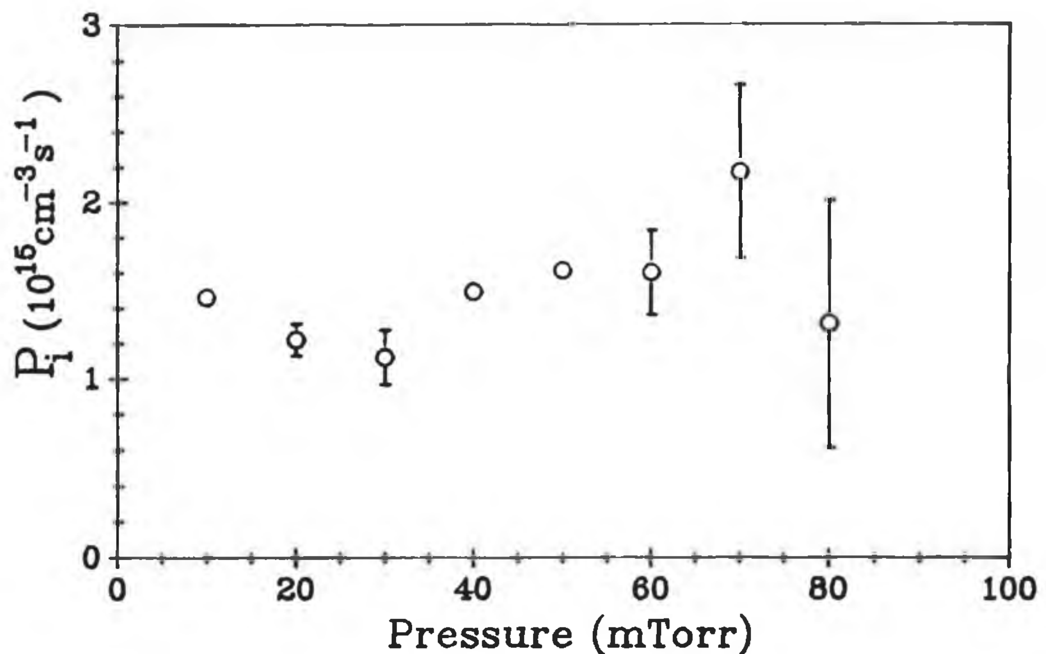

FIG.5.2: Calculated plasma production rate as a function of gas pressure in a 13.56MHz, 20watt argon plasma.

laws governing the ion current extrapolation are not accurately known. Thus, large error bars are presented on the production rate values. Also, since the driving rf power measurement is only accurate to within a factor of two, small fluctuations in the calculated production rate are to be expected.

The fast electron density

$$n_{fe} = \int_{eV_i}^{\infty} f(\varepsilon).d\varepsilon \quad \ldots \quad (5.1)$$

where eV_i is the ionization potential, is found to decrease with increasing pressure (in the regime of fig.5.2), which is as expected, since n_o increases and the production rate remains virtually constant. These fast electrons are lost via inelastic collisions with the neutral gas (neutral cooling) as the pressure increases.

At low pressures (diffusion regime), the plasma ionization balance is as follows. The loss rate of positive ions (and electrons) is governed by particle flux to the electrodes. An estimate of the current density to each electrode gives an approximate value for plasma loss rate. Typical operating conditions are: rf power = 20watts, rf driving voltage = 900V (peak-to-peak) and electrode area = 50cm^2. The sheath impedance contains

both a capacitive and a resistive term, but it is the resistive component which governs ion flux to the electrodes. Thus, the ion flux is determined by the discharge conduction current, which can be estimated as

$$I_{rms} = \text{Input power} / V_{rms} \qquad (5.2)$$

where V_{rms} is the root mean square of the rf driving voltage and I_{rms} is the root mean square of the resistive (or conduction) discharge current. The usual phase term $\cos\phi$ is not included, since we consider only real current. Therefore, the current density is 1.2mA/cm^2, corresponding to a positive ion flux of 3.8×10^{15} electrons cm^{-2}s^{-1}, and an equal electron flux. A total of 7.5×10^{15} charged particles are lost per cm^2 per second. Since the input power is only accurate to within a factor of two, so also is this estimated loss rate.

The loss rate must be balanced by a plasma ionization rate. Since the length of the glow region of the discharge is approximately 3.0cm (taking both sheath lengths as a total of 0.5cm, corresponding to the original electrode arrangement), then the ionization rate must be approximately 1.3×10^{15} electrons cm^{-3}s^{-1}. In a 20watt, 30mTorr argon plasma with n_e=1×10^{10}cm^{-3}, the production rate has been calculated (using eqn. 4.1) at 1.1×10^{15} electrons cm^{-3}s^{-1}, using the measured eedf shown in fig.5.1a, which agrees well with our estimated loss rate. Note that spatial eedf measurements have indicated that the rf argon plasma is spatially homogeneous between the

electrodes, so that the above calculation is valid. While this ionization balance is a first order approximation, a similarly good agreement between plasma production and loss is achieved over a wide range of pressures in argon. Clearly, as the pressure is increased, the accuracy of the calculated production rate diminishes (see fig.5.2). It is clear that the measured eedf's can explain the ionization rate, in the case of the argon discharge, through a single step ionization process.

5.3 EEDF's measured in nitrogen rf plasmas

Figure 5.3 shows an eedf measured in a nitrogen, cold cathode dc discharge at 300mTorr. The bulk electron group is apparently Maxwellian with an associated temperature, kT_e=0.19eV. This thermalizing of the bulk group results from electron-neutral and electron-electron elastic collisions. At energies above 2eV, the effects of inelastic collisions become dominant. In particular, a

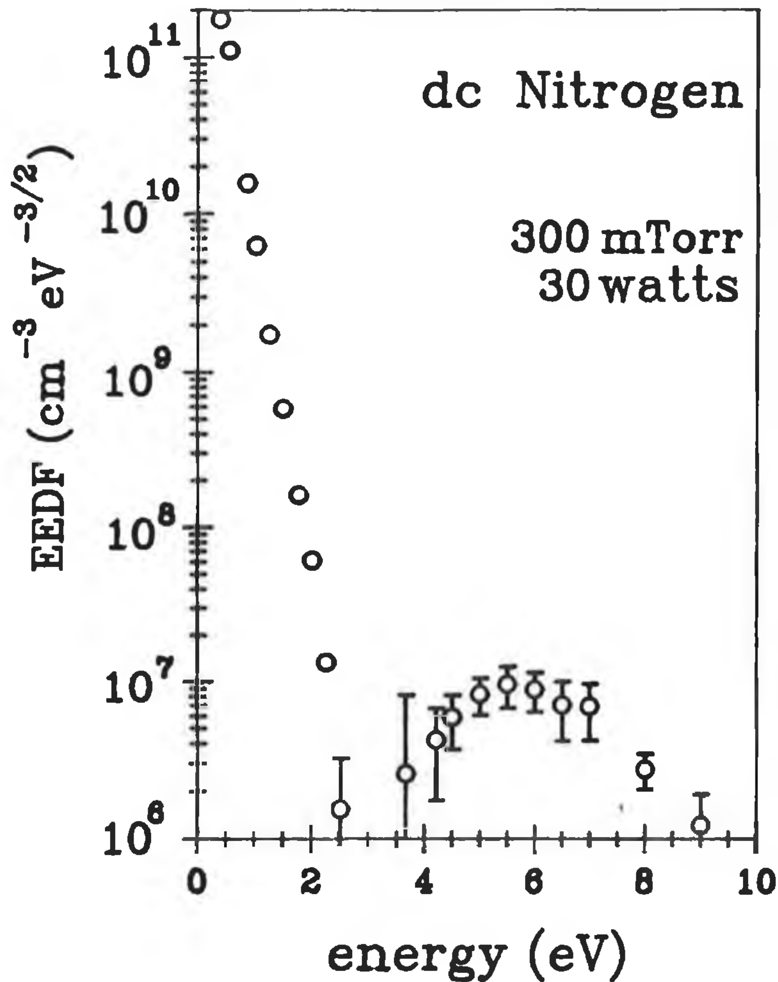

FIG.5.3: EEDF measured in a dc nitrogen discharge.

"hole" appears in the eedf between 2eV and 4eV. This feature has been reported previously in a beam produced plasma[85] and a low-pressure hot cathode discharge[86]. It has also been observed in a 100kHz discharge[60] using a time-resolved Langmuir probe. The feature is due, essentially, to the depletion of electrons due to inelastic collisions involving the vibrational excitation of the N_2 molecule. Between 2eV and 4eV, the eedf is not thermalized, because inelastic collisions (vibrational excitation of the nitrogen molecule) dominate the electron-electron collisions.

Above 4eV, the eedf can be populated by either of two mechanisms. Firstly, by superelastic collisions involving N_2 metastable states. Secondly, by an electron beam produced by secondary electrons which have been degraded via inelastic collisions. A reduction in loss rates below the ionization threshold results in a tail in the eedf. It is possible that each mechanism dominates under different conditions.

Figure 5.4 shows an eedf measured in a 20watt, 13.56MHz nitrogen plasma at 10mTorr. It contains two very distinct Maxwellian groups, with kT_e=1.1eV and kT_{fe}=3.7eV. As the gas discharge pressure is increased, the "hole" observed in the dc glow eedf appears in the nitrogen eedf.

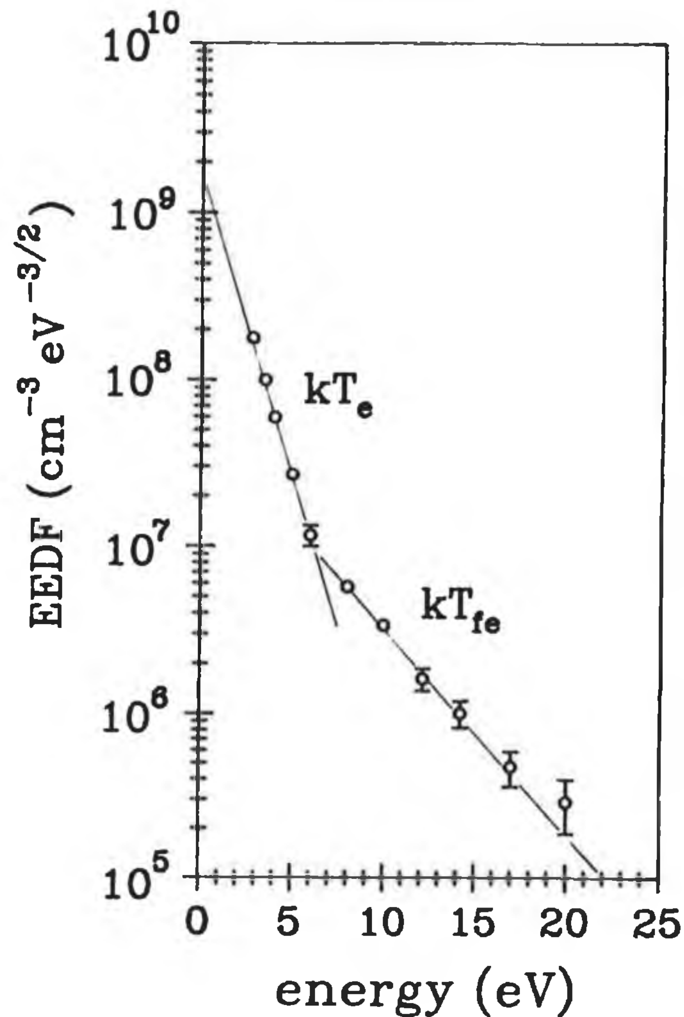

FIG.5.4: EEDF measured in a 13.56MHz, 15watt nitrogen plasma at 10mTorr.

Figure 5.5 shows an eedf measured in a 13.56MHz plasma under similar operating conditions as the dc discharge eedf of fig.5.3. It shares the essential features of the dc discharge eedf. However, the bulk electrons are hotter (with a bulk electron temperature of about 1eV), although the distribution function is not obviously Maxwellian at low energies. Between 1.5eV and 3.5eV, however, the slope of the eedf corresponds to a

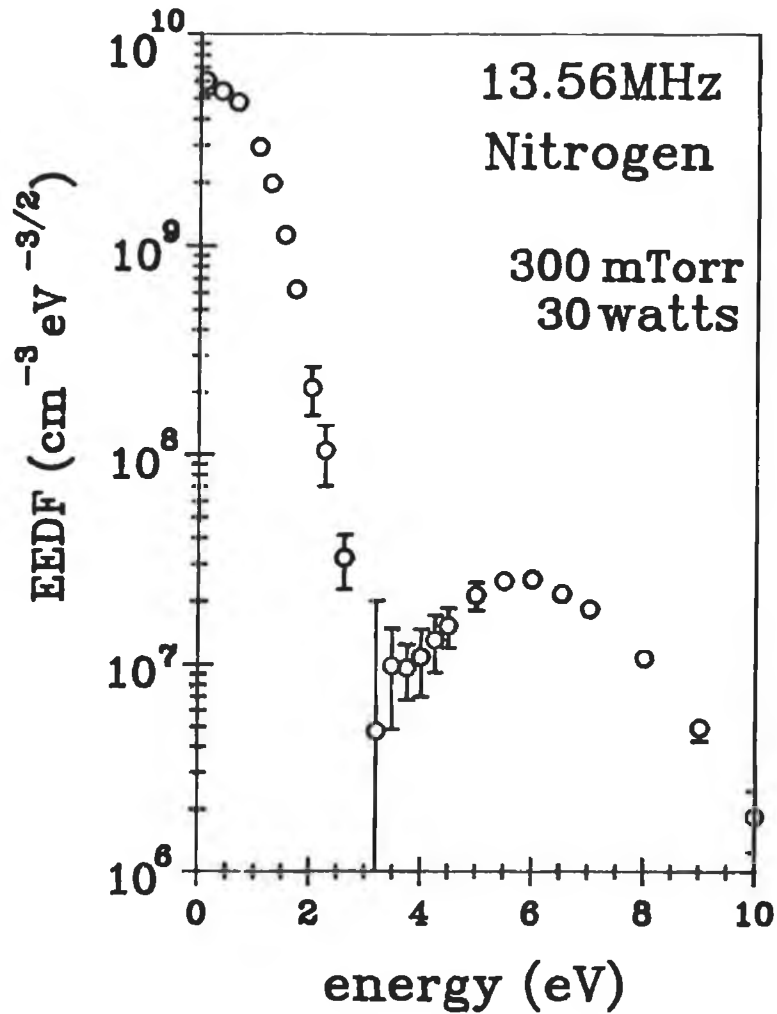

FIG.5.5: EEDF measured in a 13.56MHz, 30watt nitrogen plasma at 300mTorr.

temperature of 0.34eV. Also, the region between 2eV and 4eV is not so depopulated as in the dc case.

The density of electrons at each energy is determined by the balance of electron production and loss at that energy. Thus, the energy interval between 2eV and 4eV is

populated by either beam electrons or superelastic electrons and depopulated by inelastic collisions involving the vibrational excitation of N_2. Also, the region can be populated by bulk electrons, and since kT_e in the rf plasma is greater than kT_e in the dc plasma, this may be the reason for differing degrees of eedf density in this interval.

The apparent peak in the eedf between 5eV and 7eV could correspond to the energy of secondary electrons produced by electron-metastable collision ionization of metastable nitrogen[87], suggesting that superelastic collisions may be the mechanism for eedf population in the high energy region.

The plasma production rate for single step ionization is given by eqn 4.1. Using the measured eedf's, the calculated production rate in the rf N_2 plasma has been compared to the estimated loss rate, for typical power densities of 0.6 watts/cm^{-2}, as in the case of argon. At the low pressure (fig.5.4), the production and loss rates balance. In the case of the higher pressure eedf (fig.5.5), the plasma loss rate is at least three orders of magnitude greater than the estimated production rate (see section 5.2). There are two possible explanations. Firstly, there is a possible source of gas ionization other than from direct single step ionization (electron

impact ionization of the ground state nitrogen molecule), and this could be energy returned from excited states such as the metastable states (electron-metastable collision ionization). Secondly, the ionization may not be evenly distributed throughout the glow. Spatial eedf measurements (fig.5.7) and initial calculations suggests that this does not fully explain the imbalance[88].

Figure 5.6 shows the evolution of the eedf with increasing gas pressure. The salient feature is the increasing depopulation of the 2eV to 4eV energy interval as gas pressure increases. This corresponds to increasing electron depletion via vibrational excitation of the N_2 molecules. Note also, the depletion of fast electrons in the tail of the distribution, via neutral gas cooling, as pressure increases.

Unlike the dc plasma, the N_2 eedf's measured in the rf plasma display a Druyvesteyn like shape at low energies. A Maxwellian velocity distribution has the form

$$f(v) = n.(m/2\pi kT)^{3/2}.\exp(-mv^2/2kT) \qquad (5.3)$$

whereas a Druyvesteyn velocity distribution is given by

$$f(v) = C.\exp(-3\delta m^2v^4/8\lambda^2e^2E^2) \qquad (5.4)$$

where δ is the fractional energy transfer in an elastic collision, λ is the mean free path between collisions and E is the electric field. The essential point to notice is that the Druyvesteyn distribution varies as $\exp(-v^4)$

rather than as $\exp(-v^2)$ as for a Maxwellian. The Druyvesteyn distribution thus predicts more electrons with energies around the average energy, but many fewer electrons with energies greater than a few times the average[(1),(2)]. The reason for the Druyvesteyn shape of the nitrogen eedf's in the rf plasma is not clear, and the problems associated with probe measurements close to the plasma potential must be borne in mind. Druyvesteyn electron energy distributions are associated with the presence of dc fields in the bulk plasma resulting in very little electron-electron collisions. Rockwood[(89)] has pointed out that although electron-electron collisions may be important in atomic gases, even at low fractional ionization, they are unlikely to play any significant role in molecular gas discharges. The ambipolar field in the nitrogen rf discharge has been measured at approximately 2V/cm (see section 4.4) which may explain the observed shape.

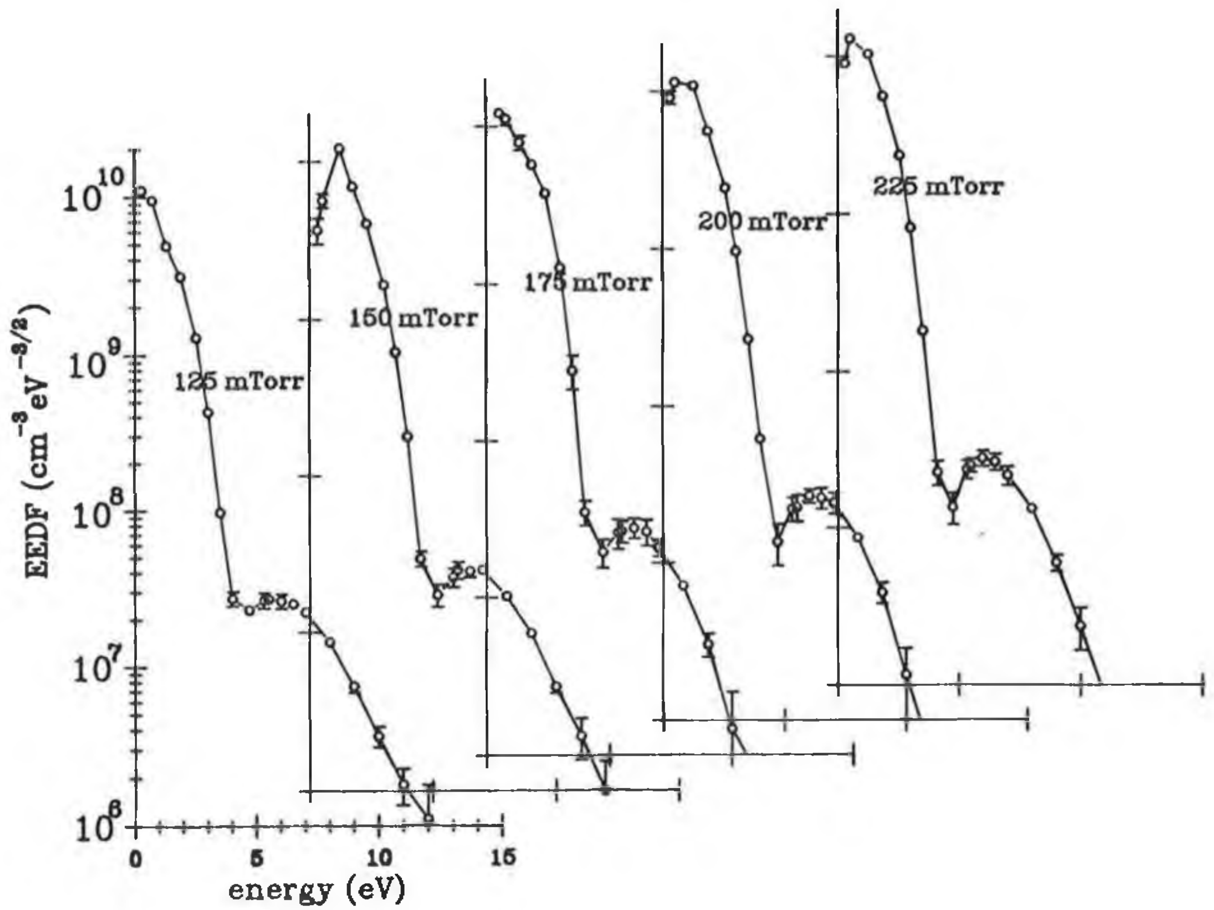

FIG.5.6: EEDF as a function of gas pressure in a 13.56MHz, 30watt nitrogen plasma.

The spatial dependence of the nitrogen rf plasma eedf has also established. The results are shown in figure 5.7, for a 20watt, 13.56MHz plasma at (a)100mTorr and (b)250mTorr. These pressures were chosen having considered the pressure dependence (figs.4.3 and 5.6) and spatial dependence (fig.4.6) of the nitrogen plasma parameters, the conditions being quite different in both cases. There are a number of salient features worthy of discussion.

In the high pressure case, fig.5.7b, the tail of the eedf can be seen to decay as a function of distance from the driven electrode. This is as expected, since the mean free path for electron elastic collisions is of the order of 1mm. The concept of "electrostatic confinement", as discussed in chapter six, requires that fast electrons, which are confined by the plasma-anode sheaths, be numerous throughout the glow. However, these electrons originate via ionic bombardment of the driven electrode, and thus tend to exist in greater densities near this electrode.

In the low pressure case, fig.5.7a, the tail of the eedf again decays with increasing distance from the driven electrode, but not as rapidly as the high pressure case. Also, the electron depletion region appears to increase in this direction which may be due the associated decrease in

electron temperature. A further feature is the anomaly apparent in the 100mTorr eedf near the driven electrode. This is only observed at these low pressures, and close to the rf sheath, regardless of input power. Referring to fig.4.6b, the potential between X=1.5 and X=2.5, at 100mTorr, is no more than 2V, so that the effect would not be smoothed by the plasma electric field. Rather, it appears to be associated with the proximity to the rf sheath (see fig.4.6a). Since, the plasma parameters, kT_e and n_e are modulated in the sheath[22], time averaged probe measurements at the sheath edge may be invalid.

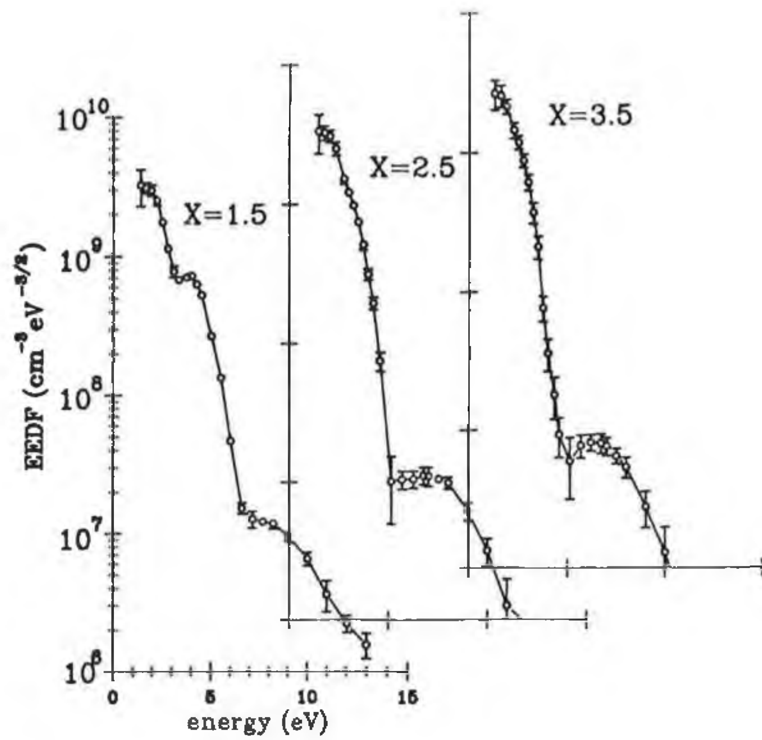

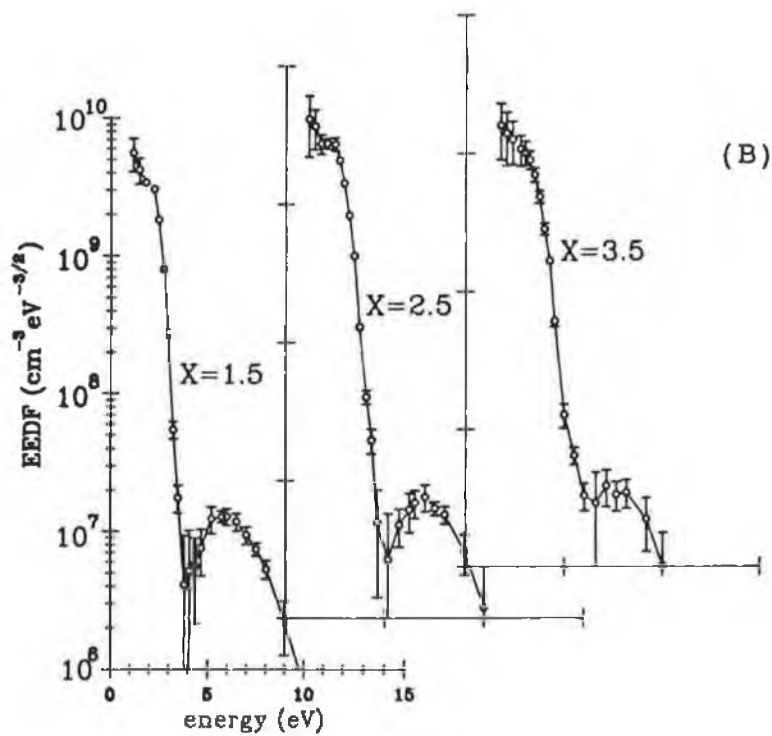

FIG.5.7: Spatial dependence of the eedf in a 13.56MHz, 20watt nitrogen plasma at (A)100mTorr and (B)250mTorr.

5.4 Afterglow eedf's and the influence of super-elastic collisions on the eedf structure

Nitrogen eedf's, measured both in dc and rf discharges, have been presented in the previous section. They are of specific interest in terms of atomic/molecular physics. In particular, they illustrate the interaction of plasma electrons with excited gas species. The "hole" observed between 2eV and 4eV is essentially due to electron depletion by excitation of the vibrational molecular levels of nitrogen. Also, it is suspected that the region between 5eV and 7eV is populated by electrons which gain energy in super-elastic collisions; i.e. electron-metastable collisions resulting in de-excitation of the metastable atom/molecule and a "fast" electron. As previously discussed, the nitrogen eedf does not account for the plasma production rate, and the ionization rate could well be dominated by electron-metastable collision ionization. Also, interactions between vibrationally excited nitrogen, $N_2(\nu)$, and metastable nitrogen, N_2^*, could be a significant ionization process, since considerable energy is stored in these molecular states. Certainly, the ionization process in N_2 is complex and worthy of further investigation. To this end, there have been several theoretical or modeling publications on the nitrogen eedf, both in dc and rf discharges[83],[84], and also in discharge afterglows[87].

In the light of the above, eedf's were measured in the N_2 afterglow, for various discharge conditions. At low pressures, in the diffusion regime, the fast electron density is known to decay rapidly (<10μs). Thus, fast eléctrons appearing in the eedf at long times (>50μs) into the post-discharge are evidence of the interaction of metastable species with the eedf. Also, recent theoretical work on the N_2 afterglow eedf has demonstrated that the eedf measured in the post-discharge can be influenced dramatically by the so-called "residence" time of the discharge on pulse. For example, if the residence time is short (of the order of 50μs), then N_2^* states can become much more numerous in the discharge than $N_2(\nu)$ states, whose population increases more slowly. The afterglow eedf of a short residence time pulsed plasma should be rich in super-elastic electrons but display little evidence of electron depletion in the 2eV to 4eV region. Conversely, if the residence time is long (of the order of 300μs), then the afterglow eedf will be determined primarily by electronic interaction with the vibrational molecular levels, which have become numerous in the relatively long on pulse. The structure will be quite different to the structure of the afterglow eedf associated with the short residence time.

Figure 5.8 is an example of an eedf measured in a nitrogen rf plasma afterglow. The plasma on time is 100μs, the off time is 300μs, so that the repeat rate is 2.5kHz. This eedf is typical of all those measured in the nitrogen afterglow. Clear evidence of metastable influence on eedf structure has been obtained. Also, in the case of the residence time experiments, the afterglow eedf's have proved to be far too noisy to separate

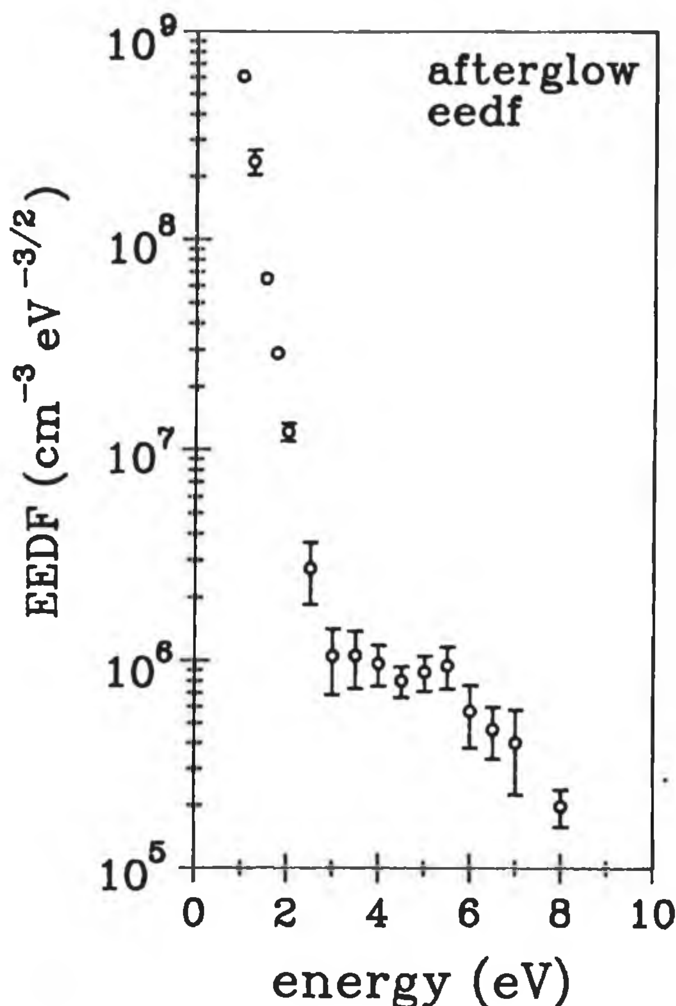

FIG.5.8: EEDF measured 15μs into the afterglow of a 13.56MHz, 15watt nitrogen pulsed plasma at 10mTorr.

metastable nitrogen and vibrationally excited nitrogen action on the eedf structure. Typical plasma off times in these experiments must be of the order of one or two milli-seconds, to ensure that the plasma decays fully. Also, low pressures are preferred, since the tail of the eedf decays more rapidly in high pressure afterglows. In order to improve the obtained results, it is necessary to increase the discharge power, thereby increasing the populations of plasma species.

Some afterglow measurements were also made on helium rf pulsed plasmas, since helium is known to contain several important metastable transitions. Figure 5.9 is a plot of the decay of the helium eedf at progressively longer times into the afterglow. The presence of super-elastic electrons is un-ambiguous. This structure, with apparent peaks in the eedf at about 7eV, can also be observed in a cw rf discharge. Figure 5.10 shows such an eedf, measured in a 20watt, 13.56MHz helium plasma at 1Torr.

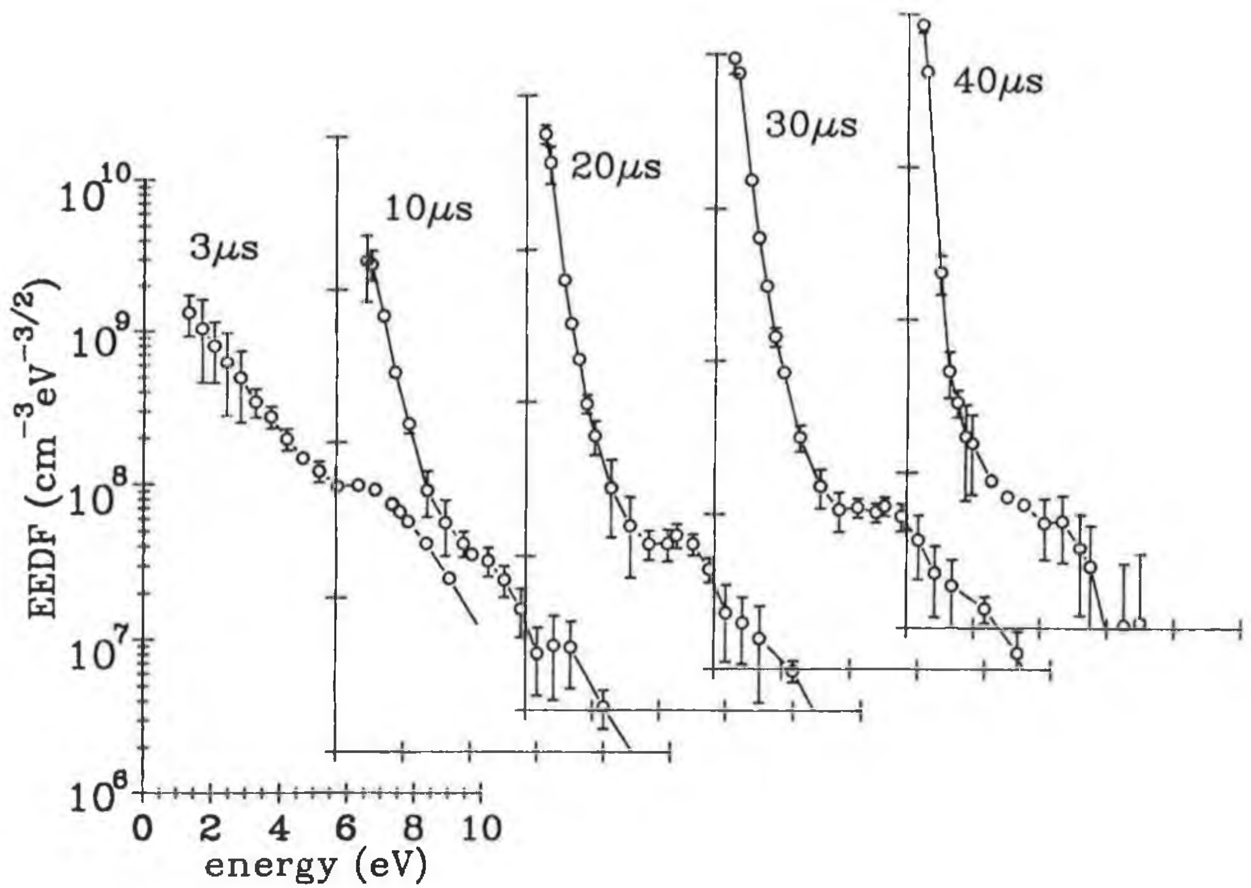

FIG.5.9: Temporal evolution of the eedf in the afterglow of a pulsed 13.56MHz, 15watt helium plasma at 150mTorr. The plasma on time is 100μs and the plasma off time is 300μs.

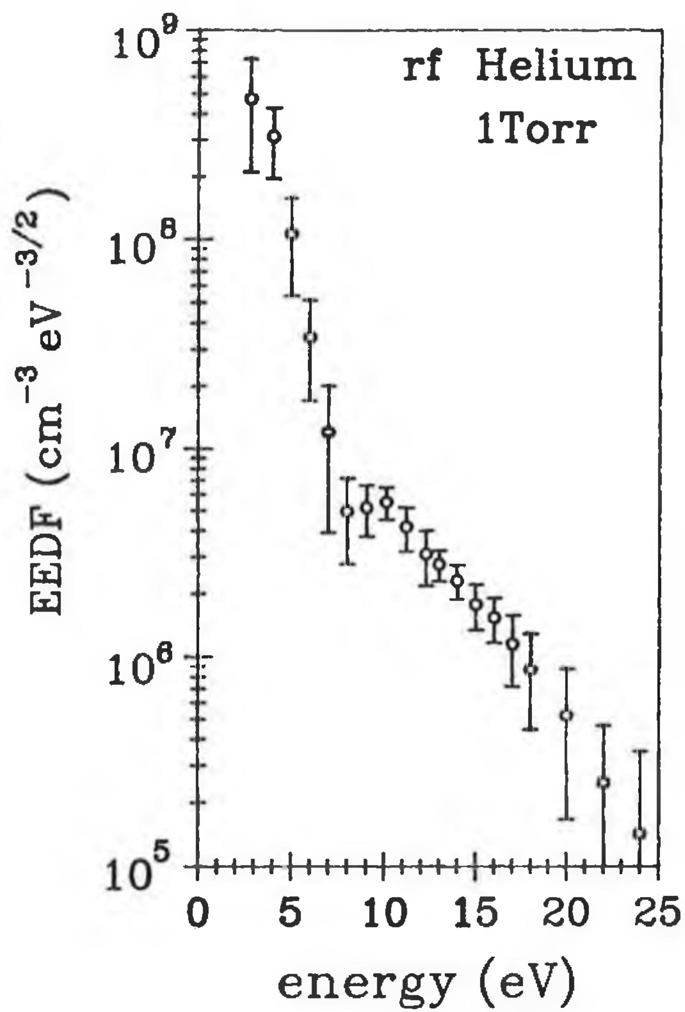

FIG.5.10: EEDF measured in a 13.56MHz, 20watt helium plasma at 1Torr.

CHAPTER SIX

ELECTROSTATIC CONFINEMENT IN RF PLASMAS

6.1 Introduction

The Langmuir probe measurements of both the eedf's and plasma parameters appear to confirm that the low pressure argon, and indeed nitrogen, rf plasma is sustained by electron impact ionization of the ground state atom or molecule by energetic electrons in the tail of the energy distribution, close to the ionization threshold (ε_{th}), with energies ε given by

$$\varepsilon_{th} < \varepsilon < 25eV$$

There appears to be no contribution from higher energy electrons ($\varepsilon > 25eV$). The electrons in the range ε_{th} to 25eV appear isotropic, despite the fact that their mean free path exceeds the chamber length. In the case of high pressure nitrogen plasmas, a source of ionization other than single step ionization may be responsible for plasma production . At low pressures (≤100mTorr), dc discharges

cannot be sustained in the described discharge configuration. A heating mechanism (namely, sheath oscillation heating) has been postulated to explain the persistence of the rf glow at low pressures. However, the fact remains that the mean free path of the ionizing electrons exceeds the chamber dimension at these low pressures, so that regardless of the existence of an electron heating mechanism, the fast electrons should be lost to the chamber walls before gas collisions occur.

Multipole or "bucket" ion sources, in which fast electrons are confined in the plasma via strong surface magnetic fields, can be operated down to pressures of about 1mTorr. The fast electrons are deflected from the chamber walls, and confined to traversing the plasma bulk, so that the chamber dimension is effectively much larger, and becomes comparable to or greater than the electron mean free path.

Clearly, a confinement mechanism peculiar to rf plasmas, which traps fast electrons, would explain both the improved efficiency at low pressures and the observation of fast electrons in the low pressure eedf's.

6.2 The confinement mechanism

In general, the plasma potential in the quasi-neutral region of a gas discharge must be positive with respect to any large electrode area to prevent excessive loss of electrons. Thus, the potential gradient across a dc discharge is typically represented as in figure 6.1. The anode is grounded, as are the walls, and the cathode is biased negatively. The plasma potential sits about 1volt positive, depending on the gas pressure. Electrons escape to the walls and to the anode down the plasma-anode sheath, which is in this case about -1volts. Bulk electrons, with energies less than 1eV cannot escape, and

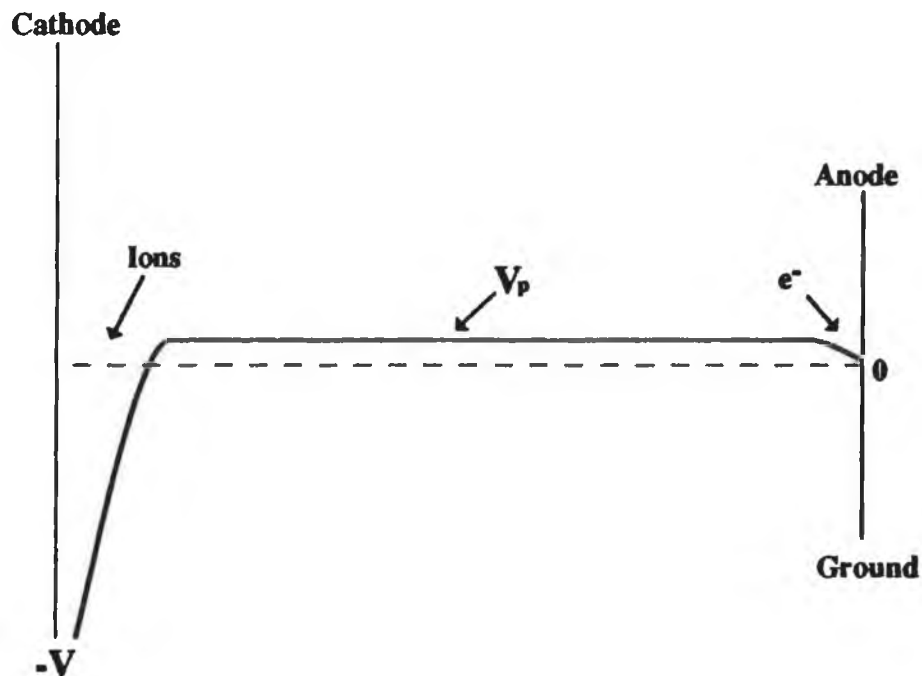

FIG.6.1: Potential gradient across a dc discharge.

thus the bulk temperature is about 1eV. The cathode sheath is very negative, so that electrons are reflected and positive ions are accelerated to the cathode.

Figure 1.3 is an illustration of the expected temporal evolution of the driving potential, $V_{rf}(t)$, and typical plasma potential, $V_p(t)$, waveforms for a capacitively coupled rf discharge. Figure 6.2 is a representation of the potential gradient across such an rf discharge at the two extremes of the cycle. When the driving potential is positive, the driven electrode acts as the momentary anode. When $V_{rf}(t)$ is negative, the grounded electrode is the momentary anode. The momentary anode sheath potential is the difference between the

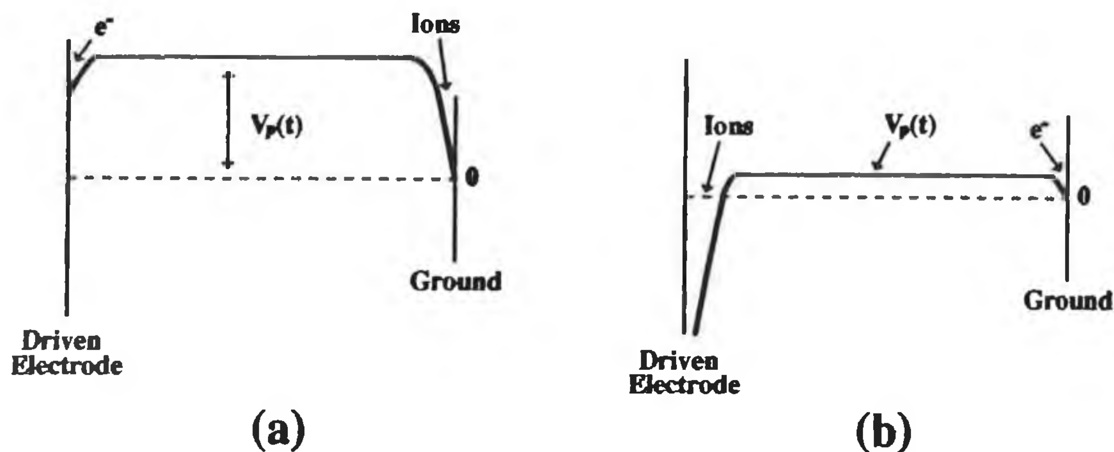

FIG.6.2: Potential gradients across an rf discharge at the peak and trough of the rf cycle.

plasma potential and the momentary anode potential. In dc plasmas this potential is of the order of 1volt, and fast electrons easily escape to the anode. Fast electrons are always confined by the cathode sheath, being repelled by the high cathode fall potential.

At low driving frequencies, where $\omega < \omega_i$, the rf sheath is resistive and the plasma potential appears as V_{p1} in fig. 1.3. The momentary anode sheath remains relatively small over the rf cycle, and fast electrons are lost as in a dc discharge. When the driving frequency is high, so that $\omega > \omega_i$, then the rf sheath is capacitive and the plasma potential appears as V_{p2}. In this case, the momentary anode sheath potential is quite large over most of the rf cycle and fast electron confinement is possible. Also shown is the intermediate case, V_{p3}, where the rf sheath contains both a capacitive and a resistive term and electrostatic confinement of ionizing electrons is also possible.

In order to estimate the magnitude of the electrostatic confining voltages, a simple simulation was executed. Typical conditions were taken as; V_{rf}=800volts (peak-to-peak), dc bias=300volts. These values are easily measured. The magnitude of the momentary anode sheath potential is then simply the difference between the plasma potential and the momentary anode potential. In the first case, (A), the plasma potential was assumed to be sinusoidal; equal to [V_{rf}(peak) - dc bias], i.e. 100V at

the peak of the rf cycle and ground (zero volts) at the trough. In the second case, (B), the plasma potential is given a 30% contribution from the second harmonic of the driving frequency, which simulates a more resistive sheath. Figure 6.3 shows the magnitude of the momentary anode potential as a function of rf period for both cases. It is apparent that ionizing electrons are trapped in the glow for the majority of the rf cycle. For example, a 20eV electron has a transit time (for a 3.5cm electrode separation) of approximately 13ns. The rf period is about 74ns, so that referring to fig.6.3, it is possible for fast electrons to traverse the glow region several times, before escaping to either electrode.

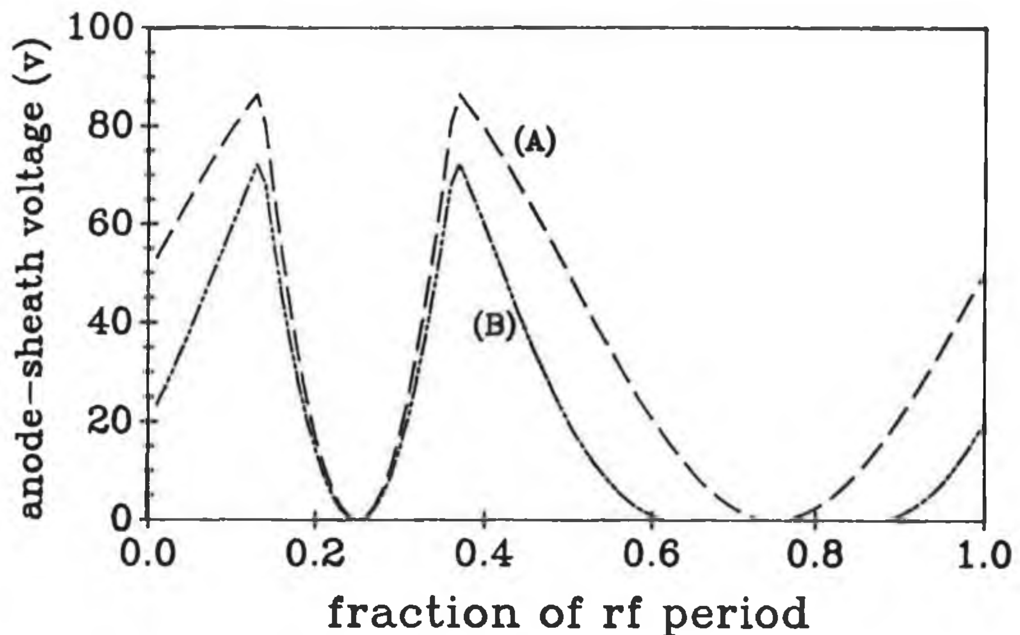

FIG.6.3: Magnitude of the anode sheath voltage as a function of the rf cycle, from a software simulation.

CHAPTER SEVEN

CONCLUSIONS

7.1 Summary of work

A tuned Langmuir probe has been used to measure plasma parameters and eedf's in argon and nitrogen rf discharges. Langmuir probe measurements have the advantages over other plasma diagnostic techniques that the eedf can be determined, and spatial resolution is possible. The technique employed, as well as sources of error, has been outlined in detail in chapter two. The tuned probe technique offsets the problem of rf convolution of the probe characteristic, so that it can be used in rf plasmas.

The recent upsurge in the use of rf plasmas as processing mediums ensures that such a diagnostic device will be well employed. The lack of diagnostic techniques on such reactors has meant that interesting (from the industry viewpoint) considerations such as etch rate,

deposition rate, surface damage, etc. are relatively unknown quantities in terms of the microscopic plasma parameters. If the plasma is well understood, and relevant parameters and functions easily monitored, then the industry can only improve in its operation efficiency.

Quite apart from understanding the actual discharge physics, it is also important to appreciate the subtlety of rf power design. Important considerations have been outlined in chapter three, including rf noise, rf impedance matching, and rf power measurement.

The tuned probe measurements reveal that the argon plasmas have a bulk temperature of between 1.5eV and 2.5eV, over a wide range of gas pressures. At low pressures the nitrogen eedf is approximately bi-Maxwellian, with a bulk temperature of about 1eV, whereas at higher pressures, the eedf is highly non-Maxwellian. Its structure is determined rather by electronic interactions with excited states of the molecule. The measured bulk temperature values are substantiated by extrapolating measurements taken in the plasma afterglow, where no perturbing effects are present. The pressure, power and spatial dependence of the bulk temperature, the plasma potential and the electron density have been presented in chapter four.

The plasma production rate calculated from the eedf's agree with the estimated loss rate in the case of argon over a wide range of pressures, whereas the eedf in high pressure nitrogen reveals that a powerful source of gas ionization other than electron impact ionization of the ground state molecule may be dominant. The influence of super-elastic collisions on the eedf structure has also been discussed in chapter five.

A description of electrostatic confinement of fast electrons in low pressure, high frequency rf plasmas was presented in chapter six. It explains the persistence of rf plasmas at pressures below which the mean free path of ionizing electrons exceeds the chamber length. The high momentary anode sheath voltages found in these plasmas results in the fact that fast electrons can only escape during a portion of the rf cycle and that the electron temperature of rf plasmas tends to be higher than in the case of dc plasmas. This fast electron trapping complements the rf sheath heating mechanism.

7.2 Suggestions for future work

The obvious, and planned, extension to this work is to apply the developed probe and knowledge to a typical processing system. For example, mixtures of argon and methane, used in deposition work, could be easily handled by the existing described arrangement. Extensive investigative work, with a functioning diagnostic tool, would be very fruitful.

In terms of the rf plasma physics, the theory of electrostatic confinement of fast electrons, which is at an embryonic stage, needs development. For instance, it is possible to construct a particle-in-cell type model, taking electrons accelerated across a sheath, passing through an almost un-collisional plasma (low pressure), and being reflected from a dynamic (voltage and spatial temporal variation) sheath. The eedf could thus be modeled and compared to the measured eedf's.

The nitrogen eedf's, which have proved interesting in terms of excited state interactions, need to be studied further. In particular, such questions as to why the observed "hole" in the eedf is not filled by electron-electron collisions (thermalized), and what role metastable atoms/molecules play in shaping the eedf. To answer the first it is necessary to compare the cross-section for electron-electron collisions and the cross-section for molecular vibrational excitation, at the

relevant eedf energy, and estimate relative reaction rates. To answer the second, again the reaction rate should be calculated, but also, via the afterglow experiments described in section 5.4, it should be possible to detect the presence of super-elastic electrons at high energies in the eedf of the afterglow plasma, if they are present. Certainly, if the pulsed plasma is operated at much higher powers, the afterglow measurements would not be so noisy.

Other outstanding work includes the need to develop suitable rf power measuring devices and examination of the behaviour of the electron density as a function of pressure in greater detail.

REFERENCES

1. B.E. Cherrington, *Gaseous electronics and gas lasers*, Oxford, Pergamon press, 1979
2. B.N. Chapman, *Glow Discharge Processes*, New York, Wiley, 1980
3. A.P. Paranjpe, Ph.D. thesis, Stanford University, 1989
4. R.W. Boswell and A.J. Perry, *LA*1, GEC90, Illinois, USA, 1990
5. R.C. Meyer, *LA*5, GEC90, Illinois, USA, 1990
6. M. Moisan and Z. Zakrzewski, *J Phys D*, 24, 1025, 1991
7. M.A. Lieberman, A.J. Lichtenberg and S.E. Savas, *IEEE Trans Plasma Sci*, 19, 189, 1991
8. M.A. Lieberman, A.J. Lichtenberg and D.F. Flamm, *Memo No. UCB/ERL M*90/10, Univ. of California, 1990
9. K.N. Leung, G.J. DeVries, W.F. DiVergilio, R.W. Hamm, C.A. Hauck, W.B. Kunkel, D.S. McDonald and M.D. Williams, *Rev Sci Instrum*, 62, 100, 1991
10. K. Köhler, J.W. Coburn, D.E. Horne, E. Kay and J.H. Keller, *J Appl Phys*, 57, 59, 1985

11. H.S. Butler and G.S. Kino, *Phys Fluids*, 6, 1346, 1963
12. Ph. Belenguer and J.P. Boeuf, *Phys Rev A*, 41, 4447, 1990
13. T.J. Sommerer, W.N.G. Hitchon and J.E. Lawler, *Phys Rev Lett*, 63, 2361, 1989
14. D. Rapp and P. Englander-Golden, *J Chem Phys*, 43, 1464, 1965
15. F.J. de Heer, R.H.J. Jansen and W. van der Kaay, *J Phys B*, 12, 979, 1979
16. A.V. Phelps and L.C. Pitchford, *JILA Information Centre Report No. 26*, Boulder, CO
17. M.J. Kushner, *IEEE Trans Plasma Sci*, 14, 188, 1986
18. V.A. Godyak and A.S. Khanneh, *IEEE Trans Plasma Sci*, 14, 112, 1986
19. V.A. Godyak and R.B. Piejak, *Phys Rev Lett*, 65, 996, 1990
20. O.A. Popov and V.A. Godyak, *J Appl Phys*, 57, 53, 1985
21. V.A. Godyak, *Sov Phys Tech Phys*, 16, 1073, 1972
22. M. Surendra and D.B. Graves, *IEEE Trans Plasma Sci*, 19, 144, 1991
23. M. Surendra, D.B. Graves and I.J. Morey, *Appl Phys Lett*, 56, 1022, 1990
24. J.P. Boeuf and Ph. Belenguer, *Non equilibrium processes in partially ionized gases*, NATO advanced study institute, Series B: Physics, edited by M. Capitelli and J.N. Bardsley, New York, Plenum, in press

25. J.P. Boeuf and E. Marode, *J Phys D*, 15, 2169, 1982

26. R.W. Boswell and I.J. Morey, *Appl Phys Lett*, 52, 21, 1988

27. V.A. Godyak, *Sov J Plasma Phys*, 2, 78, 1976

28. C.G. Goedde, A.J. Lichtenberg and M.A. Lieberman, *J Appl Phys*, 64, 4375, 1988

29. M.A. Lieberman, *IEEE Trans Plasma Sci*, 16, 638, 1988

30. M.A. Lieberman, *IEEE Trans Plasma Sci*, 17, 338, 1989

31. K.U. Riemann, *J Appl Phys*, 65, 999, 1989

32. H.R. Koenig and L.I. Maissel, *IBM J Res Develop*, 14, 168, 1970

33. A.J. van Roosmalen, W.G.M. van den Hoek and H. Kalter, *J Appl Phys*, 58, 653, 1985

34. P. Bletzinger and M.J. Flemming, *J Appl Phys*, 62, 4688, 1987

35. P. Bletzinger, *J Appl Phys*, 67, 130, 1990

36. J.V. Scanlan and M.B. Hopkins, *J Vac Sci Technol*, to be published

37. J.V. Scanlan and M.B. Hopkins, *G64*, *ICPIG XX*, Pisa, Italy, 1991

38. G.A. Hebner, J.T. Verdeyen and M.J. Kushner, *J Appl Phys*, 63, 2226, 1988

39. L. Schott, in *Plasma Diagnostics*, edited by W. Lochte-Holtgreven, Amsterdam, 1968

40. F.F. Chen, in *Plasma Diagnostic Techniques*, edited by R.H Huddlestone and S.L. Leonard, Academic Press, New York, 1964

41. J.G. Laframboise, Univ. of Toronto, Institute for Aerospace Studies, *Report No.* 100, 1966

42. M.B. Hopkins and W.G. Graham, *Rev Sci Instrum*, 57, 2210, 1986

43. M.B. Hopkins and W.G. Graham, *J Phys D*, 20, 838, 1987

44. M.B. Hopkins, M. Bacal and W.G. Graham, *J Phys D*, 24, 268, 1991

45. M.J. Druyvesteyn, *Z Phys*, 64, 781, 1930

46. M.B. Hopkins and W.G. Graham, *J Appl Phys*, 69, 3461, 1991

47. D. Hickey, *PhD Thesis*, University College Dublin, 1975

48. R.H. Sloane and E.I.R. McGregor, *Phil Mag*, 18, 193, 1934

49. N. St.J. Braithwaite, *Plasma parameters and the use of Langmuir probes*, internal report

50. J.F. Waymouth, *J Appl Phys*, 37, 4492, 1966

51. E. Blue and J.E. Stanko, *J Appl Phys*, 40, 4061, 1969

52. J.C. Molloy, *MSc Thesis*, Dublin City University, 1990

53. H. Kawano, B.M. Annaratone and J.E. Allen, *G46*, *ICPIG XX*, Pisa, Italy, 1991

54. M.J. Kushner, *J Appl Phys*, 53, 2939, 1982

55. V.A. Godyak and O.A. Popov, *Sov Phys Tech Phys*, 22, 461, 1977

56. V.A. Godyak and S.N. Oks, *Sov Phys Tech Phys*, 24, 784, 1979

57. V.A. Godyak and S.N. Oks, *Sov Phys Tech Phys*, 24, 1255, 1979

58. V.A. Godyak and Z. Kh. Ganna, *Sov J Plasma Phys*, 6, 372, 1980

59. M. Capitelli, R. Celiberto, C. Gorse, R. Winkler and J. Wilhelm, *J Phys D*, 21, 691, 1988

60. M.B. Hopkins, C.A. Anderson and W.G. Graham, *Europhys Lett*, 8, 141, 1989

61. C.A. Anderson, W.G. Graham and M.B. Hopkins, *Appl Phys Lett*, 52, 783, 1988

62. C.A. Anderson, M.B. Hopkins and W.G. Graham, *Rev Sci Instrum*, 61, 448, 1990

63. M. Surendra and D.B. Graves, *Phys Rev Lett*, 66, 1469, 1991

64. M.J. Colgan, N. Kwon, Y. Li and D.E. Murnick, *Phys Rev Lett*, 66, 1858, 1991

65. W.G. Graham, C.A. Anderson and K.R. Stalder, *E67*, *ICPIG XX*, Pisa, Italy, 1991

66. N. Hershkowitz, M.H. Cho, C.H. Nam and T. Intrator, *Plasma Chem Plasma Process*, 8, 35, 1988

67. N. St.J. Braithwaite, N.M.P. Benjamin amd J.E. Allen, *J Phys E*, 20, 1046, 1987

68. D. Maundrill, J. Slatter, A.I. Spiers and C.C. Welch, *J Phys D*, 20, 815, 1987

69. T.I. Cox, V.G.I. Deshmukh, D.A.O. Hope, A.J. Hydes, N. St.J. Braithwaite and N.M.P. Benjamin, *J Phys D*, 20, 820, 1987

70. Y.P. Song, D. Field and D.F. Klemperer, *J Phys D*, 23, 673, 1990

71. B.M. Annaratone and N. St.J. Braithwaite, *Meas Sci Technol*, 2, 795, 1991

72. J.V. Scanlan, *The development of Langmuir probes for rf plasmas*, Dublin City University, 1989

73. R.R.J Gagné and A. Cantin, *J Appl Phys*, 43, 2639, 1972

74. A.P. Paranjpe, J.P. McVittie and S.A. Self, *J Appl Phys*, 67, 6718, 1990

75. A. Cantin and R.R.J. Gagné, *Appl Phys Lett*, 30, 316, 1977

76. G. Dilecce, M. Capitelli and S. De Benedictis, *J Appl Phys*, 69, 121, 1991

77. J.V. Scanlan and M.B. Hopkins, *Rev Sci Instrum*, to be published

78. C.J. Wu, J.A. Rees and P.A. Chatterton, *E*88, *ICPIG XX*, Pisa, Italy, 1991

79. W.G.M. van den Hoek, C.A.M. de Vries and M.G.J. Heijman, *J Vac Sci Technol B*, 5, 647, 1987

80. Chris Bowick, *RF Circuit Design*, Howard Sams and Co., Indiana, USA, 1982

81. J.S. Logan, N.M. Mazza and P.D. Davidse, *J Vac Sci Technol*, 6, 120, 1968

82. R.A. Gottscho, G.R. Scheller, D. Stoneback and T. Intrator, *J Appl Phys*, 66, 492, 1989

83. J. Loureiro, C.M. Ferreira, M. Capitelli, C. Gorse and M. Cacciatore, *J Phys D*, 23, 1371, 1990

84. R. Nagpal and P.K. Ghosh, *J Phys D*, 23, 1663, 1990

85. D.R. Suhre and J.T. Verdeyen, *J Appl Phys*, 47, 4484, 1976

86. H. Amemiya, *J Phys Soc Jpn*, 55, 169, 1986

87. C. Gorse and M. Capitelli, *J Appl Phys*, 62, 4072, 1987

88. J.V. Scanlan, M.M. Turner and M.B. Hopkins, *Appl Phys Lett*, to be published

89. S.D. Rockwood, *J Appl Phys*, 45, 5229, 1974

ACKNOWLEDGEMENTS

I am greatly indebted to Michael Hopkins for his guidance and tuition in the course of this work. Without his enthusiasm and continual drive to increase our understanding of discharge physics, our knowledge of the rf plasma would not have achieved its current level. He has also ensured that I have had several opportunities to travel and present results at international conferences, which has certainly helped improve the quality of the presented work and speed its completion. I am grateful for useful discussions with the following plasma physics people; Bill Graham, Michael Grimley, James Molloy, Colin Anderson, David Cameron, Michael Murphy, Ziaul Karim and Tony Herbert. I am also indebited to the many international plasma physicists I have interacted with and especially those who have shown an interest in my work. The project has been funded by VG Quadrupoles, and I am grateful for the continued interest of Dave Seymour and Co.. I wish to acknowledge the electronics work of Alan Hughes, which has operated, without hitch, for the past two years. Much of the technical work for the project was done at UCD, and I acknowledge the help of Bart Finn and Frank Heffernan in this regard.

I also must acknowledge the help of my fellow colleagues; Paul Jenkins for sound advice at all times,

Kevin Mellon and Hugh Grimley for sparks and waterworks, Mark Daly for use of the printer, Neil O'Hare for help with some of the diagrams and the many others. Among the Physics Dept. staff, I am grateful for the advise of Greg Hughes, John Costello and for the modeling work of Myles Turner. My rowing colleagues in the Physics Dept., Colin Potter, Liam Roberts and Adrian Giessel have also been a source of inspiration.

Without the continued assistance of both Barbara (anything?) and Marion this work would not have been done in the present time scale. For this I remain in their debt. I am also grateful to the EE Dept., for the loan of equipment on several occasions.

On a personal level, I am grateful for the "blind" support of my parents, since they haven't a clue what it is I do. I have been encouraged and financially supported by both Gráinne and Fonsie, and remain also in their debt.